THE HONG KONG
POLYTECHNIC UNIVERSITY
香港理工大學
Pao Yue-kong Library
包玉剛圖書館

Copyright Undertaking

This thesis is protected by copyright, with all rights reserved.

By reading and using the thesis, the reader understands and agrees to the following terms:

1. The reader will abide by the rules and legal ordinances governing copyright regarding the use of the thesis.
2. The reader will use the thesis for the purpose of research or private study only and not for distribution or further reproduction or any other purpose.
3. The reader agrees to indemnify and hold the University harmless from and against any loss, damage, cost, liability or expenses arising from copyright infringement or unauthorized usage.

IMPORTANT

If you have reasons to believe that any materials in this thesis are deemed not suitable to be distributed in this form, or a copyright owner having difficulty with the material being included in our database, please contact lbsys@polyu.edu.hk providing details. The Library will look into your claim and consider taking remedial action upon receipt of the written requests.

Pao Yue-kong Library, The Hong Kong Polytechnic University, Hung Hom, Kowloon, Hong Kong

http://www.lib.polyu.edu.hk

This thesis in electronic version is provided to the Library by the author. In the case where its contents is different from the printed version, the printed version shall prevail.

The Hong Kong Polytechnic University

Department of Civil and Environmental Engineering

LONG-TERM BEHAVIOR OF BOND BETWEEN FRP AND CONCRETE EXPOSED TO A HUMID SUBTROPICAL ENVIRONMENT: EXPERIMENTAL STUDY AND PREDICTIVE MODELING

By

Dianyu SUN

BEng

A Thesis Submitted in Partial Fulfillment of the Requirements for the Degree of Master of Philosophy

September 2014

CERTIFICATE OF ORIGINALITY

I hereby declare that this thesis is my own work and that, to the best of my knowledge and belief, it reproduces no material previously published or written, nor material that has been accepted for the award of any other degree or diploma, except for where due acknowledge has been made in the text.

_____ (Signed)

SUN Dianyu (Name of student)

ABSTRACT

Fiber reinforced polymer (FRP) composites have been widely applied in many fields such as the aerospace industry for many years. Compared with steel which is a commonly used modern construction material, the FRP composites have the advantages of excellent corrosion resistance and high strength-to-weight ratio. The corrosion resistance of FRP can benefit the long-term performance of reinforced structures, while the high strength-to-weight ratio leads to great ease in site handling, which reduces labor cost and interruptions to existing services. While a large number of studies have been conducted for the short-term performance of FRP- strengthened reinforced concrete (RC) structures, uncertainty is still remaining in their long-term performance. Indeed, lack of proper understanding of the durability of the FRP-strengthened RC structures has in return impeded a wider adoption of this technique in practice.

In this present study, the long-term performance of FRP-to-concrete interfaces and FRP-strengthened RC beams subjected to accelerated wet-dry cycles, which simulate a sub-tropical environment, is investigated. The thesis consists of four parts of work: (1) Evaluation of the degradation of materials used in the FRP-strengthened RC structures to provide a reference for the following durability study on FRP-to-concrete interfaces and FRP-strengthened RC beams. The concrete, FRP composites and adhesive materials were tested after 8 months of accelerated dry-wet cycle exposure. (2) Examination of the long-term performance on FRP-to-concrete interfaces subjected to accelerated wet-dry cycle exposure, with the aim to establish a series of exposure-based interfacial bond-slip models; (3) Assessment of the durability of FRP-strengthened RC beams, which experienced 8 months of accelerated dry-wet cycle exposure. Finite Element (FE) analysis was conducted to simulate their mechanical performance with due consideration of the degradation of materials and FRP-to-concrete interfaces; (4) The long-term performance of FRP-strengthened RC beams under sustained load. Four beams were loaded under two different

load levels for 9 months and the beam deflections were continuously measured using the fiber optic sensing technique. FE simulations were also conducted to reproduce the time-dependent beam deflections in comparison with the test results. Static loading tests were also conducted on the beams at the end of the sustained loading.

The following findings have been obtained from the above studies: Degradations were observed in FRP-to-concrete interface after 8-month exposure, while their degree varied in different types of FRP systems. The proposed exposure-dependent bond-slip model gave a good prediction of the degraded bond behavior; (b) The load capacity of FRP-strengthened RC beams decreased by 1.4% to 10.8% after 8-month exposure in wet-dry cycles, while increase in stiffness of beams was also observed; (c) Carbon FRP (CFRP)-strengthened RC beams were subjected to 300 days sustained loading. The time dependent deflections were 1.76~2.60 times the instantaneous deflections. However, no significant change was observed on the load-carrying capacity of the strengthened beams after the sustained loading regardless of the sustained load levels. (d) The FE models developed in this study with the implementation of appropriate bond-slip models of the FRP-to-concrete interface, can effectively predict the long-term behavior of FRP-strengthened RC beams with due consideration of the effects of weathering and sustained loading.

ACKNOWLEDGEMENTS

First and most importantly, I would like to give my heartfelt thanks to my chief supervisor, Prof. Jian-Guo Dai, and my co-supervisor, Prof. Jin-Guang Teng, for their generous support and constructive support throughout my master study.

In addition, I would like to thank the senior fellows of my group: Prof. Guo Yongchang, Dr. Chen Guangming, Dr. Xiao Qiongguan, Dr. Gao Wanyang, Dr. Bai Yulei, Mr. Fu Bin and Mr. Zhao Junliang, who gave me many precious suggestions and recommendations on my study. It would have been much more difficult to complete the work without their valuable suggestions and advices.

My sincere thanks also go to all my trusted friends and colleagues in the Department of Civil and Environmental Engineering of the Hong Kong Polytechnic University: Mr. Fang Xiaoliang, Mr. Yang Yinan, Mr. Zhu Jiongyi, Mr. Zeng Junjie, Mr. Nie Xuefei, Mr. Wang Qingkai, Mr. Liu Xiao, Ms. Wu Jingyun and Ms. Wang Zihao, and Mr. Liu Long in the Department of Civil Engineering of the Guang Dong University of Technology, not only for their constructive discussions, but also their kind encouragement and assistance during my study. I would like to give my particular thanks to Mr. Liu Long, who supported and assisted me earnestly during the experiment program; and my sincere thanks to Mr. Liu Xiao, who spent his precious time helping print the manuscript of this thesis, which is greatly appreciated.

Last but not the least, I wish to express my profound gratitude to my family. Their everlasting love, support and encouragement are the most precious fortune of mine, without which I would never have so much courage and confidence to pursue my dreams.

Table of Contents

LIST OF FIGURES

LIST OF TABLES

CHAPTER 1

INTRODUCTION

1.1 GENERAL

Fiber-reinforced polymer (FRP) composites are formed by embedding continuous fibers in a resin matrix that binds the fibers together. Common FRP composites include glass fiber-reinforce polymer (GFRP), carbon fiber-reinforced polymer (CFRP), and aramid fiber-reinforced polymer (AFRP). Compared with steel which is a commonly used modern construction material, the FRP composites have many advantages, including excellent corrosion resistance and high strength-to-weight ratio. The corrosion resistance of FRP can benefit the long-term performance of reinforced structures, while the high strength-to-weight ratio leads to great ease in site handling and reduces labor cost and interruptions to existing services (Teng et al. 2002; Bank 2006). Due to these superior material properties, FRP composites have been widely applied in many fields such as the aerospace industry. The FRP composites embraced wide applications in constructions due to reduction of the price and an increasing recognition of their advantages, as well as the extremely increasing rehabilitating requirement for aged structures which are suffering continuous degradation in the past twenty years around the world (Teng et al, 2002; Holloway and Teng 2008). The FRP composites have been applied in many aspects of civil engineering, including (Chen et al. 2010): (a) retrofitting/strengthening of existing structures by bonding/wrapping to existing reinforced concrete (RC) structures; (b) replacing conventional construction materials in the construction of new structures, such as FRP bars, cables and profiles; (c) combined use with conventional materials (e.g., steel and concrete) to create hybrid structures, such as concrete-filled FRP tubes.

In general, there are two major types of applications for externally bonded FRP systems:

contact-critical applications (e.g., FRP confinement of RC columns) and bond-critical applications (e.g., FRP flexural /shear strengthening). The present study is concerned with the latter type. A bond-critical FRP system consists of five components: (a) the concrete layer; (b) FRP composites; (c) resins between the concrete and FRP composite and (d) interfaces between them (Figure 1-1). When FRP systems are used as flexural strengthening systems in RC beams, the FRP laminates are always attached on the tension flange of the beams to provide additional tension capacity, while the adhesive layer transfers shear stress between the concrete and FRP composites, so that all the components work simultaneously as a hybrid section.

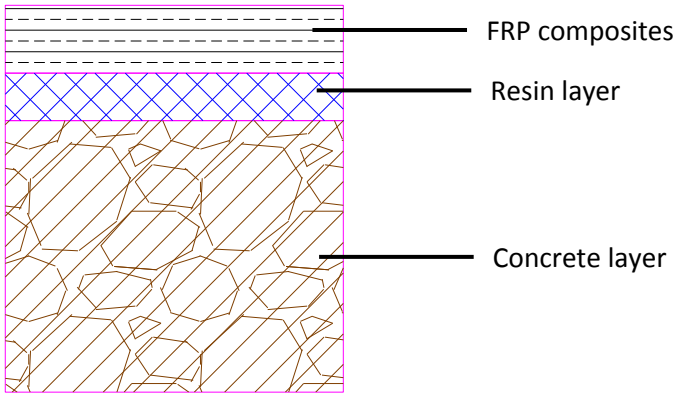

Figure 1-1 Components of the FRP-to-concrete interface

In reality, the components of interface are exposed to environmental conditions. The ambient environment can interact with the interfaces directly or indirectly. For example, moisture can penetrate into the interfaces through cracks and voids, and high temperature could affect the interfaces via heat transition or radiations. The components and interfaces can hardly forever retain their properties subjected to continuous environmental effects, i.e. degradation is supposed to occur within them; as a result, the FRP-to-concrete interface suffers deterioration in its performance, which can be detrimental due to loss of normal functions. The greater the degradation over time, the lower the structures' load-carrying capacity will

be. Therefore, the durability of the bond should be a critically important issue to be considered. The present thesis will be limited to RC beams strengthened in flexure, for whose research outcomes, particularly the exposure-dependent bond-slip model, will also have direct applications in predicting the long-term behavior of other bond-critical FRP-strengthened RC systems.

While a large number of studies have been conducted for the short-term performance of FRP-strengthened RC structures, uncertainty is still remaining in their long-term performance. The lack of proper understanding for the durability of the strengthened RC structures has impeded the wider adoption of FRP strengthening technology as it can lead to skepticism and lack of confidence in the technology. Therefore, for a wider adoption of the technology in a humid subtropical environment, the effect of the local humid subtropical climate on bond durability must be properly understood and assessed.

1.2 ENVIRONMENTAL EXPOSURE CONDITIONS

Most existing research on the durability of FRP-strengthened RC members is in terms of the environmental exposure conditions that have a significant effect on their long-term performance. These conditions include: (1) moisture (water and salt solutions); (2) alkaline environment; (3) extreme temperature and thermal cycling; (4) low temperature and freezing and thawing; and (5) ultra violet (UV) radiation. In the subtropical climate, the main features of environment include a large amount of annual rainfall and significant seasonable variations in temperature, as well as high level UV radiation. Therefore, the effects of moisture, thermal cycling and UV radiation are the main concerns in terms of durability of FRP-strengthened RC structures in the humid subtropical climate. Since it has been well established that the effect of ultra violet can be excluded or minimized by applying a layer of coating on the surface of FRP (Karbhari et al. 2013), the present study is then focused on the

effects of combined moisture and thermal cycling on the long-term performance of bond-critical FRP-strengthened RC systems in humid subtropical climates and the predictive modeling of these effects.

A wide variety of studies on the effects of moisture and temperature have been conducted using different exposure schemes. In general, these schemes include: (1) FRP types (e.g., CFRP, GFRP and AFRP); (2) Resin types (e.g., epoxies, polyesters and vinylesters); (3) Solution types including pure water, salt water and alkaline solution (Karbhari and Zhao 1998; Leung et al 2001; Wan et al. 2006; Silva and Biscasia 2008); (4) exposure period; (5) types of exposures, such as fully immersion or 100% humidity (Grace and Singh 2005), wet-dry cycles (Chajes et al. 1995; Toutanji and Gomez 1997; Mukhopadhyaya et al. 1998; Sen et al. 1999; Leung et al. 2001; Almusallam et al. 2006; Dai et al. 2008) and field exposure (Sen et al. 1999; Almusallam et al. 2006)). In particular, Sen et al. (1999) evaluated bond degradation under various exposure conditions and reported that the dry/wet cycle is the most severe factor leading to bond degradation. Due to the relatively short history of the FRP strengthening technology and the time and cost involved in conducting a larger number of field exposure tests, existing field exposure data are neither sufficient nor detailed enough to gain a good understanding of the bond durability of bond-critical FRP-strengthened RC systems and to develop design models. Indeed, given the diversity of climate and the associated environmental exposure conditions, the diversity of materials available for FRP strengthening and the time scale involved, the development of reliable empirical durability design models based on field exposure tests is generally unfeasible. As a result, existing durability researches on FRP-strengthened RC systems have been dominated by accelerated laboratory tests based on an empirical approach.

1.3 EFFECTS OF MOISTURE ON MATERIAL COMPONENTS OF FRP-TO-CONCRETE INTERFACES

Before exploring the interfacial issues of FRP-to-concrete interface, it is essential to evaluate the characteristics of fundamental components. In this session, the materials used in the FRP system are introduced and the related in-service properties are discussed.

1.3.1 Resins

The polyesters, epoxies and vinyl-esters are the most common thermal-setting matrices which are adopted for manufacturing FRP composites. The polymers are manufactured by polymerization (Hollaway 2010), by which the polymers obtain the properties of high-modulus of elasticity and high tensile strength. The matrices are cross-linked formed by network molecular structure; therefore, these resins could be formed under heat and they do not melt or soften upon reheating once formed. Also, the resins generally have good resistance to solvents. Resin adhesives are often composed of two parts: the resin and curing agent. One important thing is that the resins must be mixed in a correct mix ratio. The two parts need to co-react in a fixed ratio for a complete reaction; otherwise, un-reacted resin or curing agent will remain within the matrix, which will affect the properties of the polymer after cure. There are two methods to polymerize a thermosetting polymer, which are cold cured systems and hot cured systems. The former one is widely adopted since the resin can be cured at ambient temperature on site (generally 10-30 ℃). However, relatively long curing time is needed and the physical properties are not mature without a post-curing process, which unfortunately is generally omitted on site. By the contrast, the latter one has a restricted curing temperature process (e.g., elevated temperatures of the order of 130 ℃), which generally can only be realized in an automated production factory.

For thermosetting polymers such as epoxies, the glass transition temperature (T_g) is an important in-service property. The T_g is defined as the temperature at which the physical properties of an amorphous or an amorphous/crystalline polymer vary from a solid phase (brittle of glassy state) to a liquid phase (rubbery state). The phase change of the polymer is

over a finite temperature range and the T_g is the mid-point of this range. Polymers below the T_g are rigid, which have both stiffness and strength; while polymers above the T_g are soft elastomers or viscous liquids and have no stiffness or strength. Considering such properties of resins, it is recommended that the working conditions should be 20 ℃ below the glass transition temperature especially for cold cured systems (Hollaway 2010). For hot cured composites, the glass transition temperature could reach 200 ℃, while the cold cured systems have a much lower T_g, which normally does not exceed 100 ℃. However, the T_g of some cold cured composites can be increased by further post curing the polymer at a higher temperature, but there exists a maximum value in T_g regardless the post cure temperature.

The durability of polymers is a function of the aggressive environments and time. One of the major concerns is the ingress of moisture and aqueous solutions or the contact with an alkaline environment. As for the corrosion effects of moisture, both physical and chemical interactions are included. The absorption of the moisture will cause plasticization, saponification or hydrolysis in polymers due to interruption of weak (Van der Walls) bonding between polymer chains (Hollaway 2010). Resins subjected to long-term moist exposure may degrade in strength, stiffness and toughness. The effect of moisture on the resin matrix could be reversible or irreversible depending upon the chemical composition of the specific resins. Usually, the resin deterioration is linked with the water content, however many other factors may have contributions to the degradation. The polymer permeability, or barrier property of polymers, determines the ability of moisture resistance of polymers. Haque et al. (2003), Liu et al. (2005), Hackman and Hollaway (2006) reported that the ingress of moisture would permeate through polymers over time particularly if the polymer is permanently immersed in water or salt solutions. A fully curing process can improve the barrier property of polymers largely by advantage of a high-degree of cross-linking structure. Another effective method to improve the barrier property of the polymers is to apply an additive coating layer to the matrix (Van Ooij et al. 2005).

1.3.2 Fibers

Three types of fibers are most often used in the construction industry, which are the glass, the carbon and the aramid fibers. The three types of fibers have very different stiffness and ultimate strength, while each type of fiber has several different sub-types with different mechanical properties. Various types and mechanical properties of these fibers were discussed in detail by Hollaway and Head (2001). As for the durability of fibers subjected to moisture, (a) carbon fibers have good resistance to moisture ingress (Ceroni et al. 2006); on the contrary, (b) glass fibers are very susceptible to alkaline solvents and strong acidic environments due to the presence of silica in fibers (Mufti et al. 2005; Jones and Chandler 1985). The main reactions in an alkaline environment include pitting, hydroxylation, hydrolysis, and leaching (Hollaway 2010). Chloride ions will also corrode the glass fibers through dissolving the surface of fibers. Moisture can readily ingress into fibers and exacerbate the microscopic cracks and defects on the surface of fibers; as a result, the tensile strength of fibers decreases. In addition, the glass fibers have the high ratios of surface area to the weight, which however aggravate to some extent the corrosion. Similarly, (c) reduction in tensile strength were also observed in aramid fibers when exposed to an alkaline environment (Uomoto and Nishimura 1999)

1.3.3 Fiber reinforced polymers (FRP)

The primary aim of a fiber reinforced polymer is to provide an average behavior of the composite to make the component materials efficiently functioned. Besides the basic properties of resins and fibers, the mechanical performance of FRP composites is highly dependent upon the quality of the fiber-matrix interface. This interface provides physical and chemical connection between the fiber and the polymer, thus its characteristics will also affect the durability performance of the composite. The ingress of moisture into this interface will weaken the bond between the fibers and the matrix, which as a result, impedes the components working compositely. Therefore, if a composite is composed of matrix and fibers which are moisture-permeable or solvent susceptible respectively, it is supposed to

suffer more severe durability problems. Matthews and Rawlings (1999) reported that the fiber to polymer tensile strength ratio, which represents the sensitivity of the composite to matrix properties, is the dependent factor of corrosion resistance of FRP composites against moisture. CFRP composites have a much higher strength ratio than that of GFRP, which makes them less susceptible to moist corrosion. Many field exposure tests and accelerated tests were conducted to evaluate the durability of FRP composites (e.g., Katsuki et al. 1997; Uomoto 2001), which can be summarized as follows: (a) CFRP composites have good durability characteristics; (b) AFRP composites have good solvent corrosion resistance except in acidic environment; and (c) GFRP composites have poor alkaline resistance.

1.3.4 Concrete substrate

The main moisture reactions on concrete include: (a) freezing and thawing; (b) chemical attack from solvents; (c) corrosion of embedded metal; and (d) alkali-aggregate reaction. (Mather 2004). In a sub-tropical environment, the freeze-thaw effect is not a problem since there is no extremely low temperature. The other reactions can be alleviated or suppressed by proper methods, e.g., using a proper type of concrete, increasing the thickness of concrete cover and, producing a careful curing process. However, these issues should be still considered if when durability of FRP-strengthened RC structures is concerned. The deterioration of concrete substrate is detrimental for externally bonded FRP systems since the performance of the strengthening system relies much on the concrete substrate. Moreover, the ingress of moisture at fluctuating temperature induces cracks and exacerbates the voids inside the concrete. A porous substrate will aggravate the extent of moisture contact of the interfaces, which is detrimental for the durability of the external bonded FRP systems largely if no precautions are taken.

1.4 EFFECTS OF MOISTURE ON FRP-TO-CONCRETE INTERFACES

1.4.1 Short-term behavior of FRP-to-concrete interface

When concrete structures are strengthened using externally bonded fiber-reinforced polymer composites (e.g., flexural strengthened RC beams), the bond between the FRP and the concrete generally plays a key role in transferring forces between them. For the external FRP to be effective in enhancing the load-carrying capacity of the structure, effective stress transfers between the FRP and the concrete are required. Many researchers have conducted extensive research on the short-term bond behavior between FRP and concrete (e.g., Teng and Chen 2001, Dai et al. 2005). Substantial experimental and theoretical work exists on the bond strength of FRP to steel or concrete joints, which indicated that the strength of the FRP-to-concrete interface is relatively weaker than both side materials in a repairing system because of the stress concentration and rapid change of stress level along the bond line (Teng et al. 2002). An important feature of FRP- bonded concrete joints is the existence of effective bond length which suggests that the bond strength cannot increase continuously with the increase of bond length. Although the bond strength is not likely to further develop when the bonded length is beyond the effective bond length longer bond length can improve the ductility of the bond (Teng et al. 2002). Considering these phenomena, several bond strength models or bond-slip models have been developed in the past few years (e.g., Chen and Teng 2004; Dai et al. 2005; Lu et al. 2005). However, it is apparent that since none of these models have taken the environmental effects into account, they cannot be applied for long-term design directly.

1.4.2 Mechanisms of moisture effects on the FRP-to-concrete interface

The durability of bond subjected to moisture is determined by many factors: (a) the basic in-service properties of the component materials, namely the concrete, resins and FRP composites, which have been discussed in detail in section 1.3; (b) the interfacial characteristics between materials (i.e., the resin-to-concrete interface and resin-to-fiber interface); (c) the environmental conditions; and (d) the method and quality of manufacturing of the bond including the applying process and curing process. There exist

microscope voids and defects in the material components, making the bond permeable to moisture and solvents. The moisture can ingress into the interfaces through various sources such as, capillary action along the longitudinal fibers, water penetrating through the cracks and voids of the concrete and diffusion through the matrix. Although the FRP materials commonly have good corrosion resistance, some aspects of the composites have been observed to deteriorate when subjected to long term exposure to specific moist environment. The extent of deterioration depends on many factors such as the types of resins and FRP used in the strengthening systems, ambient temperature, stress state of the bond, pre-existing cracks. The presence of moisture in the interface between concrete and FRP composites will weaken the bond chemically (plasticization, saponification or hydrolysis effect) and physically (exacerbating the voids and defects). The internal stress will be produced in the polymer matrix due to moisture-induced swelling. As a result, irreversible damage is developed through matrix cracking and delamination in the concrete-matrix and fiber-matrix interfaces.

1.4.3 Existing experiments and findings on the moisture-affected durability of FRP-to concrete interfaces

Substantial research has been conducted to study the effects of moisture or synergistic effects of temperature and moisture on the FRP-to-concrete interfaces. Strength reductions obtained from these tests ranged from 0~45% decrease in the bond strength or maximum 60% loss in mode I/II fracture energies. Changes in failure mode were also observed in some cases (e.g., Shreshta et al. 2012).

Karbhari et al. (1997) developed a modified peel test to explore the durability of concrete joints bonded with different types of FRP materials and subjected to different moisture exposure regimes for 60 days, which were (a) ambient conditions at 20 ℃; (b) immersion in fresh water at 20 ℃; and (c) immersion in synthetic sea water at 20 ℃. Degradation in bond which is represented by the fracture energy release rate varied among different FRP systems.

The CFRP systems achieved a better moisture resistance regardless of the nature of the solvents and loss in fracture energy was very limited; while the Mode II fracture energy release rate of GFRP-to-concrete interfaces decreased by over 50% in cases of both fresh and sea water. The authors also concluded that interfaces in which the resins have a higher T_g lead to a better corrosion resistance under relatively high temperatures as well as accelerated wet-dry cycling exposures.

Mukhopadhyaya et al. (1998) assessed the durability of double-lap GFRP bonded concrete joints under various exposure conditions, namely wet-dry cycling in 5% sodium chloride solution (wet for one-week and dry for another week in one cycle; 18 cycles, 18±2℃), freeze-thaw cycling (450 cycles and two days per cycle) and a combination of chloride immersion and freeze-thaw cycles. The author reported an increased bond transfer length and a larger magnitude of shear stress distribution and the plate slip of joints in all of the exposure regimes. However, the bond strength is not largely affected considering the relatively short exposure duration.

Sen et al. (1999) explored the durability of FRP-to-concrete interface using shear and torsion tests on CFRP bonded concrete slabs. Five epoxy systems were used and the exposure in three conditioning environments for 17 months were evaluated: (a) wet/dry cycles in 15% salt water (4-day submergence in 60℃ salt water and 4-day drying in ambient temperature); (b) combined wet/dry and thermal cycles in 15% salt water and (c) outdoor (field exposure). The result indicated that the most severe deterioration in bond occurred in wet/dry cycles, in which the greatest loss (0~60%, according to the epoxy system adopted) in bond cohesion strength was found.

Wan et al. (2006) explored the durability of CFRP-to-concrete interface saturated in fresh water at room temperature for maximum 8 weeks. A progressive degradation in bond was

reported. The fracture energy of bond decreased by 77% at the end of exposure. The author also studied the effect of the presence of water on the interface when applying the FRP fabrics. The higher the moisture content on the substrate, the poorer the bond performance would be within the tested moisture content range (8%~58%).

Frigione et al. (2006) studied the water resistance of FRP bonded concrete joints using flexural tests. The author reported 30% decrease in bond strength of joints after one month of immersion in distilled water at a temperature of 23 ± 1℃. A reduction in the glass transition temperature and the stiffness of the epoxy resins used was also reported in the study.

Dai et al (2008) firstly assessed the effect of the presence of moisture on the CFRP-to-concrete interface during FRP application process. Both dry and wet substrates in two humidity degrees (48% and 90%) were evaluated. The results of single-shear pullout tests on the FRP bonded concrete joints indicated that there was little influence of the concentration of moisture in the concrete substrates before bonding, if a proper primer was used. The author further studied the durability of bond subjected to 8-month wet-dry cycles (4-day submergence in 60℃ sea water and a 3-day dry period per cycle). The joints suffered about 40% loss in pull off strength, regardless the substrate treatment when FRP composites were bonded.

Dai et al. (2010) further evaluated the durability of FRP bonded concrete joint and FRP-strengthened RC beams subjected to wet-dry cycles for 8 months, 14 months and 2 years. Results indicated asymptotical degradation nature of FRP-to-concrete interfacial tensile bond strength with the exposure time.

Tuakta et al. (2011) conducted peel and shear fractures tests on FRP bonded concrete joints

after being exposed to maximum 8 wet-dry cycles. Three exposure durations were adopted: 1, 2 and 3 weeks, and the number of cycles were 1 to 8. In each cycle, the drying was four days and the lengths of wet period were different according to the duration of each cycle. The water temperature was 23℃ or 50℃. The author reported maximum 58% loss in peel fracture toughness and 55% in shear fracture toughness when joints were still wet. The decrease in fracture toughness was considerable even in the early stage of exposure and was more severe in a higher temperature, longer submerging period, and more cycles. However, when the joints were fully dried, they could regain a proportion of fracture toughness (95% in early weeks and almost no regain in ending weeks.). The author also reported a high correlation between the fracture toughness of bond and moisture content: the larger the moisture content, the lower the fracture toughness in bond would be.

Shrestha et al. (2012) conducted a single-shear pullout tests on FRP bonded concrete joints subjected to fully immersion of water in variations of durations from one month to 6 months. Test results showed 11% to 14% decrease in bond strength in FRP bonded concrete joints using polythiol-polyamine combined hardener primer and 2% to 10% decrease in the bonded joints using polyamine hardener primer, respectively. The properties of resins after continuous water immersion were also evaluated by the author. The tensile strength of the resins after water immersion were found higher than the original ones in most cases, while the shear strength of resins showed slight decrease after exposure.

1.4.4 Approaches of studying deterioration in bond

Generally, two types of approaches are adopted to study the deterioration and failure mechanisms of FRP bonded concrete systems: (1) the strength-based and (2) the fracture-based approach. In the strength-based approach, bond degradation is evaluated by measuring the interfacial bond properties of bonded joints, including interfacial tensile bond strength, interfacial shear strength using pull-off tests (e.g., Sen *et al.* 1999) and single-lap or double-lap shear tests (Mukhopadhyaya *et al.* 1998), and also evaluated by tests of the flexural

capacity and ductility of FRP bonded RC beams (e.g., Chajes *et al.* 1995; Toutanji *et al.* 1997; Leung *et al.* 2001; Grace *et al.* 2005; Dai *et al.* 2010). Some researchers also used (2) Mode I or/and Mode II fracture toughness to evaluate bond degradation affected by moisture (Karbhari *et al.* 1997; Lyons *et al.* 2002; Davalos *et al.* 2005; Wan *et al.* 2006; Au and Buyukozturk 2006; Tuakta *et al.* 2011) between FRP and concrete. In this approach, the degradation of bond is indicated with the bond fracture toughness or interfacial energy release rate, which can be evaluated with the peel and shear fracture tests. Using this approach, the local deterioration in bond can be captured by tracking how crack propagates along the interface from a pre-existing crack at the interface. Compared to strengths, interfacial fracture toughness appears to be a more generic and useful indicator in capturing exposure-induced degradation of bond because the effects of material stiffness and member size are naturally included in the indicator. A drawback of this approach is that engineers are usually unfamiliar with fracture mechanics approaches and the approach is generally difficult to apply as explicit solutions are seldom available.

1.4.5 Existing bond durability design approaches

As for short-term loading, in predicting the long-term performance of FRP-strengthened RC members, the key challenge still lies in the prediction of debonding failures, as FRP rupture and concrete crushing are comparatively easier to model. The current state of the art in predicting debonding failures of bond-critical FRP-strengthened RC members after environmental exposure is far from satisfactory. In design guidelines, material strength reduction and partial safety factors are usually given to account for the long-term deterioration of material properties, but no provisions are given to account for the deterioration of bond strength except for UK's Concrete Society (2004) guideline. In the Concrete Society (2004) guideline, the deterioration of bond strength is accounted for through the reduction of elastic modulus of FRP. The elastic modulus, however, is assumed to be independent of the effect of environmental exposure in other design guidelines and does not appear to be the main reason causing the deterioration of bond. Obviously these

recommended material strength reduction and partial safety factors are satisfactory only when the fracture of FRP is a dominant mechanism. A safe and economical bond durability design approach is therefore urgently needed.

1.5 EFFECTS OF MOISTURE ON FRP-STRENGTHENED RC BEAMS

1.5.1 Existing experimental explorations and findings on the moisture-affected durability of FRP-strengthened RC beams

Some of the previous studies reported that after a relatively long-term exposure (over one year or 100 cycles), noticeable decrease in the beam load capacity can be observed, and such degradation cannot fully recover (e.g., Grace and Singh, 2005; Silva and Bisacia, 2007; Tuakta *et al.* 2011); while contrary results were discovered by some other scholars in the tests within a shorter term (e.g., Silva *et al.* 2007; Dai *et al.* 2010), in which even an increase in beam strength was discovered.

Charjes *et al.* (1995) accessed the durability of flexural strengthened RC beams with FRP systems using small-scale beams strengthened with variations of FRP composites. Three types of fabrics were used, which were aramid, glass and graphite composite fabrics. The beams were subjected to chloride exposure for 50 or 100 wet/dry cycles at room temperature (wet for 16hrs and dry for 8hrs). The tests indicated 10%~20% decrease in beam strength after 50 cycles and 19%~36% decrease after 100 cycles. Among the three types of FRP-strengthened beams, the graphite-reinforced beams proved to be the most durable, losing less than 15% of their strength increase over the un-strengthened beams.

Toutanji et al. (1997) evaluated the durability of CFRP and GFRP-to-concrete interfaces and FRP-strengthened RC beams subjected to a 75-day exposure scheme including 300 wet/dry cycles (four-hour submergence in 3.5% salt solutions and 2-hour drying in hot air at 35 ℃

and 90% humidity in each cycle). The results indicated that the load-carrying capacity of the strengthened beams decreased by 10%~45% after exposure.

Karbhari *et al.* (1998) conducted an investigation of durability performance for in situ formed externally composite strengthening systems. Two types of CFRP systems and one GFRP system were evaluated. The strengthened members were placed into different environmental conditions for 120 days, namely (a) ambient conditions at 20 ℃; (b) immersion in fresh water at 20 ℃; and (c) immersion in synthetic sea water at 20 ℃. Most severe decrease in beam strength (45%) and increase in mid-point deflection (68%) were observed in GFRP-strengthened RC members submerged to sea water. Additionally, better performance of CFRP composites over GFRP composited were also indicated by the test results.

Grace *et al.* (2005) studied the durability of the CFRP-strengthened RC beams subjected to variations of adverse environmental conditions, such as 100% humidity, saltwater, alkali solution, freeze-thaw, thermal expansion, dry-heat and repeated load cycles etc. The author concluded that long term exposure to humidity is the most detrimental to FRP-strengthened RC beams. Beams subjected to 10,000 hrs. of 100% humidity (at 38±2 ℃) experienced an average of 33% reduction in beam strength.

Almusallam (2006) conducted a durability study on GFRP-strengthened RC beams subjected to (a) field exposure; (b) wet-dry cycles in fresh water; (c) wet-dry cycles in saline water and (d) wet-dry cycles in alkaline water environment. All the wet-dry cycles consisted of two-week submergence in the solutions and two-week drying, and the exposure temperature was 23±2 ℃. The test duration was 24 months, however, no noticeable changes on the flexural strength of beams were observed in all aforesaid environments.

Mukherjee *et al.* (2007) evaluated the durability of GFRP-strengthened RC beams subjected

to 60 ℃ pure water immersion for varying durations (0-9 months), or subjected to field exposure for 12 months. At the meantime, varying service load was applied to simulate the real service conditions in a tropical environment. The author reported 13.5% higher beam load capacity after 9-month exposure in water and an 18.9% lesser beam load capacity after field exposure. Increase in stiffness was also observed in all beams after exposure.

Silva *et al.* (2007) evaluated the durability of CFRP and GFRP-strengthened RC beams subjected to salt water immersion (5% salt water) for 1000, 5000 and 10000 hours by bending tests. The author reported that although considerable degradations in bond were visually observed, the load carrying capacity was not affected.

Soudki *et al.* (2007) evaluated the durability of CFRP-strengthened RC beams subjected to wet/dry cycles (room temperature; 24-hour submergence in 3% salter water and 24-hour drying per cycle). The author reported asymptotical decrease in the ultimate capacity of the CFRP-strengthened RC beams from 100 cycles to 300 cycles. 11% to 28% decrease in beam load capacity was reported after 300 cycles' exposure. However the beam stiffness was not affected, as reported by the author.

Dai et al. (2008) studied the durability of CFRP-strengthened RC beams subjected to 8-month wet-dry cycles (4-day submergence in 60 ℃ sea water and a 3-day dry period per cycle). A decrease in stiffness and a slightly increase in the beam strength were reported.

As reported above, the effect of moisture on the performance of FRP composites has been one of the most widely studied durability issues. Although strength reductions in FRP-to-concrete interface and FRP strengthened RC beams were discovered and analyzed by many studies listed above, strength reductions reflect the effects of many factors other than those of bond degradation, such as the effects of the size of the beam, stiffness of the bonded FRP reinforcement and the steel reinforcement ratio. As a result, those test results cannot be

easily generalized and thus can hardly serve as the basis for the development of a reliable practical durability design approach.

1.5.2 Simulations of long-term performance of FRP-strengthened RC beams under environmental effects

The existing research on debonding failures under short-term loading has relied heavily on the understanding and modeling of the basic shear stress-slip. The power of an accurate bond-slip model in predicting the short-term behavior of FRP bonded concrete joints and FRP-strengthened RC beams has been extensively demonstrated by many researchers in developing FE and simple design models for debonding failures of FRP-to-concrete joints (e.g., Chen and Teng 2011; Dai *et al.* 2006; Lu *et al.* 2007) and RC beams (e.g., Chen *et al.* 2011) strengthened in shear or flexure with bonded FRP systems. The bond-slip model therefore provides a unified basis for predicting the debonding failure of bond-critical FRP-strengthened RC members. It is therefore clear that if the approach established for short-term loading is to be successfully applied in studying debonding failures after long-term environmental exposure, a reliable bond-slip model that reflects the effects of environmental exposure should first be developed. Such an exposure-dependent bond-slip model can then be implemented in an FE model similar to that presented in Chen *et al.* (2011) to predict the long-term performance and debonding failure after environmental exposure. The FE model after suitable verification with test data can then be employed to generate data for the development of a bond durability design approach. However, so far, none of such exposure-dependent bond-slip model is feasible yet.

1.6 EFFECTS OF SUSTAINED STRESS ON FRP-STRENGTHENED RC BEAMS

In reality, the sustained stress level in the externality bonded system due to permanent or

quasi-permanent loading is very low, if at the time of strengthening, such loading is already present. Therefore, for such applications, the effect of sustained loading on the durability of bond-critical FRP-strengthened RC members is not a major issue. However, significant stresses can arise in the FRP system, if the FRP system is pre-stressed or is used to support additional sustained loading, or if the original RC structure is expected to further deteriorate/deform to shed stresses into the FRP system. In such cases, the stresses in the FRP may interact with the effect of environmental exposure to causes additional degradation of the bond between FRP and concrete.

Creeps in the concrete and FRP-to-concrete interface are dominant phenomena when FRP strengthened RC beams are subjected to sustained stresses (e.g., Benyoucef et al. 2006; Chami et al. 2007). Previous experiments observed that there is a significant proportion of beam's long term deflection contributed by the cohesive creep in FRP-strengthened RC beams as a function of the strengthening ratio of FRP systems (Reda et al. 2010). The interaction between creeps in the concrete and FRP systems can induce strain redistribution in the FRP-strengthened RC beams, due to which a significant increase in the axial force may occur in the FRP laminates (Hamed et al. 2010). Creep in FRP-strengthened RC beams may lead to premature failure in beams over time, in spite of the relative lower sustained loads than short-term failure loads. Experimental studies have found both positive and negative influences of FRP reinforcement for long-term performance of RC beams under sustained stresses. Tan et al. (2006) reported that RC beams strengthened with FRP composites can reduce the long-term deflection of beams largely compared with those without FRP strengthening. Choi et al. (2007) studied the creep mechanism of epoxy under shear stress, concluding that the shear stress to shear strength ratio in adhesive layer was a primary factor affecting the long-term behavior of the FRP-to-concrete interfaces. Ahmed et al. (2011) studied the time-dependent behavior of cracked or un-cracked CFRP strengthened RC beams subjected to six month's sustained loads. The long-term deflection in controlled RC beams were 64% and 65% of their instantaneous deflections, while long-term deflections

in FRP strengthened RC beams were only 42% to 46% of their instantaneous deflections.

At the meantime, simulations of the creep behavior in FRP-strengthened beams have been intensively studied. Bazant and Wu (1974) developed an exponential algorithm for creep modeling; another closed-form high-order solution was developed by Rabinovich and Frostig (2000) considering the creep and shrinkage on equilibrium and deformation compatibility requirements in and between all parts of the composited beams. Another closed-form solution for the interfacial shear and normal stresses in FRP-strengthened RC beams was developed by Benyoucef et al (2006), which can be used in the simulation of plate end failure; Tan and Saha (2008) developed empirical equations for predicting the crack width and its variation with time. Choi et al (2010) conducted FE modeling for FRP-strengthened RC beams, which took into account both the creep of concrete and viscoelasticity of epoxy adhesive on the FRP-to-concrete interface. Taha et al. (2010) developed another simulation model using Finite Element method, in which perfect bonds between interfaces of different materials were assumed. Hamed and Bradford (2010) also developed a creep model, in which the viscoelasticity and shear deformability of adhesive were considered. A theoretical model was further developed by Hamed and Bradford (2012), in which creep of different materials, time-dependent cracking and tension-stiffening of concrete were all considered.

For most FRP-strengthened RC beams, the stress level in the FRP is low as explained above. Therefore, the present study is focused on the durability of such FRP-strengthened RC beams subjected to environmental exposure. However, the interaction between sustained stresses and environmental exposure will also be explored to clarify the contradictory conclusions in the existing literature and to ascertain the effect of this interaction. It is expected that this interaction effect is important for at least some of the strengthening applications.

1.7 OBJECTIVES AND SCOPE

This chapter has presented a comprehensive review of the existing knowledge relevant to durability study on the bond behavior between FRP-to-concrete interfaces under environmental and load effects. A lack of research on the critical mechanisms of bond degradation and the missing of reliable design guideline for durability study were issued: Although intensive study was conducted on this area, little has been discussed on the bond degradation as the key factors of reductions in bond strength, or the methodology adopted is hardly feasible for real design; Moreover, the existing design code misunderstood the mechanism of durability issue in FRP-to-concrete interface by defining reduction factors for material properties (e.g., FRP stiffness) of FRP composites. The review also issued the blank on the study of interactive effects between environmental exposure and sustained stresses. A lack of study on the above issues makes the long-term performance of FRP-to-concrete interface skeptical in real practices, and evaluations on these gaps are necessary to make the FRP-strengthened RC structures reliable.

Against the above background, this thesis is proposed to study the long-term performance of the FRP-to-concrete interface experimentally and to develop a powerful predictive tool for this performance. The realization of this aim requires a combined experimental and theoretical approach. The experimental work includes both accelerated laboratory tests and actual field exposure tests. The relationship between them needs to be examined and established. The theoretical work includes the development of a bond-slip model, FE modeling of member behavior, and the development of a durability design procedure. To represent the seasonal cycles of moisture and temperature of the humid subtropical climate, the environmental exposure conditions to be considered will involve combined moisture and thermal cycling. Both types of cyclic actions are known to lead to long-term degradation of the bond between FRP and concrete. In summary, the present study has the following

specific objectives:

(a) To gain an in-depth understanding of the long-term bond behavior between FRP and concrete in a humid subtropical climate and in sustained stress load;

(b) To establish an exposure-dependent bond-slip model for FRP-to-concrete interfaces that reflects the effects of long-term moisture and thermal cycling;

(c) To develop a Finite Element (FE) predictive model for the long-term performance of FRP-strengthened RC beams that incorporates the exposure-dependent bond-slip model; and

(d) To formulate a safe and economic approach for the durability design of FRP-to-concrete interfaces with due consideration of the humid subtropical climate.

1.8 ORGANIZATION OF THESIS

The organization of the present thesis is illustrated in Figure 1-2. **Chapter 2** discusses the long-term performance of material components in a FRP-strengthened RC system. Firstly, the exposure scheme is introduced; secondly, the material test methods are introduced, including concrete strength tests, tensile tests of steel reinforcement, FRP composites and epoxies, as well as Dynamic Mechanical Analysis (DMA) of epoxies. Test results and discussions are reported afterwards.

Chapter 3 presents the experimental and numerical studies on the behavior of concrete-to-FRP interface. In the experiment part, both accelerated laboratory tests and field exposure tests were designed and prepared. The performances of four types of FRP-to-concrete interface exposed in wet-dry cycles for 0 month and 8 months were evaluated. The specimen preparations, test procedures and instruments are introduced in sequence. Test observations and results are introduced and discussed. Based on the test, analytical studies were conducted. In the analysis part, the method proposed by Dai et al. 2005 was used to develop

the exposure-dependent bond-slip models. The analytical results are described and discussed, which proves that the regressed bond-slip models can give a good indication for effects of exposure conditions.

Chapter 4 presents the experimental and analytical explorations for long-term performance of FRP-strengthened RC beams. In the experiment part, both accelerated laboratory tests and field exposure tests were designed and prepared. The beams with four different FRP systems subjected to 0-month and 8-month exposure in wet-dry cycles were tested. Test observations and results are described in detail and comparisons between exposure period and FRP types are discussed. In the analysis part, a study on FRP debonding strain is conducted. Moreover, Finite Element (FE) simulations were conducted. The FE models were built to simulate all components of the beams, including the materials and interfaces. The proposed bond-slip models in chapter 3 were implemented in the FE models so as to represent the degradation in bond. The models predict the tests well for exposed beams of all types.

Chapter 5 introduces the effects of sustained load on the FRP-strengthened RC beams. Two variables were evaluated herein, which were the load level and the type of FRP composites. The loading set-up and test procedures are described accordingly. Both the time-dependent behavior and the load capacity of beams are described and discussed. An FE model was developed to simulate the time-dependent behavior of beams, and the results and findings are discussed as well.

Chapter 6 gives a general summary for conclusions drawn from previous chapters. Limitations of present study are mentioned in this chapter, and the on-going experiment and recommendations for future study are described accordingly.

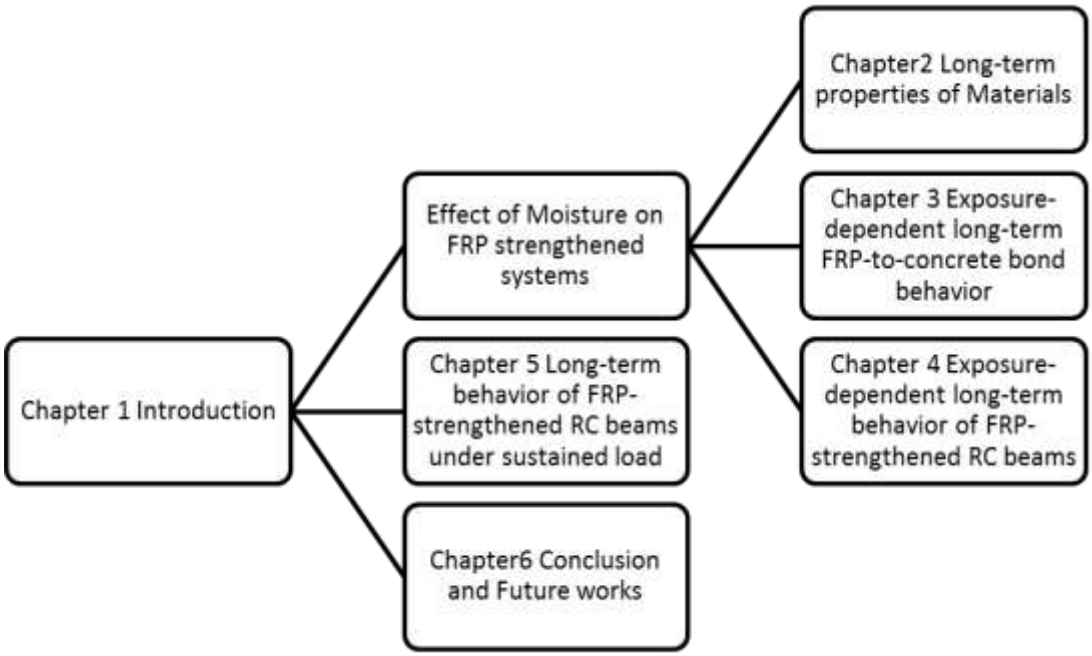

Figure 1-2 Organization of the thesis

CHAPTER 2

EXPOSURE-DEPENTDENT LONG-TERM PROPERTIES OF MATERIALS

2.1 INTRODUCTION

In practice, the FRP-to-concrete interfaces generally consist of five parts: (a) the concrete layer; (b) FRP composites; (c) resins between the concrete and FRP composite and (d) two interfaces between them (Figure 1-1). The mechanical properties of these materials composing the FRP-to-concrete interfaces play an important role in FRP-strengthened RC structures. The strength of concrete layer is generally most critical since most of the failure of a FRP-to-concrete interface occurred in the concrete layer. In addition, many researchers reported that the stiffness of FRP composites affect the sufficient shear stress transfer length (e.g., Dai et al. 2010) and effective bond length (Chen and Teng 2001). Also, since the resin layer transfers the shear stress between concrete and FRP composites so that they work as a composite section, the stiffness and toughness of the resin are important issues controlling the bond behavior. There is no doubt that variations in properties of components induced by environmental effect in FRP-to-concrete interface can affect its performance accordingly. Therefore, in order to clarify the durability of FRP-to-concrete interface, accurate evaluations of material properties with due consideration of environmental effects must be studied first. This chapter focuses on the exposure-dependent material properties of the material components in FRP-to-concrete interface. In this chapter, the exposure scheme is firstly introduced, after which the material tests are introduced. The specimen preparations and test procedures are introduced by the sequence of concrete, steel reinforcement, FRP composites and epoxy resins. Comparisons of the mechanical properties of materials before

and after exposure are the main focus of the present chapter; in addition, the DMA tests of epoxies are also reported in the ending part of this chapter.

2.2 EXPOSURE SCHEME

Since no established accelerated testing procedure for bond durability suited to the subtropical climate has been found in the existing literature, an appropriate accelerated testing scheme needs to be established for the present project. This scheme has considered the following features of the local climate: (1) The subtropical climate has no extremely low temperature and the recorded highest temperature in Hong Kong is 36 ℃. However, a maximum temperature of around 50 ℃ can be reached for an FRP system bonded to concrete under direct sunlight based on the information given in the Structures Design Manual of the Highways Department of the Hong Kong Government. (2) The annual average humidity in a subtropical area is high at about 82% and the average rainy day per year is about 142, indicating that there is frequent dry and wet cycling. (3) Based on the DMA analysis for epoxies (Section 2.4.3), the glass transition temperature (T_g) of epoxy adhesives used in this study are approximately 60 ℃ (Table 2-11). Some researchers reported that if the adhesives are exposed in a much higher temperature than the T_g, irreversible damage is likely to occur in the interface (Bai *et al.* 2012). Considering these features, the proposed exposure scheme for use in the present project consists of submergence in 40 ℃ sea water for 16 hours and exposure in 40 ℃ dry air for 32 hours in each cycle (Figure 2-1). Heated air ventilation was used to dry the specimens more efficiently. It was observed that the proposed accelerated exposure scheme enabled the specimens to dry and wet efficiently in each cycle; the moderately high temperature adopted accelerated the diffusion of moisture while avoiding changing the material degradation mechanisms. An environmental chamber was built to conduct the exposure cycling (Figure 2-2).

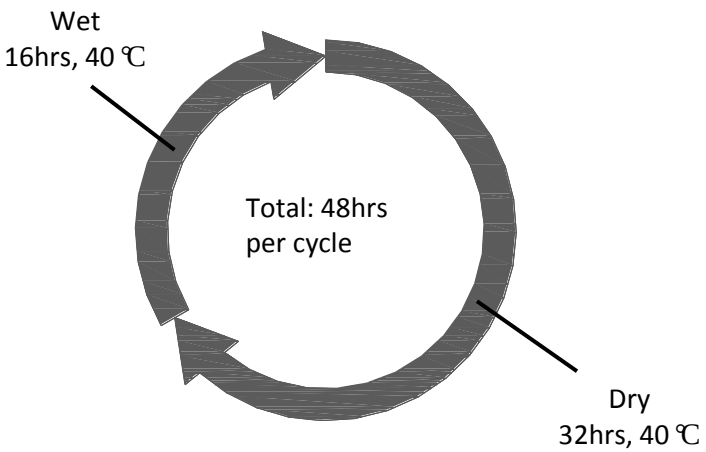

Figure 2-1 Wet-dry cycles in accelerated laboratory tests

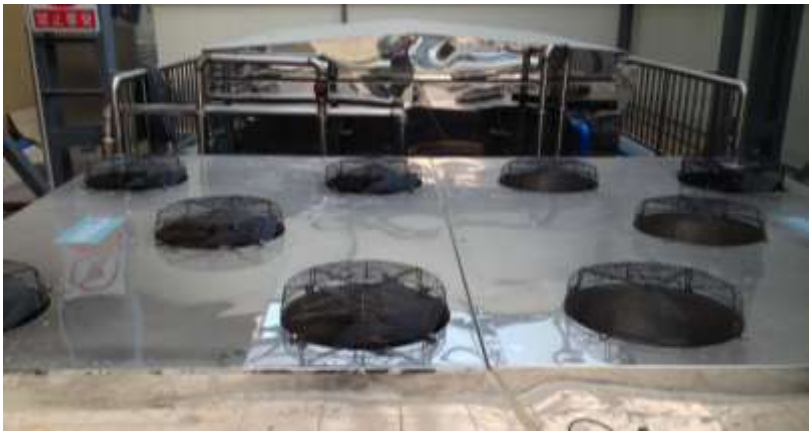

Figure 2-2 Environmental chamber consisting of heated water tanks and air ventilations

2.3 MATERIAL PROPERTY TESTS

In this study, a long-term experiment project was designed which lasts as long as 144 months. The material specimens, FRP bonded concrete joints and FRP-strengthened RC beams were subjected to different environmental exposure schemes. There were totally 10 groups of specimens in terms of exposure period: five groups for accelerated laboratory tests (0, 8, 12, 18 and 24-month) and five groups for field exposure tests (24, 36, 60, 96 and 144-month). This chapter mainly introduces the material part.

Notations of the specimen name (e.g., L-GS-8m-1):

The 1st alphabet: exposure scheme. L = accelerated laboratory tests**;** F = field exposure tests;

The 2nd word: specimen type or FRP type in beams and joints, in which GS=GFRP sheet, CS = CFRP sheet, CP = CFRP plate；

The 3rd number: Duration of exposure, e.g., 18m = 18 months; and

The 4th number: Number of the specimen.

2.3.1 Concrete

50 standard concrete test cylinders were cast in the same batch. All the cylinders in the present studies were cast using the ready-mixed concrete. The maximum aggregate size of concrete was 10 mm. The concrete was well cured indoors at 20±2 ℃ for 28 days.

Table 2-1 Information of concrete cylinder specimens for accelerated laboratory tests

Serial No.	Specimen type	Specimen size (mm)	Exposure duration	Quantity
L-Cylinder	Cylinder	Φ150×300	0 month	5
			8 months	5
			12 months	5
			18 months	5
			24 months	5

Table 2-2 Information of concrete cylinder specimens for field exposure tests

Serial No.	Specimen type	Specimen size (mm)	Exposure duration	Quantity
F-Cylinder	Cylinder	Φ150×300	24 months	5
			36 months	5
			60 months	5
			96 months	5
			144 months	5

The concrete compressive strength and Young's modulus were tested using standard cylinders according to ASTM C39/C39M and C469/C469M accordingly. The 7-day strength of concrete was 18.75 MPa, and the 28-day strength of concrete was 40.99 MPa. After 8 months, the concrete strength increased to 43.82 MPa (Table 2-3), which was 6.9% higher

than the 28-day strength of concrete.

Table 2-3 Material properties of concrete

Test time	Specimen No.	Compressive strength *f*c (MPa)		Elastic modulus *E*c (GPa)	
		Test	Avg.	Test	Avg.
7 Day	A	18.75	18.75	/	/
	B	18.76		/	/
28 Day	A	40.9	40.99	22.57	21.29
	B	41.97		20.43	
	C	40.12		20.87	
8 month	A	43.43	43.82	19.93	21.43
	B	44.01		22.62	
	C	44.01		21.76	

2.3.2 Steel reinforcement

Steel reinforcement was installed in the RC beams. Two ribbed steel bars in diameter of 8mm or 10mm were used for the compression or tension reinforcement respectively, while the plain steel bars in diameter of 8mm were used for the stirrups. The mechanical properties of steel bars are listed in Table 2-4. A relatively thick concrete cover was produced in the RC beams to suppress the corrosion of the steel reinforcement since it is not the focus of present study. The half potential method was adopted to monitor the corrosion in steel reinforcement. According to the test results (Table 2-5), the steel bars seem not corroded after 8-month exposure. However, the decrease in the half potential indicated the trend of steel corrosion to some extent.

Table 2-4 Material properties of steel reinforcement

Type	Diameter (mm)	Yielding strength f_y (MPa)	Young's modulus E_s (GPa)
Tension reinforcement	10	419	174
Compressive reinforcement	8	402	176
Stirrups	8	350	177

Table 2-5 Half-cell potential of steel reinforcement in exposed beams

Beam	Half-cell potential (mV; average of five test points along beams)	
	Before exposure	After 8-month exposure
L-CP1-8m	+78	-73
L-CP2-8m	+36	-54
L-CS-8m	-45	-191
L-GS-8m	-44	-99

Note: if potentials over an area are:

(a) >-200mV, greater than 90% probability that no reinforcing steel corrosion is occurring;

(b) -200~-350mV, corrosion activity is uncertain;

(c) <-350mV, greater than 90% probability that corrosion is occurring.

Figure 2-3 Test on half-cell potentials of steel reinforcement in RC beams

2.3.3 FRP composites

Three types of FRP composites were used in the present investigation: (a) CFRP sheet, with a nominal thickness of 0.167mm per layer; (b) GFRP sheet, with a nominal thickness of 0.172mm per layer and (c) CFRP plate with a thickness of 1.2mm (Table 2-6 and Table 2-7). The purpose of using different types of FRP composites was to evaluate the influences of exposure on different types of FRP composites, which can be a practical reference for selection of FRP types in real engineering. Tensile tests were conducted following the procedure in ASTM D3039/D3039M-08. The specimens were designed in dimension of 250mm×25mm (Figure 2-4). The CS and GS coupons were cut from a single-layer CS or GS

sheet formed in a wet lay-up process, while the CP coupons were cut from pultruded CFRP plates directly. When manufacturing the CFRP and GFRP sheets, the fibers were fully infiltrated by well-mixed resin using a brush. The sheets were then placed in a customized glass mold and cured for 7 days.

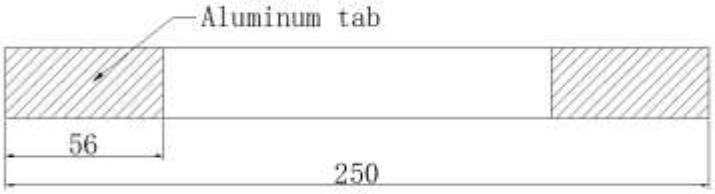

Figure 2-4 Dimension of FRP composite coupons

Table 2-6 Information of FRP specimens for accelerated laboratory tests

Serial No.		Specimen type	Specimen size	FRP type	Adhesive type	Exposure duration	Quantity
L-GS	L-GS-0m	FRP coupons	250×25	GFRP sheet	Sika330	0 month	8
	L-GS-6m					8 months	8
	L-GS-12m					12 months	8
	L-GS-18m					18 months	8
	L-GS-24m					24 months	8
L-CS	L-CS-0m	FRP coupons	250×25	CFRP sheet	SW-3C	0 month	8
	L-CS-6m					8 months	8
	L-CS-12m					12 months	8
	L-CS-18m					18 months	8
	L-CS-24m					24 months	8
L-CP	L-CP-0m	FRP coupons	250×25	CFRP plate		0 month	8
	L-CP-6m					8 months	8
	L-CP-12m					12 months	8
	L-CP-18m					18 months	8
	L-CP-24m					24 months	8

Table 2-7 Information of FRP specimens for field exposure tests

Serial Number		Specimen type	Specimen size	FRP type	Adhesive type	Exposure duration	Quantity
F-GS	F-GS-18m	FRP coupons	25×250	GFRP sheet	Sika330	18 months	8
	F-GS-36m					36 months	8
	F-GS-60m					60 months	8
	F-GS-96m					96 months	8
	F-GS-144m					144 months	8
F-CS	F-CS-18m	FRP	25×250	CFRP sheet	SW-3C	18 months	8

	F-CS-36m	coupons				36 months	8
	F-CS-60m					60 months	8
	F-CS-96m					96 months	8
	F-CS-144m					144 months	8
F-CP	F-CP-18m	FRP coupons	25×250	CFRP plate		18 months	8
	F-CP-36m					36 months	8
	F-CP-60m					60 months	8
	F-CP-96m					96 months	8
	F-CP-144m					144 months	8

After being exposed in the chamber for 8 months, the coupons were tested at a speed of 2mm/min. For each type of specimen, at least five identical coupons were tested. The test data were regarded improper and removed if the following were observed: (a) obvious defects in specimens; (b) tabs slipped during loading and (c) failure occurred inside the tab area or the plate split during loading. Both the original and exposed mechanical properties are listed in Table 2-8.

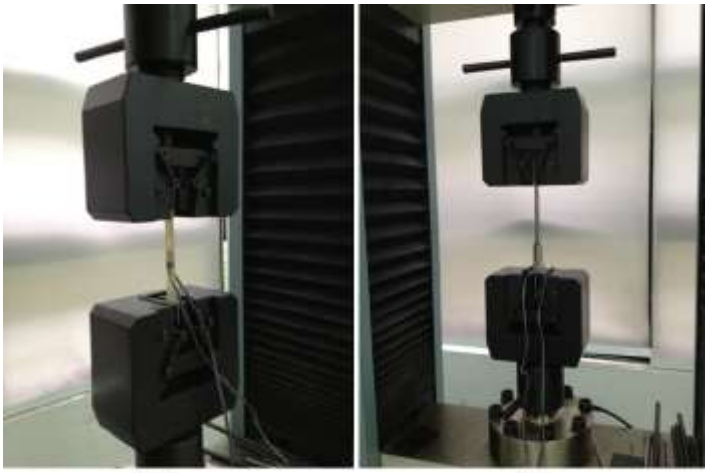

Figure 2-5 Coupon tensile tests: (a) resin (b) FRP composites

(a-1) (a-2)

Figure 2-6 Failure of CFRP sheet coupons: (a) 0-month (b) 8-month

(b-1) (b-2)

Figure 2-7 Failure of GFRP sheet coupons: (a) 0-month (b) 8-month

(c)

Figure 2-8 Failure of FRP specimen (a-1) CS-0m (a-2) CS-8m (b-1) GS-0m (b-2) GS-8m (c) CP-8m

Table 2-8 Material properties of FRP composites

Coupon	Tensile strength f_{frp} (MPa)		Young's modulus E_{frp} (GPa)		Ultimate strain ε_{frp}	
	Test	Avg.	Test	Avg.	Test	Avg.
CS-0m-1	4659.61	4584.78	255	236	1.53%	1.59%
CS-0m-2	4899.07		233		1.63%	
CS-0m-3	4779.79		230		1.73%	
CS-0m-4	4319.91		233		1.56%	
CS-0m-5	4265.51		229		1.52%	
CS-8m-1	4763.63	4859.80	261	239	1.74%	1.93%
CS-8m-2	4951.08		228		1.97%	
CS-8m-3	4249.96		212		1.97%	
CS-8m-4	5046.83		231		1.99%	
CS-8m-5	5287.50		265		1.99%	
GS-0m-1	1530.29	1552.31	113	113	1.49%	1.45%
GS-0m-2	1561.45		114		1.47%	
GS-0m-3	1541.79		117		1.13%	
GS-0m-4	1510.29		104		1.63%	
GS-0m-5	1617.74		117		1.54%	
GS-8m-1	951.16	793.72	121	121	0.82%	0.71%
GS-8m-2	795.32		124		0.84%	
GS-8m-3	924.16		118		0.84%	
GS-8m-4	514.20		122		0.41%	
GS-8m-5	783.77		120		0.66%	
CP-0m-1	2402.77	2398.29	178	167	1.68%	1.61%
CP-0m-2	2390.28		162		1.59%	
CP-0m-3	2398.34		164		1.62%	
CP-0m-4	2415.63		168		1.65%	
CP-0m-5	2384.45		162		1.49%	
CP-8m-1	2697.61	2693.95	161	161	1.64%	1.61%
CP-8m-2	2799.54		162		1.63%	
CP-8m-3	2704.58		162		1.57%	
CP-8m-4	2762.51		160		1.68%	
CP-8m-5	2505.49		160		1.51%	

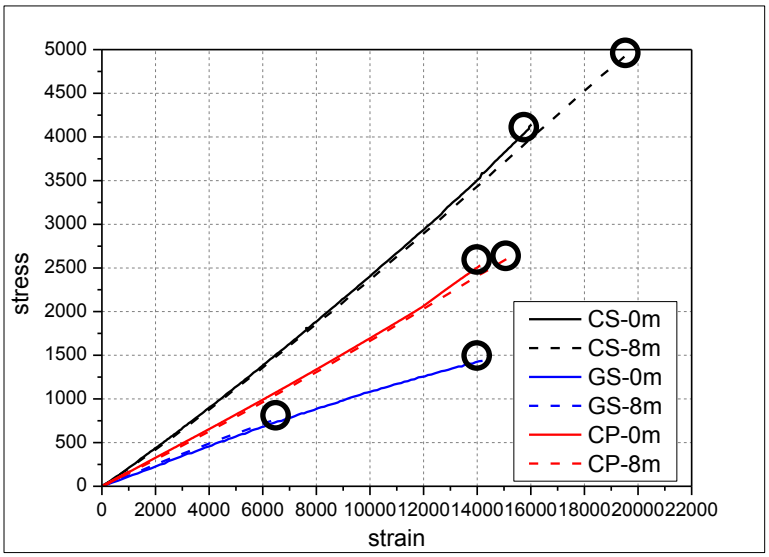

Figure 2-9 Strain-stress responses of FRP composites

According to the tensile tests, the CFRP sheets and CFRP plates obtained a 6.0% and 12.3% higher ultimate strength, respectively, while the Young's modulus remained almost the same after exposure. On the contrary, the ultimate strength of GFRP sheets decreased by 48.9%, showing very severe degradation in GFRP composites. Such changes of GFRP sheets properties have affected the performance of FRP-to-concrete interface.

2.3.4 Epoxies

Based on the recommendations of the manufactures, several commercial epoxy adhesives were used for the different types of FRP composites: SW-3C for CFRP sheets, Sika330 for GFRP sheets, and Sika30 and Araldite106 for CFRP plate (Table 2-9). The properties of epoxies are listed in Table 2-10. The purpose of using two types of epoxy for CFRP plates was to compare the contribution of adhesive stiffness on the behavior of the FRP-to-concrete interface. Tensile tests for epoxy specimens followed the procedure in ASTM D638-10. Stainless steel frames were custom-made to cast the epoxy coupons into standard shapes (Figure 2-10). All of the epoxy adhesives were cured indoors at an ambient temperature of 20±2 ℃ for 7 days.

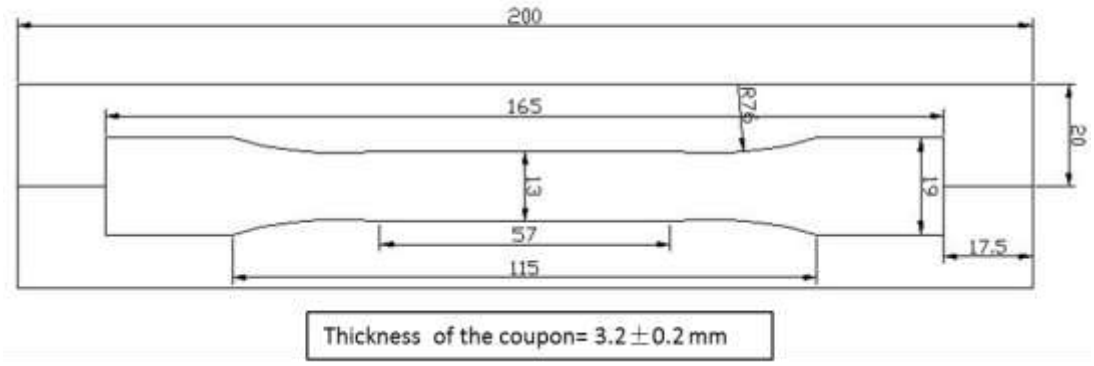

Figure 2-10 Dimension of adhesive coupons and molds (ASTM 638-10, thickness: 3.2mm)

Table 2-9 Information of epoxy specimens for accelerated laboratory tests and field exposure tests

Serial No.	Specimen No.	Exposure duration	Quantity	Serial number	Serial No.	Exposure duration	Quantity
L-SW3C (for CFRP sheet)	L-SW3C-0m	0 month	8	F-SW3C (for CFRP sheet)	F-SW3C-18m	18 months	8
	L-SW3C-6m	8 months	8		F-SW3C-36m	36 months	8
	L-SW3C-12m	12 months	8		F-SW3C-60m	60 months	8
	L-SW3C-18m	18 months	8		F-SW3C-96m	96 months	8
	L-SW3C-24m	24 months	8		F-SW3C-144m	144 months	8
L-Sika330 (for GFRP sheet)	L-Sika330-0m	0 month	8	F-Sika330 (for GFRP sheet)	F-Sika330-18m	18 months	8
	L-Sika330-6m	8 months	8		F-Sika330-36m	36 months	8
	L-Sika330-12m	12 months	8		F-Sika330-60m	60 months	8
	L-Sika330-18m	18 months	8		F-Sika330-96m	96 months	8
	L-Sika330-24m	24 months	8		F-Sika330-144m	144 months	8
L-Sika30 (for CFRP plate)	L-Sika30-0m	0 month	8	F-Sika30 (for CFRP plate)	F-Sika30-18m	18 months	8
	L-Sika30-6m	8 months	8		F-Sika30-36m	36 months	8
	L-Sika30-12m	12 months	8		F-Sika30-60m	60 months	8
	L-Sika30-18m	18 months	8		F-Sika30-96m	96 months	8
	L-Sika30-24m	24 months	8		F-Sika30-144m	144 months	8
L-Aral106 (for CFRP plate)	L-ARAL106-0m	0 month	8	F-Aral106 (for CFRP plate)	F- Aral106-18m	18 months	8
	L-ARAL106-6m	8 months	8		F- Aral106-36m	36 months	8
	L-ARAL106-12m	12 months	8		F- Aral106-60m	60 months	8
	L-ARAL106-18m	18 months	8		F- Aral106-96m	96 months	8
	L-ARAL106-24m	24 months	8		F- Aral106-144m	144 months	8

Table 2-10 Material properties of epoxy adhesives

Types of adhesives	SW-3C	Sika330	Sika30	Araldite 106
Purpose	CFRP sheet	GFRP sheet	CFRP plate	CFRP plate
Viscosity(mPas/25℃)	6000	6000	<1000	30000
Density(kg/l)	1.65	1.3	1.65	/
Resins/hardener by weight	2:1	4:1	3:1	10:8
Pot life (min)	25	90	90	100

Setting time (hrs/20 ℃)	3	12	12	10
Glass transition temperature Tg (℃)	64.92	62.09	60.33	60.14

Note: the data above were provided by the manufactures except the glass transition temperatures tested by the writer using DMA.

After being exposed in the chamber for 8 months, the coupons were tested using the same test instrument at a speed of 2mm/min. For each type of epoxy, at least five coupons were tests. Improper test results were ignored if there were defects in specimens or coupons failed in anchoring zone. The mechanical properties of epoxy adhesives are listed in Table 2-11. It can be seen that after curing for 8 months, all types of epoxy coupons gained a higher ultimate strength, while the Young's modulus did not change. It is believed that the high temperature used in the exposure scheme has accelerated the chemical reaction in epoxies, which is known as the post curing effect.

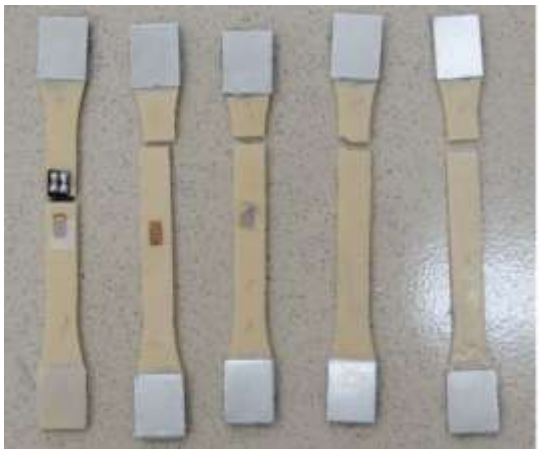

(a-1)

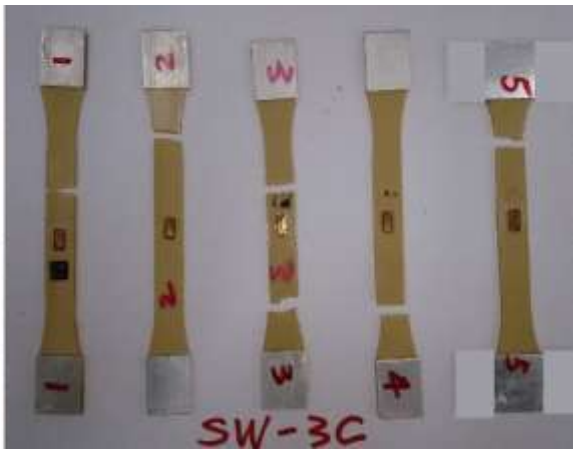

(a-2)

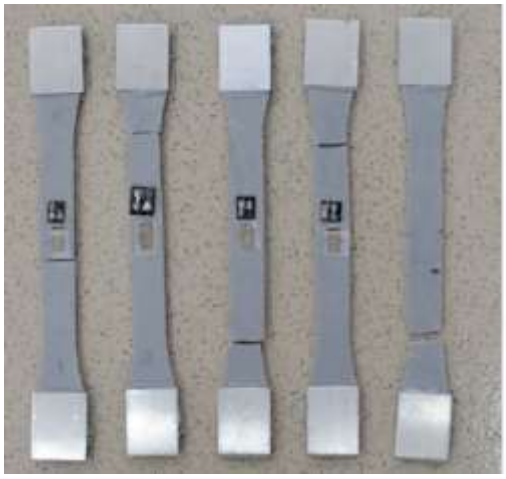

(b-1) (b-2)

(c-1) (c-2)

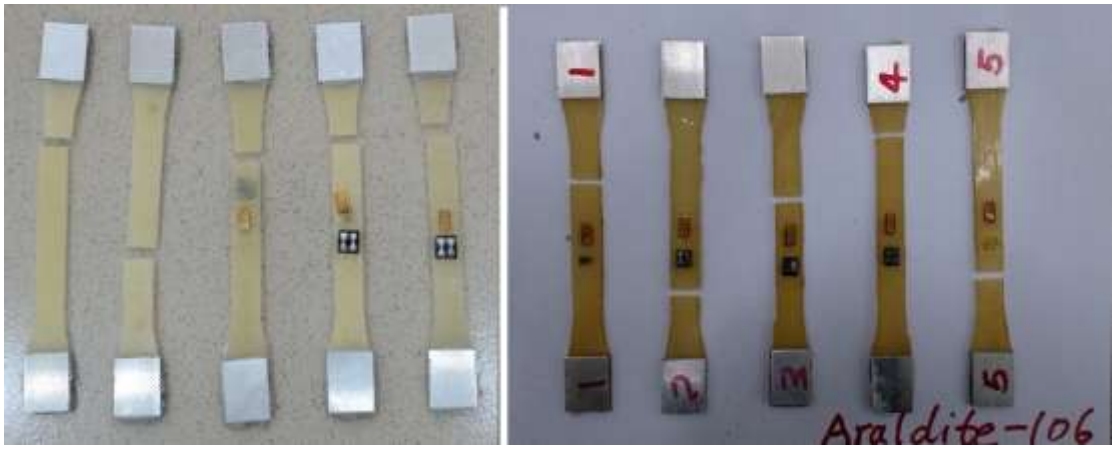

(d-1) (d-2)

Figure 2-11 Failure of epoxy coupons (a-1) SW3C-0m (a-2) SW3C-8m (b-1) Sika330-0m (b-2) Sika330-8m (c-1) Sika30-0m (c-2) Sika30-8m (d-1) Aral106-0m (d-2) Aral106-8m

Table 2-11 Mechanical properties of epoxy adhesives before and after exposure

Epoxy		0-month				8-month			
		Tensile strength f_a (MPa)		Young's modulus E_a (GPa)		Tensile strength f_a (MPa)		Young's modulus E_a (GPa)	
		Test	Avg.	Test	Avg.	Test	Avg.	Test	Avg.
3C	1	32.0	36.5	2.33	2.49	59.9	50.34	3.08	2.90
	2	41.5		2.45		50.0		3.14	
	3	38.0		2.49		39.8		2.62	
	4	40.2		2.59		52.5		2.87	
	5	32.9		2.36		49.4		2.98	
	6	34.3		2.69		/	/	/	/

Sika-330	1	35.2	30.9	4.02	4.27	41.1	43.5	4.39	4.65
	2	28.7		4.11		46.0		4.22	
	3	33.2		3.96		41.4		4.60	
	4	28.0		4.05		45.5		6.26	
	5	28.1		4.18		43.7		3.78	
	6	32.2		5.29		/	/	/	/
Sika-30	1	14.8	16.2	12.73	11.40	19.7	24.7	12.91	11.09
	2	16.5		11.69		26.9		10.48	
	3	17.8		11.24		24.3		11.56	
	4	16.2		9.90		23.8		10.40	
	5	16.2		10.52		28.9		10.12	
	6	15.6		12.30		/	/	/	/
Araldite-106	1	24.1	24.4	0.88	0.90	24.5	21.2	1.42	1.34
	2	25.2		0.98		21.9		1.31	
	3	24.2		0.95		17.4		1.35	
	4	21.8		0.89		20.3		1.26	
	5	26.8		0.79		22.1		1.34	

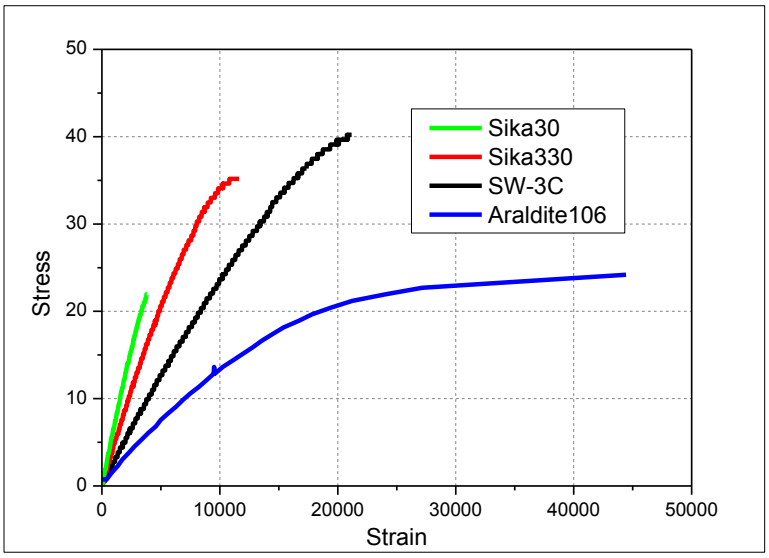

Figure 2-12 Strain-stress responses of epoxy

Glass transition temperatures (T_g) of epoxies were evaluated. The Dynamic Mechanic Analysis (DMA) method was adopted for the tests and the guideline ASTM E1640-09 was followed in this study. The specimens were cut into rectangular shapes between 1×5×20 and 1×10×20 mm to satisfy the load capacity of the analyzer (Figure 2-13) and strain amplitude

requirement of the guideline. No sawing or heating was applied on the specimens during preparations in order to avoid changing the heat history of the specimens. In the test, specimens were anchored in tension mode in the oven with a nitrogen environment. Mechanical oscillation at a fixed frequency of 1Hz was applied on the specimens, and the oven was heated at the fixed rate of 1 ℃ per minute from 20 ℃ to 100 ℃. The changes in the viscoelastic response of the materials were monitored as a function of temperature. The glass transition region was marked by a rapid decrease in storage modulus and a rapid increase in the loss modulus and tangent delta. The value of T_g can then be indicated by the peak of the tangent delta (Figure 2-14), which marks the transition from a glassy to a rubbery solid. According to the test results, T_gs of the epoxies were among 60-65 ℃ (Table 2-10).

Figure 2-13 DMA for glass transition temperature (T_g) tests of epoxy

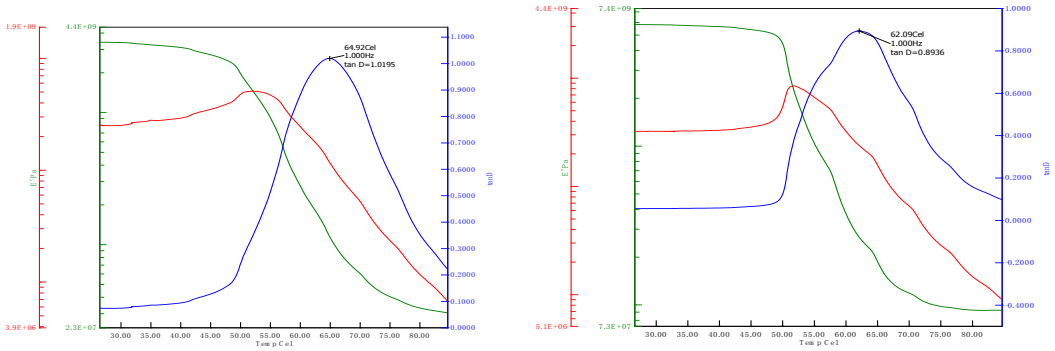

(a) (b)

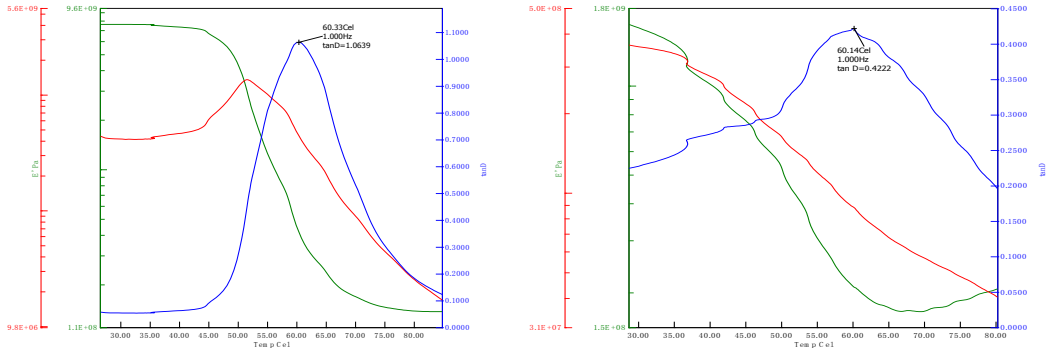

(c) (d)

Figure 2-14 DMA test report of epoxy (a) SW-3c (b) Sika 330 (c) Sika 30 (d) Araldite-106

2.4 CONCLUSIONS

In this durability study, the exposure scheme was designed very carefully. According to DMA analysis on epoxies, the T_g of epoxy adhesives were 60-65 ℃. The temperature of water and air ventilation was set to 40 ℃, 20 ℃ below the T_g of epoxy. The wet-dry cycle consisted of 16-hour sea water submergence and 32-hour drying to simulate the natural subtropical environment. After 8-month exposure, the concrete compressive strength and tensile strengths of CFRP sheets, CFRP plates, experienced a 6.9%, 6.0% and 12.3% increase, while the Young's modulus remained the same. On the contrary, the ultimate tensile strength of the GFRP sheets decreased by 48.9%. The GS composites have already undergone severe degradation in the tensile strength. As for epoxies, the SW-3C, Sika330, Sika30 and Araldite106 obtained 37.9%, 40.8%, 52.4% increase in tensile strength and little change in their stiffness, while the Araldite106 underwent 15.0% decrease in the tensile strength but a 48.9% increase in its stiffness. The test results for epoxies show that the 8-month exposure is beneficial for most of the adhesives due to the post-curing effects except Araldite 106.

CHAPTER 3

LONG-TERM BOND BEHAVIOR OF FRP-TO-CONCRETE INTERFACES

3.1 INTRODUCTION

The properties of bond between FRP and concrete are the key factors controlling debonding failures in FRP-strengthened structures. To represent such phenomenon, in most of the recent existing researches, the study of debonding failures of FRP-strengthened RC members under short-term loading has relied heavily on the understanding and modeling of the basic bond shear stress-slip model (or simply bond-slip model) (e.g., Dai et al. 2005; Lu et al. 2005). Moreover, the power of an accurate bond-slip model in predicting the short-term behavior of FRP bonded concrete joints and FRP-strengthened RC beams has been extensively demonstrated by many researchers in developing FE and simple design models for debonding failures of FRP-to-concrete joints (e.g., Chen and Teng 2001; Dai et al. 2006, Lu et al. 2007) and RC beams strengthened in shear or flexure with bonded FRP systems (e.g., Hollaway and Teng 2008). However, in real engineering, the long-term properties of the materials as well as the interfaces in a FRP-strengthened RC system can be affected largely by environmental conditions (e.g., wet-cry cycles and temperature) and their performances will vary from that of short-term bond behavior. As a result, the long-term interfacial behavior cannot be properly represented by the short-term models without considering weathering effects. According to the above considerations, there is the need to establish a reliable exposure-dependent bond-slip model, in which the weathering effects are considered properly, so that the long-term behavior of bond-critical RC members strengthened with FRP composites can be well predicted.

Existing studies suggest that the main failure mode of FRP-to-concrete joints in bond tests is cracking of concrete under shear which occurs commonly at a few millimeters from the adhesive-concrete interface (Chen and Teng 2001). This is the most acceptable failure mode since failure in concrete means a good cohesion between the concrete and FRP composites. In such cases, therefore, the bond strength of the joint depends significantly on the concrete strength. In addition, due to various reasons (such as the deterioration in materials, the existence of moisture on the interfaces or the poor application quality), the failure may occur in other forms, namely the adhesive failure (failing inside the adhesive), failure in the concrete-resin interface or FRP-resin interface and FRP rupture.

The near-end supported single-lap shear test, which has been widely accepted and applied due to its simplicity and reliability, is adopted herein to measure the bond behavior. The stress state of the interface is similar to that in a shear test specimen in various debonding failure modes. Although the single-lap shear test can be realized in a number of ways with some variations, the results obtained are not dependent on the set-ups strongly if the following basic mechanics are set closely (Chen et al. 2001):(a) bond length; (b) width of FRP plate/sheet; (c) width of concrete prism and (d) free zone length. Moreover, a sufficiently long bond length is helpful to minimize the effect of unintended loading offsets and a sufficiently high support block can help avoid non-interfacial failures (Yao et al. 2004).

Generally, there are two methods of obtaining local stress-slip curves of the FRP-to-concrete interface from a single-lap shear test: (a) from axial strains of the FRP laminate measured with closely spaced strain gauges (e.g., Nakaba et al. 2001); (b) from load-displacement (slip at the loaded end) curve (e.g., Ueda et al. 2003). In the present study, the former method was followed, by which the shear stress of a specific location on the FRP-to-concrete interface can be deduced, while the corresponding slip can be obtained by a numerical integration of the measured axial strains of the plate.

3.2 EXPERIMENT OUTILIE

3.2.1 Design of specimens

An FRP bonded concrete joint specimen in a single-lap shear test consisted of a concrete prism, FRP laminates and the adhesive layer. 120 FRP bonded concrete joints in total were prepared. Amongst the specimens, the dimensions of the concrete prism and FRP laminates (length and width of FRP sheet/plate) were identical (Figure 3-1). The specimens were distinguished by exposure scheme and FRP systems (Table 3-1 and Table 3-2). 60 joints were prepared for accelerated laboratory tests (L series). Another other 60 were for field exposure tests (F series). L series specimens were exposed in an environmental chamber and subjected to accelerated wet-dry cycles in five different durations. The specimens were submerged in 40℃ hot sea water for 16 hours and then exposed to air ventilations for 32 hours in each wet-dry cycle (Figure 2-1). F series specimens were exposed outdoors in a natural subtropical environment in five different durations. Technically it is very hard to estimate the equivalent durations between accelerated lab test and field exposure due to the lack of existed control tests. However, according to reviews of previous study, the degradation of bond in field exposure is much slower than the accelerated lab test, for which reason relatively longer exposure durations were set for field exposure tests in present study. Explanations have been added to the thesis. In each series, four types of FRP-adhesive combinations were adopted, which were 2-layer CFRP sheets (0.167mm for each layer); 2-layer GFRP sheets (0.172mm for each layer); 1-layer CFRP plate (1.2 mm for each layer) bonded with Sika30 or Araldite106. The main difference between two plate adhesives is their stiffness. The Sika30 has a shear modulus of 5 GPa, while the shear modulus of Araldite106 is 1 GPa (section 2.3.4). The purpose of using two different types of epoxy for the FRP plate is to examine whether a more ductile adhesive layer could improve the bond

performance.

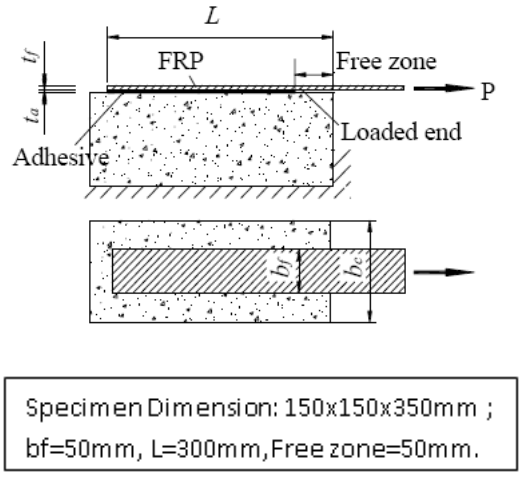

Figure 3-1 Dimension of FRP bonded concrete joints

Table 3-1 Information of FRP bonded concrete joints for accelerated laboratory tests

Serial number		Specimen type	Specimen size	FRP type	Adhesive type	Exposure duration	Quantity
L-**GS:** 3×5	L-**GS**-0m-1,2,3	Bonded joints	150×150×350	**G**FRP **s**heet	Sika330	0 month	3
	L-**GS**-8m-1,2,3					8months	3
	L-**GS**-12m-1,2,3					12 months	3
	L-**GS**-18m-1,2,3					18 months	3
	L-**GS**-24m-1,2,3					24 months	3
L-**CS:** 3×5	L-**CS**-0m-1,2,3	Bonded joints	150×150×350	**C**FRP **s**heet	SW-3C	0 month	3
	L-**CS**-8m-1,2,3					8months	3
	L-**CS**-12m-1,2,3					12 months	3
	L-**CS**-18m-1,2,3					18 months	3
	L-**CS**-24m-1,2,3					24 months	3
L-**CP1**: 3×5	L-**CP1**-0m-1,2,3	Bonded joints	150×150×350	CFRP plate	Sika30	0 month	3
	L-**CP1**-8m-1,2,3					8months	3
	L-**CP1**-12m-1,2,3					12 months	3
	L-**CP1**-18m-1,2,3					18 months	3
	L-**CP1**-24m-1,2,3					24 months	3
L-CP2: 3×5	L-**CP2**-0m-1,2,3	Bonded joints	150×150×350	CFRP plate	Araldite106	0 month	3
	L-**CP2**-8m-1,2,3					8months	3
	L-**CP2**-12m-1,2,3					12 months	3
	L-**CP2**-18m-1,2,3					18 months	3
	L-**CP2**-24m-1,2,3					24 months	3

Table 3-2 Information of FRP bonded concrete joints for field exposure tests

Serial number		Specimen type	Specimen size	FRP type	Adhesive type	Exposure duration	Quantity
F-GS: 3×5	F-GS-18m-1,2,3	Bonded joint	150×150×350	GFRP sheet	Sika330	18 months	3
	F-GS-36m-1,2,3					36 months	3
	F-GS-60m-1,2,3					60 months	3
	F-GS-96m-1,2,3					96 months	3
	F-GS-144m-1,2,3					144 months	3
F-CS: 3×5	F-CS-18m-1,2,3	Bonded joint	150×150×350	CFRP sheet	SW-3C	18 months	3
	F-CS-36m-1,2,3					36 months	3
	F-CS-60m-1,2,3					60 months	3
	F-CS-96m-1,2,3					96 months	3
	F-CS-144m-1,2,3					144 months	3
F-CP1 3×5	F-**CP1**-18m-1,2,3	Bonded joint	150×150×350	CFRP plate	Sika30	18 months	3
	F-**CP1**-36m-1,2,3					36 months	3
	F-**CP1**-60m-1,2,3					60 months	3
	F-**CP1**-96m-1,2,3					96 months	3
	F-**CP1**-144m-1,2,3					144 months	3
F-CP2 3×5	F-**CP2**-18m-1,2,3	Bonded joint	150×150×350	CFRP plate	Araldite106	18 months	3
	F-**CP2**-36m-1,2,3					36 months	3
	F-**CP2**-60m-1,2,3					60 months	3
	F-**CP2**-96m-1,2,3					96 months	3
	F-**CP2**-144m-1,2,3					144 months	3

3.2.2 Specimen preparations

A total of 150 concrete prisms were cast using normal commercial concrete in the same batch. The concrete was well mixed and vibrated after being poured into the wooden frames. All the prisms were cured more than 28 days before FRP sheet/plates were applied. 120 concrete prisms in the best quality were selected. The concrete substrate was firstly grounded with a jet-chisel so that the weak layer composed of cement laitance, loose and friable materials was removed. The grinded surface was then carefully cleaned using high-pressure air so that the surface was laitance and contaminant free and open textured. The free zone of the bonded surface was covered using insulating tapes to prevent excessive adhesive sticking on the substrate (Figure 3-3).

Figure 3-2 Mold frames and concrete prisms for bonded joint tests

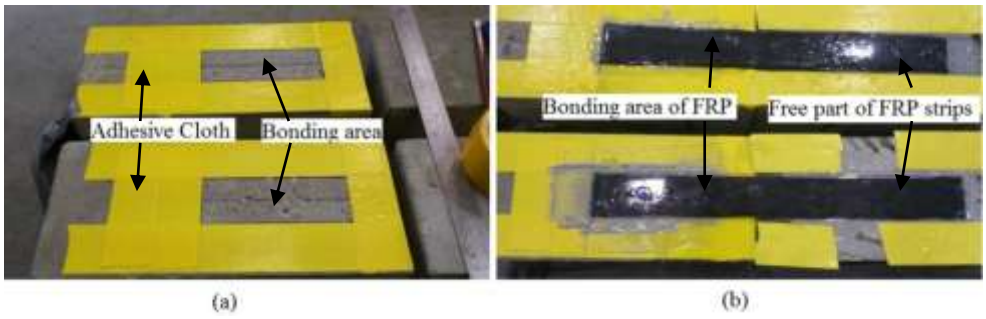

Figure 3-3 Preparation of FRP bonded concrete joints (a) treatment of concrete substrate; (b) applying FRP sheets using wet lay-up method

The procedures of applying the FRP laminates varied according to types of FRP. For CS and CP1, one thin layer of well mixed epoxy primer (SW-3P for CS and Sika 330 for CP1, respectively) was applied on the concrete substrate. The primers used for GS and CP2 were identical to the sheet/plate resins since the resins already had a very ideal viscosity to fill the void on the concrete substrate. CFRP sheets and GFRP sheets were applied using the wet-layup method. The sheets were uniformly impregnated with resins first, and were then applied onto the primer and leveled with a rub roller along the fiber direction. Differently, when the CFRP plates were applied, the plate surface was firstly brushed with sandy paper, solvent wiped and fully dried. The plate surface was then coated with a layer of adhesive in a triangular section shape. Afterwards, the plate was attached onto the concrete substrate and pressed uniformly with a roller to squeeze out excessive adhesive. After one-day curing, insulating tapes and excessive adhesives were removed carefully, so that a clean and regular bond was achieved. The specimens were cured indoors (20±2℃) for more than 7 days before being placed into the chamber or outdoors.

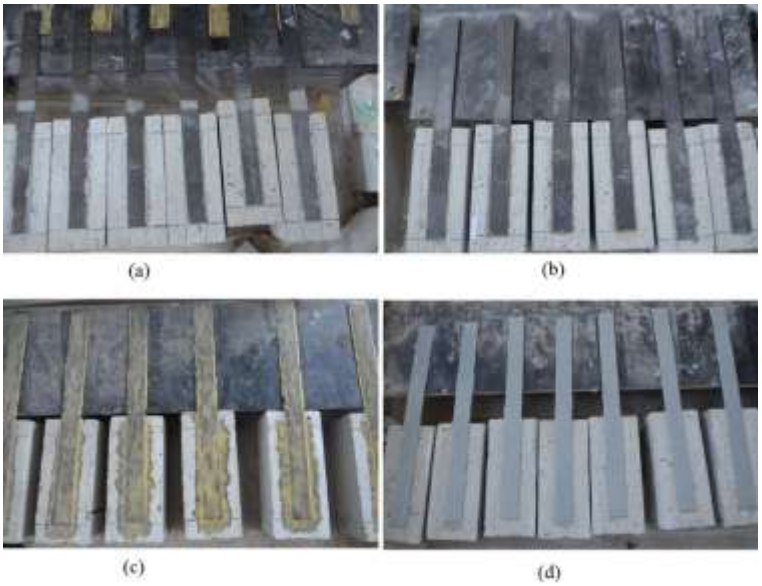

Figure 3-4 FRP bonded concrete joint specimens: (a) CP1 (b) CP2 (c) CS and (d) GS

3.2.3 Test procedure and instrumentation

A steel rig for the single-lap shear test was carefully designed and manufactured to carry out the single-lap shear tests. The instrument consisted of a platform, load head, hydraulic oil jack and load cell (Figure 3-5). Before the specimen was loaded, the alignment was adjusted very carefully so that the direction of the applied force was not only horizontal (Figure 3-7), but also coincided with the centerline of the FRP laminate (Figure 3-8). The load was applied manually using a hydraulic oil jack. The increase of load was monotonic with a constant increment of 25% of the debonding load per minute predicted by Chen and Teng's model (2001). In this way, the loading time of all tests was about 4-6 minutes.

Strain gauges and linear variable displacement transducers (LVDTs) were adopted. Strain gauges of 5mm in gauge length were attached at spacing of 20mm along the centerline of FRP laminate from the loaded end towards the free end (Figure 3-6) for the purpose of obtaining dense and accurate local strain distributions. Another 5mm strain gauge was

attached in the free zone of the laminate, 25mm from the loaded end. Meanwhile, three strain gauges of 5mm in gauge length were installed symmetrically along the transverse direction of FRP laminate at spacing of 15mm and a distance of 150mm from the loaded end to check the load alignment. Apart from strain gauges, two LVDTs were installed on both the loaded end and the free end for displacement monitoring.

Figure 3-5 Loading set-up

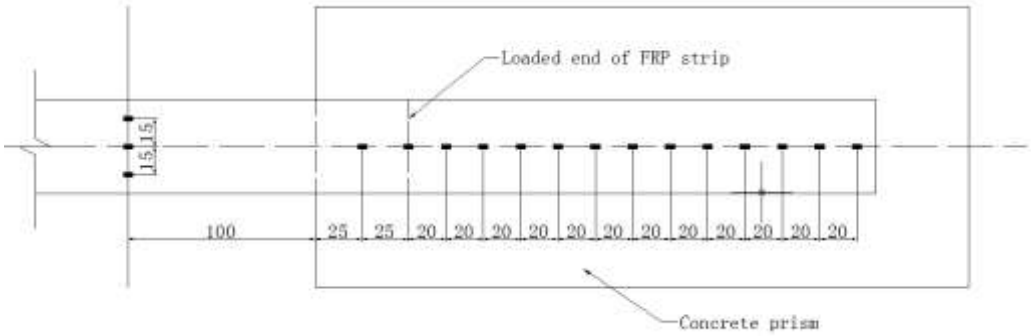

Figure 3-6 Layout of strain gauges on FRP laminates

Figure 3-7 Adjustment of horizonal plane of FRP plates

(a)

(b)

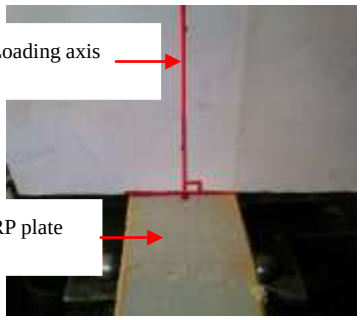

(c)

(d)

Figure 3-8 Adjustment of loading axis: (a) laser calibrator; (b) free end of the FRP laminate; (c) loaded end of the FRP laminate; (d) reaction plate of oil jack

3.3 EXPERIMENTAL OBSERVATIONS

Due to very long durations of the proposed experiments and limited time for the master study, 0-month and 8-month accelerated laboratory tests were completed so far. For simplicity, all the 0-month and 8-month specimens mentioned in the rest of present chapter refer to accelerated laboratory tests unless otherwise noted.

3.3.1 Strain evolutions in FRP during exposure

Strains in different types of FRP laminates were monitored using FBG fiber optic sensors during environmental exposure. The sensors were applied indoors at room temperature (20 ℃). The fiber optic sensors were attached on the FRP laminates at spacing of 50mm. Details of the installation procedures of FBG sensors will be introduced in chapter 5. When the specimens were monitored after being exposed for 4 months, residual strains were discovered in the FRP laminates (Figure 3-9). When the joints were submerged in heated water, different thermal expansions occurred in FRP laminates and concrete due to the thermal incompatibility of these two materials. The thermal expansion of FRP composites was larger than that of concrete under the same temperature, but the cohesive interaction impeded the relative slip between FRP laminates and concrete. As a result, interfacial stress was induces and the strains in FRP distributed in an arched shape. Because the interfacial bond stress-slip was nonlinear, strains in FRP induced by the heat expansion could not fully recover to the original state although the temperature was dropped to original state. Therefore, the residual strains remained as observed in the specimens after exposure.

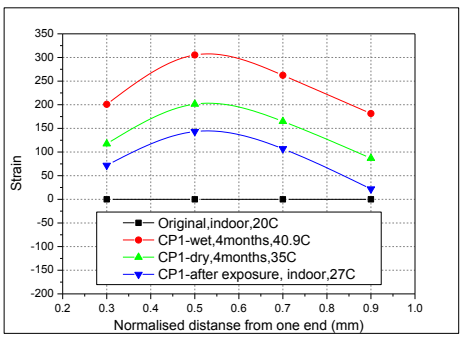

(a)

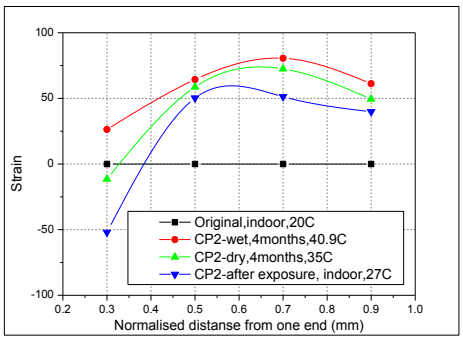

(b)

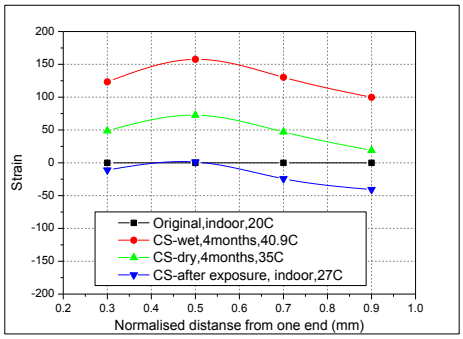

(c)

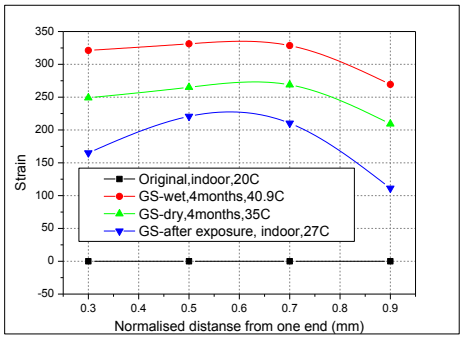

(d)

Figure 3-9 Strain variations in FRP laminates during exposure in different specimens (a) CP1 (b) CP2 (c) CS and (d) GS

3.3.2 Failure modes of FRP bonded concrete joints

For the FRP-to-concrete interface under single-lap shear test, there are several types of failure modes (Chen and Teng, 2001): (a) Concrete failure; (b) FRP sheet fracture; (c) Concrete-to-adhesive interface failure; (d) Adhesive failure; (e) Deamination in FRP sheets and (f) FRP-to-adhesive interface failure. In the present tests, all of the failure modes were observed except the concrete-to-adhesive interface failure, which only exists theoretically. Figure 3-24 in the appendix illustrates the failure modes of all tested specimens.

Amongst the tested specimens, the most often observed failure was the concrete failure (Figure 3-10). Specimens CS, GS-0m, CP2-0m, CP1-0m-2 and CP1-8m failed in this mode (Figure 3-10). The failure process started with visible concrete cracking near the loaded end of the concrete prism. Surface cracks in concrete were observed on both sides of FRP laminates, with an angle of 45 degree to the longitudinal axis of the FRP laminate. As the load increased, the FRP laminate initiated to debond from cracked concrete at the loaded end. The cracks then propagated towards the far end of the FRP laminate, which led to a complete brittle debonding. The thickness of the debonded concrete layer varied between 1mm and 5mm, and the surface of concrete was very uneven.

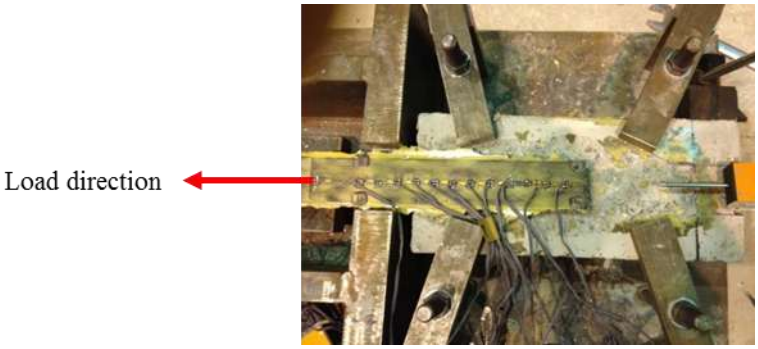

Figure 3-10 Concrete failure

In addition, adhesive failure occurred in specimen CP1-0m-1 and CP1-0m-3 (Figure 3-11). The debonding initiated by delamination between the plate resin and the primer at the loaded end; however, the debonding surface partly propagated into the concrete layer as load increased. This might be caused by the insufficient curing and large difference in stiffness between the resin and primer. When the joint was loaded, high stress concentration was induced between the primer and resin. As a result, delamination of the adhesives occurred instead of concrete cracking. Interestingly, the bond strengths in these two specimens were even larger than CP1-0m-2 specimen which failed in concrete, indicating that the interface provided very good load capacity despite the adhesive failure.

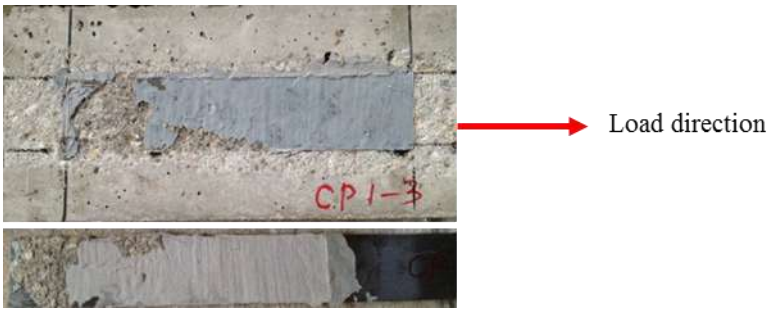

Figure 3-11 Adhesive failure

Combined plate delamination and plate-adhesive delamination occurred in all of CP2-8m

specimens (Figure 3-12) which is very different from CP2-0m's concrete failure. A thin layer of FRP laminate delaminated from the plate when debonding. Apparent plate-adhesive delamination could be observed as well. Such large change in failure mode indicated that the interface has degraded during exposure. The cohesion between the FRP and resin has been weakened. However, no reduction in bond strength of CP2-8m was found.

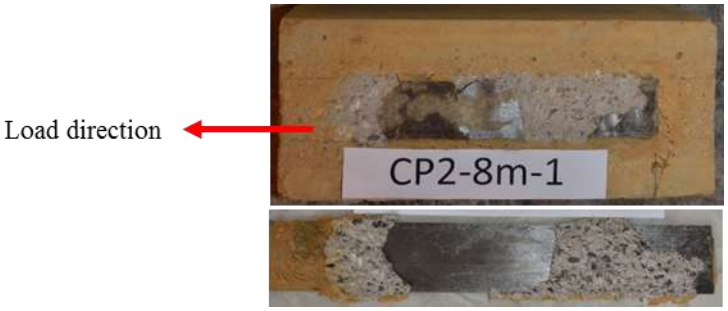

Figure 3-12 Combined plate-adhesive interface debonding and FRP delamination

In GS-8m, FRP sheets fractured instead of debonding when being loaded (Figure 3-13). As described in Section 2.3.3, the ultimate strength of the GFRP laminate decreased by 49% after 8-month exposure. Such degradation in GFRP composites directly affected the failure mode of the joints.

Figure 3-13 FRP sheet fracture

Plate splitting occurred due to poor alignment in the specimen CP2-0m-1 (Figure 3-14). The

FRP plate was split into two parts along the longitudinal direction while being loaded. The imbalance of load distribution in the section induced one part of the FRP debonding prematurely. The ultimate load was obviously lower than the bond strength of specimens failing in concrete since only half part of the bond was in service. Considering these features, the test results were ignored in the following analysis.

Figure 3-14 Plate splitting due to eccentric loading

In addition, FRP-adhesive interfacial premature failure was observed in a trial test (Figure 3-15). The main reason of such failure was improper treatment of the FRP surface which led to insufficient cohesion between the adhesive and FRP plate. The load capacity of such joint was extremely small (less than 1 kN). By abrading the polished surface using sandy papers with 240# sandy paper and solvent-wiping and fully drying the plate, such premature could be suppressed.

Figure 3-15 Plate-adhesive failure due to improper surface treatment

3.4 ANALYTICAL OBSERVATIONS

3.4.1 Ultimate bond strength and debonding strains

The ultimate bond strengths are listed in Table 3-3. Variations in bond strength are observed, which were 4.13 kN (13.7%) and 0.72 kN (2.8%) increase in CP1 and CP2, while 0.86 kN (3.2%) and 2.39 kN (16.4%) decrease in CS and GS, respectively. It indicates that the exposure has improved the CP1's bond strength largely; however the influences on CP2 and CS were not that apparent. The GFRP composites suffered great loss in tensile strength (48.9%) after exposure, which led to the inferior ultimate load of the specimens due to FRP fracture, and thus the bond strength could not be acquired.

Table 3-3 Results of single-shear pullout tests

Specimen	$E_f t_f$	A(με)		B(mm^{-1})		G_f (N/mm)		P_{max} (kN)			$P_{pre.}/P_{exp.}$	Slip (mm)			$S_{pre.}/s_{exp.}$	Failure mode
	kN/mm		Avg.		Avg.		Avg.	Exp.	Avg.	Pre.		$s_{exp.}$	$s_{exp.avg.}$	$S_{pre.}$		
CP1-0m-1	198	3190	3110	10.57	12.30	0.987	0.938	30.94	30.16	30.39	1.01	0.527	0.494	0.470	0.95	AF
CP1-0m-2	198	3004		13.47		0.875		29.14				0.387				CF
CP1-0m-3	198	3134		12.86		0.953		30.4				0.569				AF
CP1-8m-1	198	3863	3535	9.03	9.52	1.448	1.217	37.47	34.29	34.43	1.00	0.376	0.472	0.533	1.13	CF
CP1-8m-2	198	3327		10.94		1.074		32.27				0.461				CF
CP1-8m-3	198	3415		8.59		1.131		33.12				0.580				CF
CP2-0m-1	198	\	2683	\	12.72	\	\	25.5	25.85	26.1	1.01	\	0.371	0.404	1.09	PS
CP2-0m-2	198	2717		11.49		0.716	0.698	26.35				0.423				CF
CP2-0m-3	198	2650		13.95		0.681		25.7				0.319				CF
CP2-8m-1	198	\	2745	\	7.53	\	0.732	26.45	26.57	24.76	0.93	\	0.349	0.380	1.09	AF
CP2-8m-2	198	2829		6.39		0.776		27.44				0.342				AF
CP2-8m-3	198	2661		8.67		0.687		25.81				0.355				AF
CS-0m-1	81.5	6793	6766	4.12	6.73	1.834	1.821	27	26.89	27.03	1.01	0.878	1.089	1.055	0.97	CF
CS-0m-2	81.5	6997		9.69		1.946		27.81				1.260				CF
CS-0m-3	81.5	6509		6.37		1.684		25.87				1.130				CF
CS-8m-1	81.5	6519	6550	8.12	8.20	1.689	1.717	25.91	26.03	26.28	1.01	1.054	0.931	1.040	1.12	CF
CS-8m-2	81.5	5895		10.37		1.381		23.43				0.846				CF
CS-8m-3	81.5	7236		6.12		2.081		28.76				0.892				CF
GS-0m-1	25.99	7261	7736	17.36	16.58	0.995	1.133	13.7	14.60	14.72	1.01	1.480	1.621	1.270	0.78	CF
GS-0m-2	25.99	8305		15.67		1.301		15.67				1.929				CF
GS-0m-3	25.99	7642		16.70		1.102		14.42				1.453				CF
GS-8m-1	25.99	\	\	\	\	\	\	10.37	12.21	\	\	0.041	0.157	\	\	FF
GS-8m-2	25.99	\		\		\		12.35				\				FF
GS-8m-3	25.99	\		\		\		13.91				0.273				FF

Note: a) E_f=Elastic modulus of FRP; t_f=thickness of FRP; A, B= parameters in Dai et al. (2005)'s model; τ_{max}=maximum bond stress; s_{max}=slip corresponding to the maximum bond stress; P_{max}=ultimate load;

CF=cohesive failure; AF=adhesive failure; PS=plate splitting; FF=FRP fracture b) Data marked as '\' are ignored due to specific failure of specimens.

The bond strengths and debonding strains are illustrated as the function of FRP stiffness $E_f t_f$ in Figure 3-16 and Figure 3-17. The ultimate load had a positive correlation with the FRP stiffness; on the contrary, the debonding strain in FRP descended as the FRP stiffness increased. According to Dai et al. (2005), the bond strength can be denoted by the following equation:

$$P_{\max} = b_f \sqrt{2E_f t_f G_f} \qquad \text{(eq. 3-1)}$$

Eq. 3-1 indicates that the FRP stiffness is very important variable to describe the FRP's contribution on the FRP-to-concrete interface regardless of the type or the Young's modulus of the FRP materials. The figures interpreted the relationship between bond strength and FRP stiffness properly.

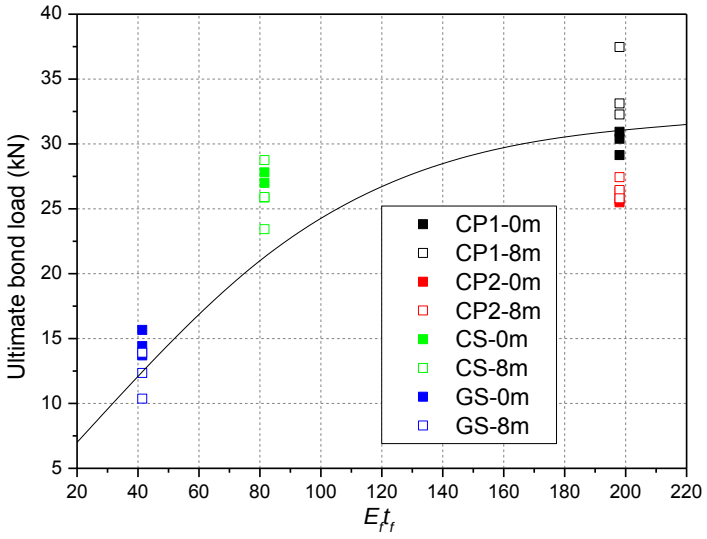

Figure 3-16 Ultimate bond strength vs FRP stiffness

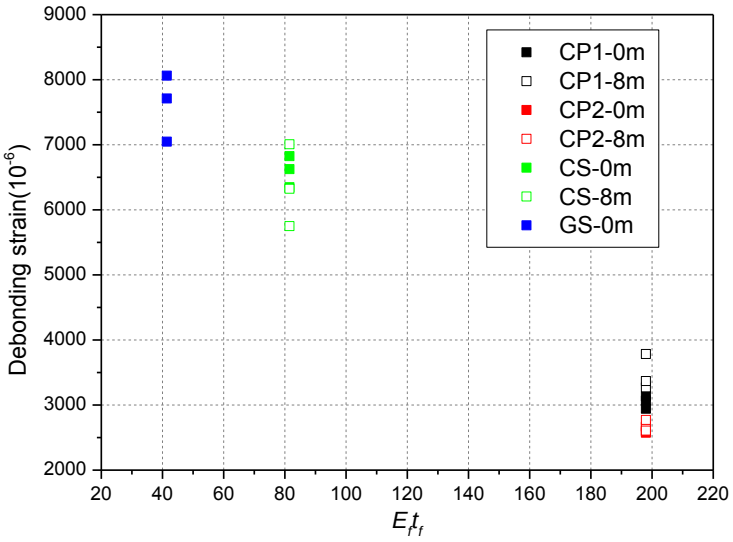

Figure 3-17 FRP debonding strain vs FRP stiffness

The test bond strengths were predicted using Teng and Chen (2001)'s model. Comparisons are illustrated in Figure 3-18. Good agreement was found for GS, CP1 and CP2, while the predicted results of CS are relatively conservative. Moreover, because of the difference in FRP stiffness, the ratio of effective bond length to the whole bond length varied. Since there is no exposure-dependent parameter indicating the environmental effects in the Teng and Chen's model, the strength variations after exposure cannot be predicted.

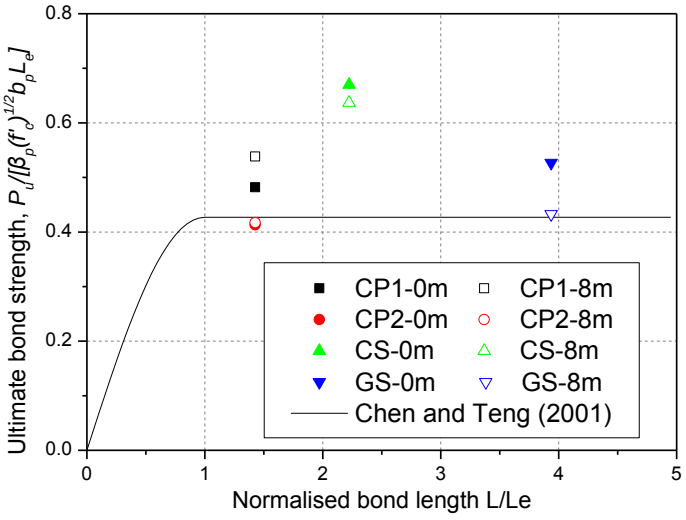

Figure 3-18 Bond strengths vs bond length

3.4.2 Bond-slip relationships of FRP-to-concrete interfaces

3.4.2.1 Theoretical background

According to Dai et al. (2005), the strain-slip response at the loaded end of the FRP laminate can be represented by the following equation:

$$\varepsilon = f\left[\delta(x)\right] = A\left(1-e^{-B\delta(x)}\right) \qquad \text{(eq. 3-2)}$$

where A and B are two parameters which can be determined by regression analysis from a bonded joint test. The physical meaning of A is the maximum strain in FRP if the bond length is longer than the effective bond length. B controls the shape of the bond stress-slip curve. A large parameter B denotes a brittle bond-slip curve in which the ascending and descending path is steeper. Noting that

$$\tau = \frac{E_p t_p}{(1+\alpha)} \frac{d\varepsilon(x)}{dx} \qquad \text{(eq. 3-3)}$$

and

$$\varepsilon(x) = \frac{d\delta(x)}{dx} \qquad \text{(eq. 3-4)}$$

in which $\alpha = E_p t_p b_p / E_c t_c b_c$, b_p and t_p= width and thickness of the FRP laminate; b_c and t_c = width and thickness of the concrete prism; and E_p and E_c = Young's modulus of the FRP and concrete, respectively.

Combining eq. 3-3 to eq. 3-4 yields the following bond stress-slip model:

$$\tau(x) = A^2 B \frac{E_p t_p}{(1+\alpha)}\left(e^{-B\delta(x)} - e^{-2B\delta(x)}\right) \qquad \text{(eq. 3-5)}$$

The interfacial facture energy of bond, G_f is defined as

$$G_f = \int_0^{\infty} \tau ds \qquad \text{(eq. 3-6)}$$

By substituting eq. 3-5 into eq. 3-6, the following equation can be obtained:

$$A = \sqrt{\frac{2G_f}{E_p t_p}(1+\alpha)} \qquad \text{(eq. 3-7)}$$

And the bond stress-slip model can be rewritten as

$$\tau(x) = 2G_f B\left(e^{-B\delta(x)} - e^{-2B\delta(x)}\right) \qquad \text{(eq. 3-8)}$$

If a sufficient long bond length (at least longer than the effective bond length) is provided so that the loaded end slip is large enough, the bond strength can be calculated using the following equation:

$$P_{\max} = b_f \sqrt{2G_f \frac{E_f t_f}{1+\alpha}} \qquad \text{(eq. 3-9)}$$

It is obvious that eq.3-1 is a special case for eq3-9, in which the stiffness of concrete substrate is assumed ultimately large, in which case, (1+α)=1 and eq.3-1 can be deduced by eq.3-9.

3.4.2.2 Determination of G_f and B

Using eq. 3-9, the G_f can be obtained from the test pull load P_{max} without difficulty:

$$G_f = (1+\alpha)\frac{P_{\max}^2}{2E_p t_p b_p^2} \qquad \text{(eq. 3-10)}$$

The strain distribution along the FRP laminate, $\varepsilon(x)$ at different pull load P can be obtained as (Dai et al. 2013)

$$\varepsilon(x) = \frac{A}{1 + e^{BA(L-x)} \cdot \frac{P_{\max} - P}{P}} \qquad \text{(eq. 3-11)}$$

Comparatively, eq3-2 denotes the strain-slip response at the loaded end of a bond, while eq3-11 denotes the load strain in bond as a function of the load level and location. If the strain

distributions at different load levels $\varepsilon_{i,j}$ are obtained from tests (i=1, 2,…, m denotes the number of load level, j=1, 2,…, n denotes the number of strain gauge), the value of B can be determined through least-square minimization of the difference between the test and predicted strain values with the use of eq. 3-11, i.e. the B can be obtained by minimizing the following equation:

$$e = \sum_{i=1}^{m}\sum_{j=1}^{n}\left[\left(\varepsilon_{i,j}\right)_{pre.} - \left(\varepsilon_{i,j}\right)_{test}\right]^2 \qquad \text{(eq. 3-12)}$$

The parameters G_f and B determined from previous tests are listed in Table 3-3. The regressed strain curves are illustrated in Figure 3-25 in the appendix. The parameters varied depending on FRP types and the exposure history. The maximum G_f and B were found in CS-0m and GS-0m, and the minimum G_f and B were found in CP2-8m and CS-8m, respectively. The B in CP1-0m and CP2-0m was very close, and B decreased in both CP1-8m (22.6%) and CP2-8m (40.8%) after exposure. On the contrary, B in CS increased by 23.3%. G_f increased by 29.7% in CP1, 4.8% in CP2, but decreased by 5.7% in CS. The parameters of GS-8m were not obtained due to the fracture failure in FRP laminates.

3.4.2.3 Predicted bond-slip model and load-slip curves

Once the parameters G_f and B are obtained, the bond stress-slip relationship can be obtained using eq. 3-8. The predicted bond-slip models are illustrated in Figure 3-19. In comparison of bond-slip models, (a) the ascending stiffness of the curve in CP1-8m did not change largely, but the area beneath the curve became larger due to a larger G_f; (b) the stiffness of CP2 became much smaller due to a large decrease of parameter B; (c) a steeper acending and descending path was found in the curve of CS-8m, however the area beneath the curve was did not change largely.

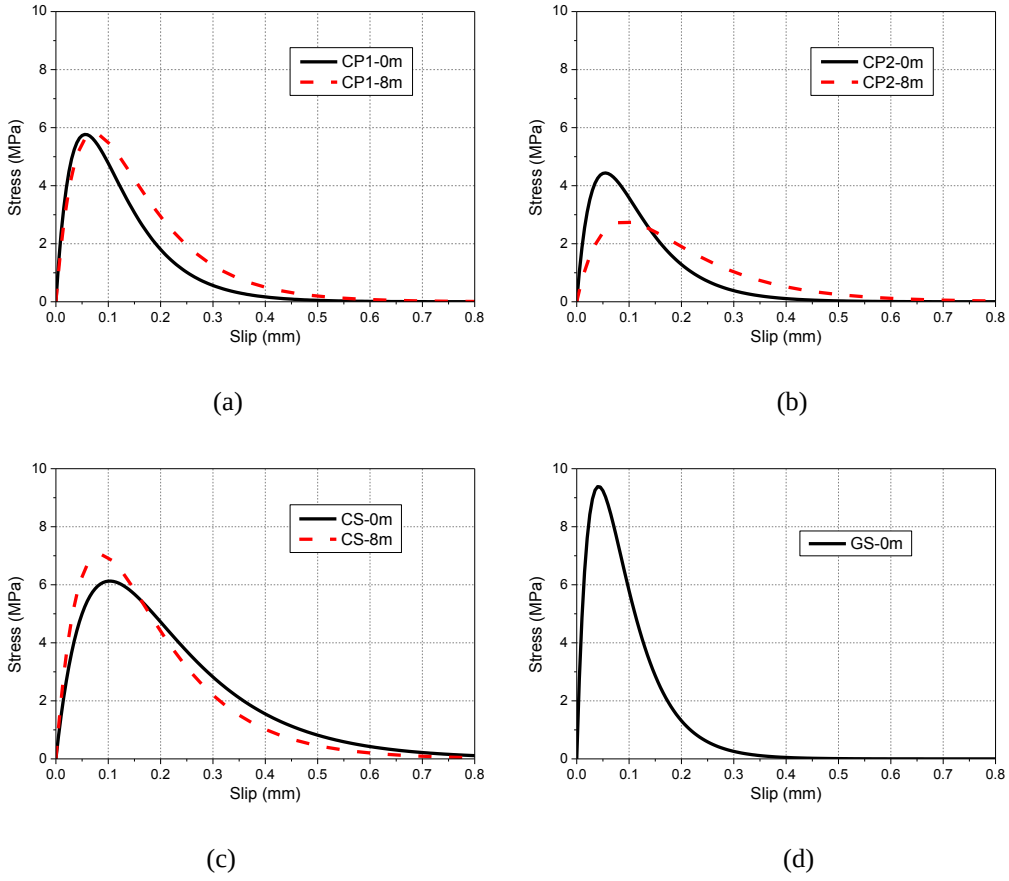

Figure 3-19 Proposed bond stress-slip curves of FRP-to-concrete interfaces of different specimens (a) CP1 (b) CP2 (c) CS (d) GS

3.4.2.4 Validation of the bond-slip models and discussions

The proposed bond stress-slip models could then be used to predict the bond behavior by an interating process. The FRP laminate can be devided into a finite number of elements along the longitudinal direction. Without loss of generality, it assumes that there are n elements and n+1 nodes (Figure 3-20).

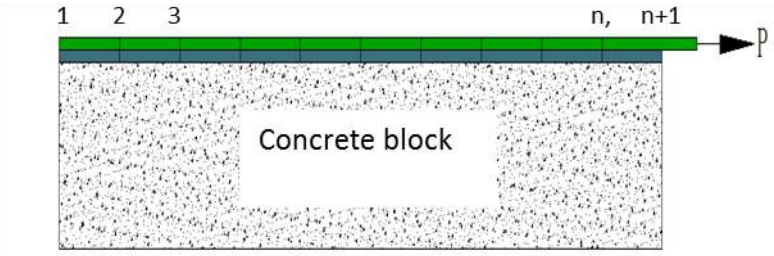

Figure 3-20 Illustration of nodes and elements in the model

The free end of the bond is not constraint, i.e.

$$\varepsilon_1 = 0\,;\ F_1 = 0 \qquad \text{(eq. 3-13)}$$

If the slip at the node 1 s_1 is known, the stress at the node 1 can be obtained as

$$\tau_1 = 2BG_f\left(e^{-Bs_1} - e^{-2Bs_1}\right) \qquad \text{(eq. 3-14)}$$

For *i*st node, it is assumed that the stress in *i*st element remains constant and equals the stress at *i*st node. Such assumption can be reasonable if a considerable large number of elements are used. The load-transfer relationship between the *i*st and (*i*-1)st node can be expressed as follows:

$$\begin{cases} F_i = F_{i-1} + bl\tau_{i-1} \\ \varepsilon_i = \dfrac{F_i}{E_f t_f b} \\ s_i = s_{i-1} + l(e_{i-1} + e_i)/2 \\ \tau_i = 2BG_f\left(e^{-Bs_i} - e^{-2Bs_i}\right) \end{cases} \qquad \text{(eq. 3-15)}$$

Therefore, if the condition in (*i*-1)st node is known, the status of *i*st node, i.e. F_i, ε_I, s_i, and τ_i can be obtained accordingly. As a result, given any free end slip s_1, the force and slip at the loaded end can be deduced. Due to the nature of the local bond stress-slip model, there is always a maximum load corresponding to a certain free end slip value.

A MATLAB program was compiled to conduct the calculation. It was found that the accuracy was acceptable (99.5%) if the more than 1000 elements were defined. The program started from a very small trial value of free end slip (less than 1e-6 mm) and output the bond status. The input value was increased gradually in loops until the load at the loaded end began to drop, which meant that the maximum load had been found. The increment of the free end slip in each loop was set reasonably small (smaller than 1e-6 mm) in order to guarantee the accuracy of results. During the calculation, the bond status at every calculated load levels was recorded.

The predicted bond strengths are listed in Table 3-3. A comparison between the predicted and test results is illustrated in Figure 3-21. The differences between most of the predicted and test results are within 1%, which is reasonable since the parameters of the models were regressed from the test results. The stain distributions at maximum load were also simulated, which are illustrated in Figure 3-25 in the appendix. The average parameters in the regressed bond stress-slip model were used to predict the strain distribution at peak load. However, there existed variations in the results of identical tests, which seem inevitable and reasonable. A comparison between test and predicted loaded end slip at peak load is listed in Table 3-3, in which good match was also found.

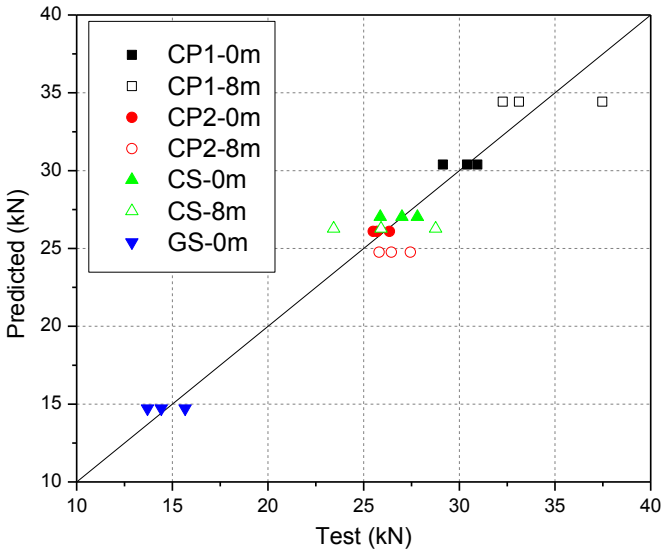

Figure 3-21 Test versus predicted bond strength

The predicted load-slip curves show very good agreement with test curves (Figure 3-26 in the appendix). For ease of comparison, all the predicted curves are illustrated in Figure 3-22. The load-slip responses are all exponential curves. The stiffness of bond was relatively large at the beginning of loading but softened gradually as the slip increased. The specimen CP1 and CP2 had a similar initial stiffness, while the stiffness of CS and GS were lower. As a matter of fact, according to eq. 3-2, the stiffness of bond is controlled by many parameters,

namely the FRP stiffness, the parameter *B* and the fracture energy. GS-0m achieved the best ductility due to its large ratio of bond length to effective bond length. The influences of wet-dry cycles varied in different types of specimens: (a) In CP1-8m, a stiffened load-slip curve and higher ultimate load were observed, which was mainly contributed by the post cured resins. As discussed previously, two of the CP1-0m failed in the primer-adhesive interface; comparatively, after 8-month exposure, all the specimens failed totally in concrete. The post curing in the wet-dry cycles provided a better cohesion between the primer and resin, which led to a better stress transfer capability. (b) On the contrary, in CP2-8m, the load-slip responses behaved almost linearly in a much lower stiffness compared with CP2-0m. Such change mainly resulted from the degradation of cohesion between the FRP plate and epoxy. As described previously, the CP2-8m failed mostly in FRP-adhesive interfaces other than in the concrete. The change in failure mode led to less efficient stress transfer through the FRP-to-concrete interfaces. Noting the formation of strain distributions in the FRP plate in CP2-8m (Figure 3-26), the effective bond length of CP-8m could even be larger than the bond length. It is well known that if there is no sufficiently long bond provided, the ductility of bond can be very poor. Therefore, the load-slip curves in the CP2-8m specimens were almost linear due to the insufficient bond length. (3) The CS-8m became slightly stiffer but achieved lower bond strength; however the changes were not very obvious. (4) Linear load-slip curves were observed in GS-8m due to fracture of FRP laminates, which was not simulated in the predicted model.

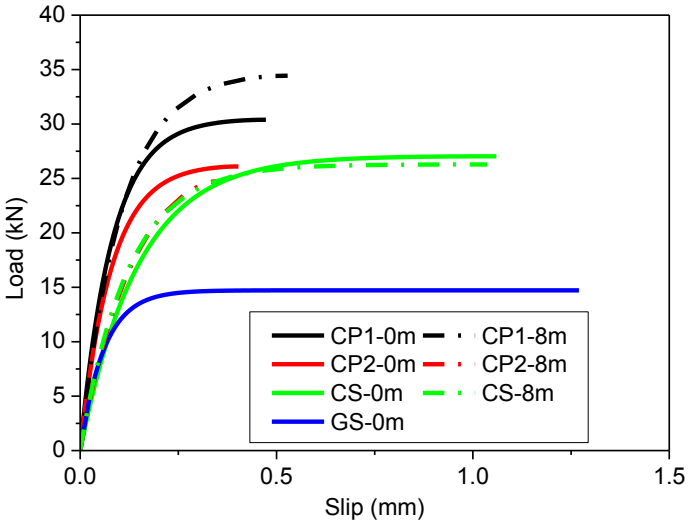

Figure 3-22 Predicted load-slip curves of FRP bonded concrete joints

Moreover, Figure 3-23 demonstrates the stress distribution in the interface at peak load. Stress distributions varied correspond to the variations of bond stress-slip curves.

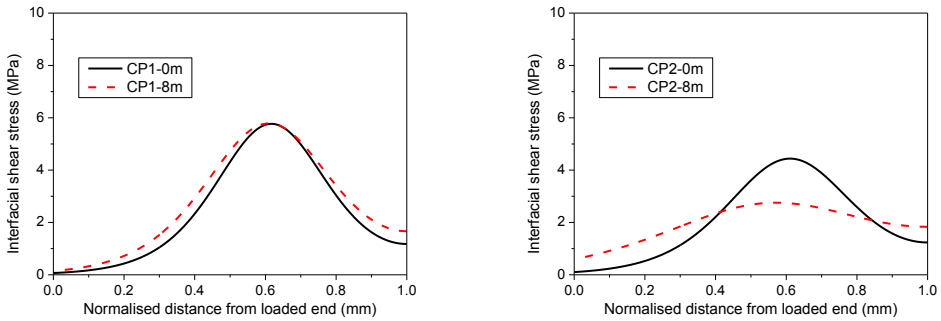

(a)

(b)

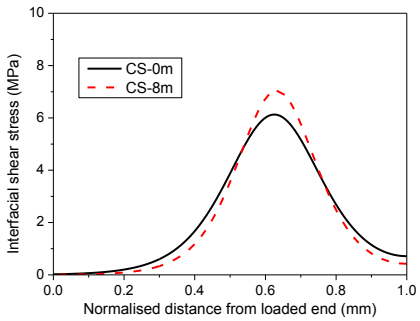

(c)

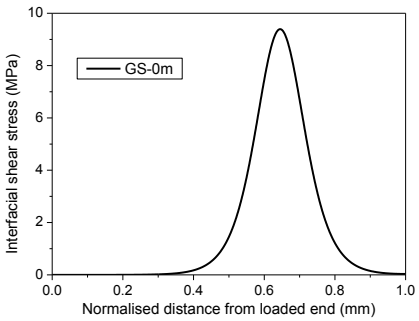

(d)

Figure 3-23 Predicted interfacial shear stress distributions in different specimens (a) CP1 (b) CP2 (c)

According to the regression analysis by Dai et al. (2005), the G_f has a negative correlation with the normalized shear stiffness of adhesive layer G_a/t_a:

$$G_f = 0.446\left(G_a / t_a\right)^{-0.352} f_c^{0.236}\left(E_f t_f\right)^{0.023} \quad \text{(eq. 3-16)}$$

in which G_a=shear stiffness of adhesive and t_a=thickness of adhesive layer. In present study, the thickness of adhesives was controlled according to the product handbook so as to provide best cohesion performance, which was 3mm for Sika30 (in CP1) and 0.1mm for Araldite106 (in CP2). The tensile modulus of adhesives, which is close and proportional to the shear modulus of the adhesive, was obtained as: $E_{a,Sika30}$=11.4MPa and $E_{a,Aral106}$=0.90MPa. As a result, the ratio $E_{a,Sika30}/t_{a,Sika30}$=3.8N/mm^3< $E_{a,Aral106}/t_{a,Aral106}$=9.0 N/mm^3, i.e. the adhesive layer in CP1 is 'softer' than the adhesive in CP2. Using eq. 3-16, the ratio of predicted fracture energy between CP1 and CP2 can be calculated as:

$$\frac{G_{f,CP1}}{G_{f,CP2}} = \left(\frac{G_{a,Sika30} / t_{a,Sika30}}{G_{a,Aral106} / t_{a,Aral106}}\right)^{-0.352} = 1.35 \quad \text{(eq. 3-17)}$$

which is very close to the ratio obtained from tests (=1.4, Table 3-3). Therefore, the discussion above proves the assumption that a soft adhesive can indeed improve the bond performance.

3.5 CONCLUSIONS

This chapter has presented both experimental and analytical studies on the exposure-dependent behavior of FRP-to-concrete interfaces. Four types of FRP-to-concrete interfaces were subjected to 8-month exposure in wet dry cycles. Single-lap shear tests were used to evaluate the bond performance after exposure. Analytical study was also conducted and exposure-dependent bond stress-slip curves were proposed. The following conclusions were made based on above work:

(a) Arch-shape strain distributions emerged in the FRP laminates during exposure, and the residual strains were not likely to fully recover even the bonded joints were fully dried and placed back to the original indoor environment.

(b) The wet-dry cycles caused changes in the failure mode of joints. Although most of the specimens (CP1-8m, CP2-0m, CS, GS-0m) failed in concrete, two of CP1-0m failed in the adhesive layer; CP2-8m failed in the adhesive-epoxy interface combined with FRP delamination; and GS-8m failed by FRP sheet fracture. Changes in the failure mode indicating that the exposure has brought out different effects on the interfaces or the FRP composites. The exposure improved the cohesion between the primer and resins in CP1, while weakened the cohesion between the FRP plate and adhesive in CP2 and the strength of GFRP sheets.

(c) Variations in bond strengths were also observed: 13.7% and 2.8% increase in CP1 and CP2 while 3.2% and 16.4% decrease in CS and GS, respectively. The ultimate bond strength of GS series decreased largely due to rupture of GFRP sheets.

(d) Predicted bond stress-slip models were proposed. The parameters were regressed from the tests. Bond degradation was well interpreted by the variations in parameters B and G_f. Good agreement was found in predicted and test results.

(e) It is proved that a soft adhesive layer could improve the bond performance. In present study, CP1 with a softer adhesive layer achieved a higher bond strength than CP2 using the same FRP plate but a harder adhesive layer.

Although the experimental and analytical study has successfully interpreted the long-term behavior of the FRP-to-concrete interfaces after 8-month exposure, it is insufficient to come

up with a formula to predict the long-term bond performance due to limited test duration and sampling. Further studies have been designed to fulfill such target, which will be discussed in Chapter 6.

APPENDIX

(a)

(b)

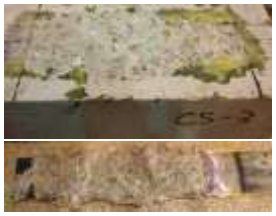

(c)

(d)

(e)

(f)

(g)

(h)

Figure 3-24 Failure in specimen (a) GS-0m (b) GS-8m (c) CS-0m (d) CS-8m (e) CP1-0m (f) CP1-8m (g) CP2-0m (h) CP2-8m

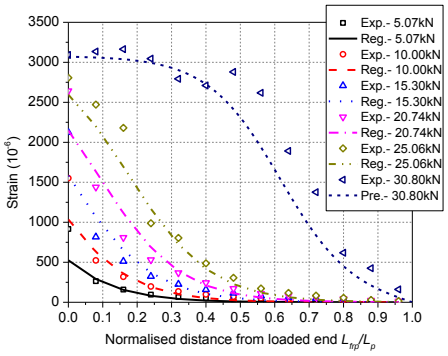

(a-1)

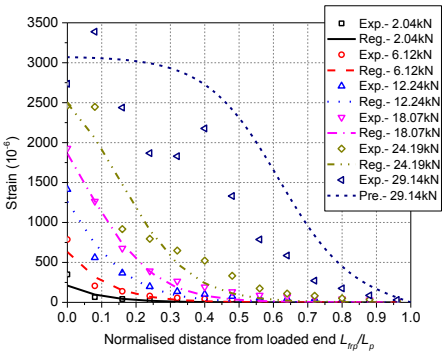

(a-2)

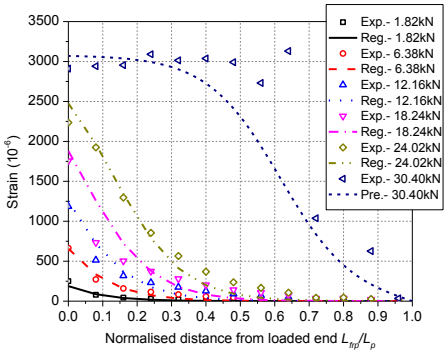

(a-3)

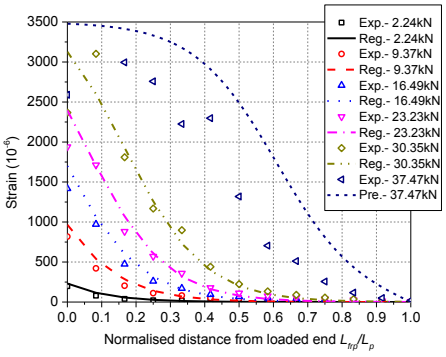

(b-1)

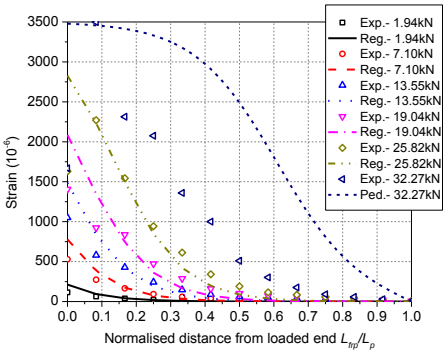

(b-2)

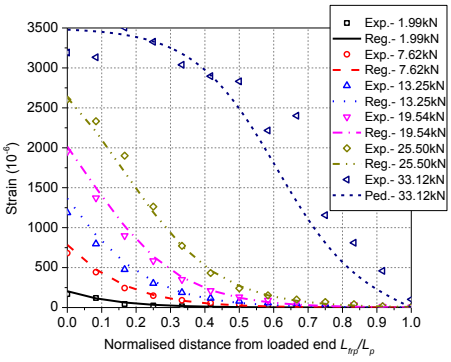

(b-3)

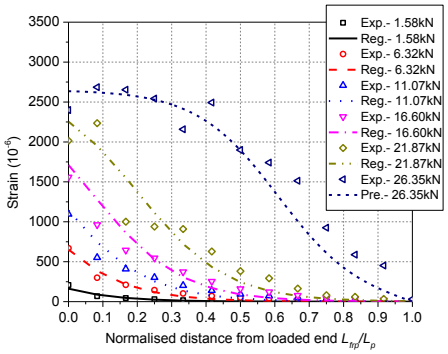

(c-1)

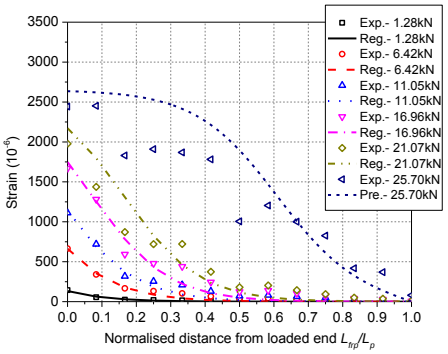

(c-2)

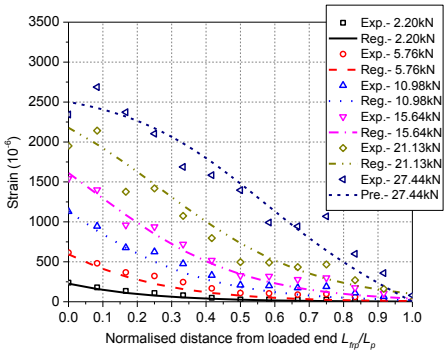

(d-1)

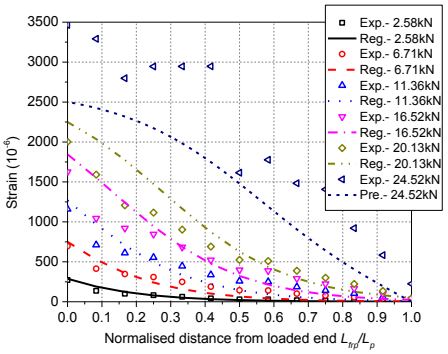

(d-2)

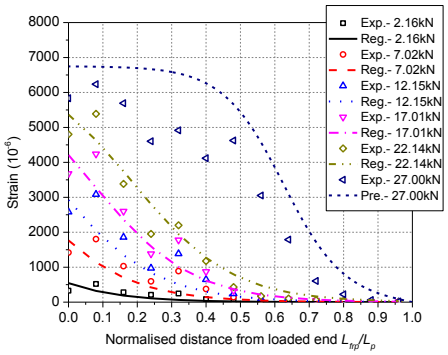

(e-1)

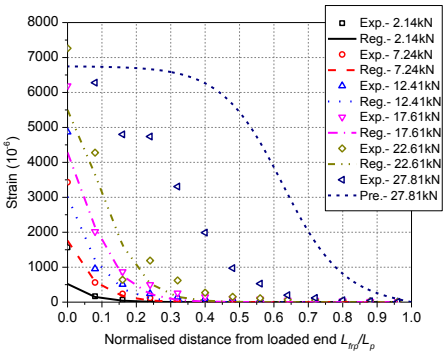

(e-2)

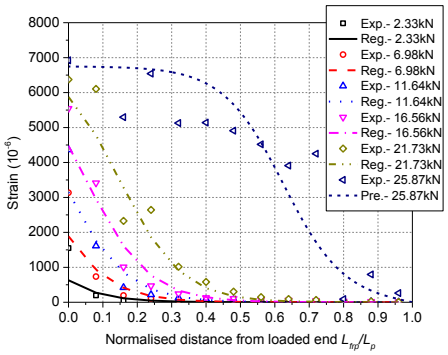

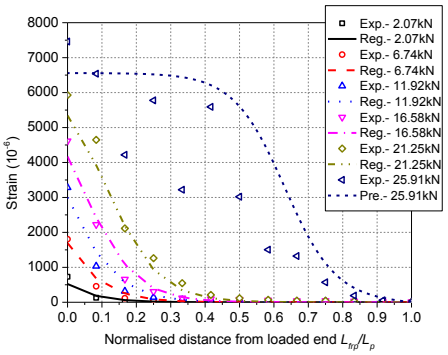

(e-3)

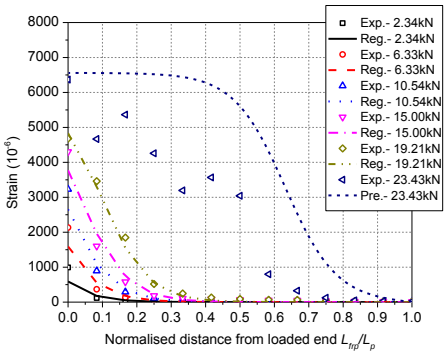

(f-1)

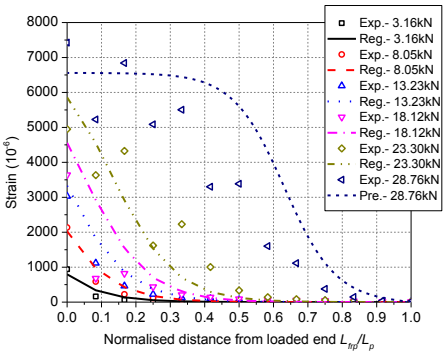

(f-2)

(f-3)

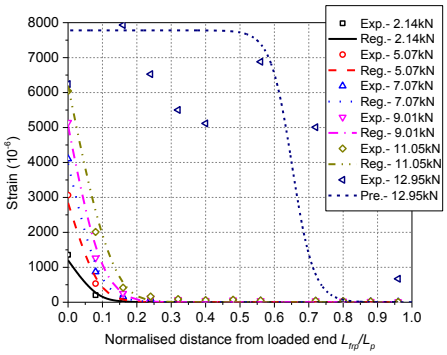

(g-1)

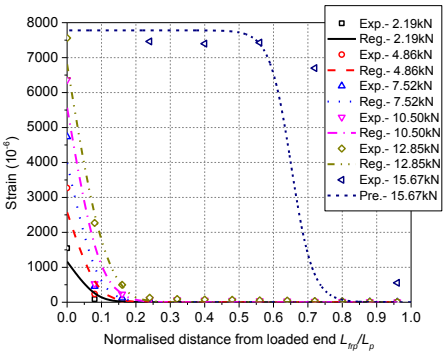

(g-2)

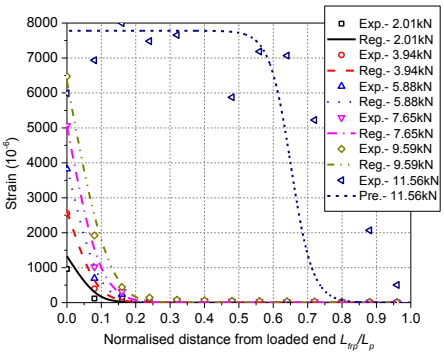

(g-3)

Figure 3-25 Test vs. predicted strain distributions in FRP at ultimate load in different specimens (a) CP1-0m (b) CP1-8m (c) CP2-0m (d) CP2-8m (e) CS-0m (f) CS-8m (g) GS-0m

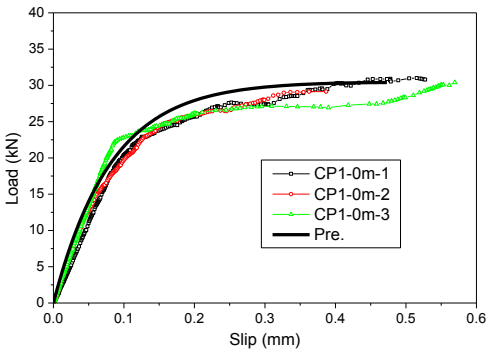
Load (kN)
Slip (mm)
CP1-0m-1
CP1-0m-2
CP1-0m-3
Pre.

(a)

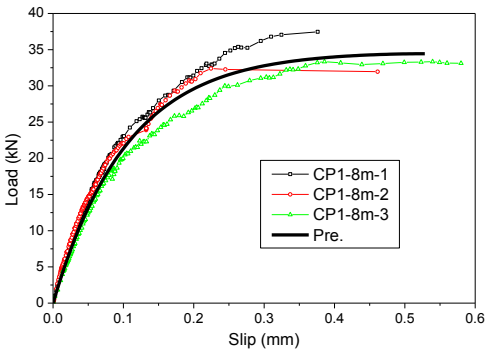
Load (kN)
Slip (mm)
CP1-8m-1
CP1-8m-2
CP1-8m-3
Pre.

(b)

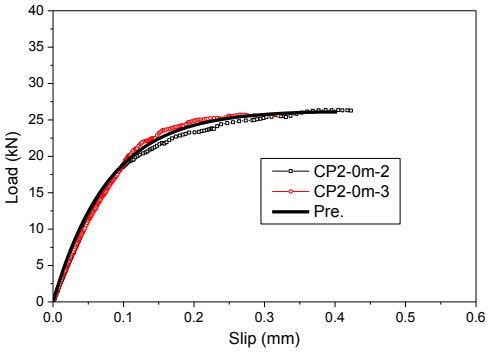
Load (kN)
Slip (mm)
CP2-0m-2
CP2-0m-3
Pre.

(c)

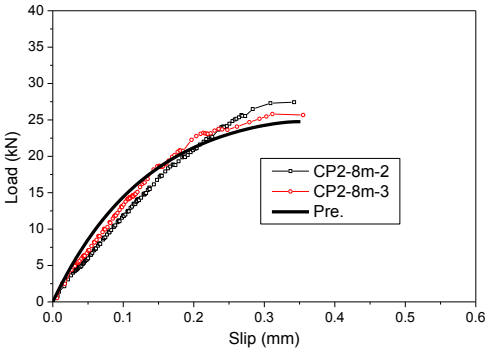
Load (kN)
Slip (mm)
CP2-8m-2
CP2-8m-3
Pre.

(d)

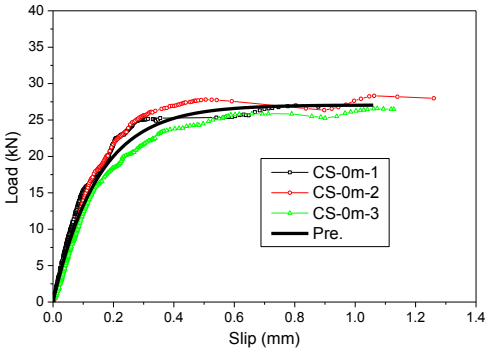
Load (kN)
Slip (mm)
CS-0m-1
CS-0m-2
CS-0m-3
Pre.

(e)

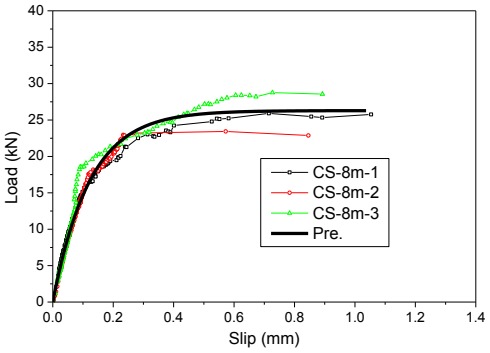
Load (kN)
Slip (mm)
CS-8m-1
CS-8m-2
CS-8m-3
Pre.

(f)

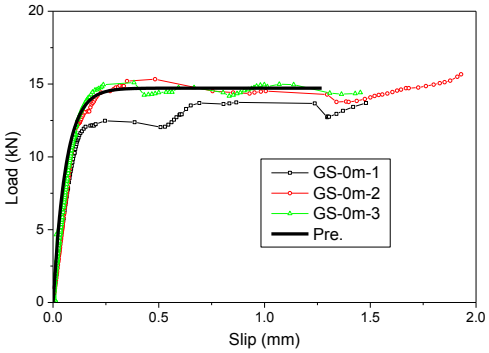
Load (kN)
Slip (mm)
GS-0m-1
GS-0m-2
GS-0m-3
Pre.

(g)

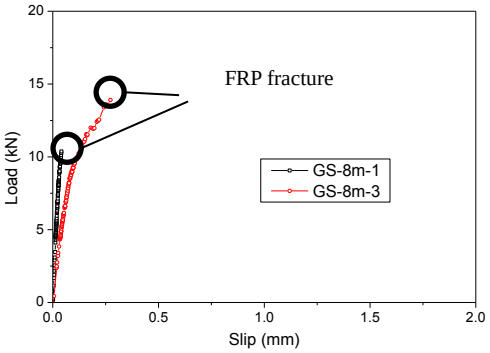
Load (kN)
Slip (mm)
FRP fracture
GS-8m-1
GS-8m-3

(h)

Figure 3-26 Test and predicted load-slip curves of specimens (a) CP1-0m (b) CP1-8m (c) CP2-0m (d) CP2-8m (e) CS-0m (f) CS-8m (g) GS -0m (h) GS-8m

CHAPTER 4

LONG-TERM BEHAVIOR OF FRP-PLATED RC BEAMS

4.1 INTRODUCTION

Bonding FRP reinforcement in the form of pultruded or wet-layup plates to RC beams (i.e., FRP-plated RC beams) has been widely used as a strengthening technique. The performance of FRP-strengthened RC beams depends on the bond of FRP-concrete interface, through which concrete stress is transferred to FRP reinforcement. As a practical strengthening technique, the bond between FRP and concrete is required to be robust not only in short-term but also in long-term. Recently, study on the long-term performance of bond of the FRP-concrete interface and FRP-strengthened RC beams is gaining increasing interest.

4.2 EXPERIMENTAL PROGRAM AND TEST OBSERVATIONS

4.2.1 Design of specimens

Forty FRP-strengthened beams were designed and prepared in this experimental program. These beams are expected to fail by IC debonding, as IC debonding is one of the most common failure modes of FRP-plated RC beams, and strongly depends on the bond between concrete and the FRP plate. All the beams had the same dimensions: 150 mm in width, 200 mm in height and 2150 mm in length as illustrated in Figure 4-1. Two 10 mm steel bars and two 8 mm steel bars were used as the internal tensile and compressive reinforcement, respectively. In order to avoid undesirable shear failure, 8mm stirrups were set at the spacing of 100 mm center to center. Two-layer CFRP sheets (0.167 mm for each layer), four-layer

GFRP sheets (0.172 mm for each layer) and one-layer pultruded CFRP plate of 1.2 mm in thickness were adopted as the flexural reinforcement aiming at IC debonding failure in beams. The FRP sheets/plates used were all 100 mm in width. The distance from plate end to the near support is very small (50 mm) so as to reduce the normal stress in the plate end, which prevents the FRP plate-end debonding. The mechanical properties of materials in beams have been described in Chapter 2.

These beams were distinguished from each other type of FRP sheets and bonding adhesives, exposure conditions and exposure durations. Detailed arrangement of beams is given in Table 4-1. The same as these used in FRP bonded concrete joint tests, four types of FRP-epoxy combinations were used in beams, i.e. CFRP sheet (CS), GFRP sheet (GS), CFRP plate-Sika30 (CP1), and CFRP plate-Araldite106 (CP2). For each FRP-epoxy combination, five beams were prepared for accelerated lab tests and another five for field exposure tests. The exposure durations were set the same as the FRP bonded concrete joints.

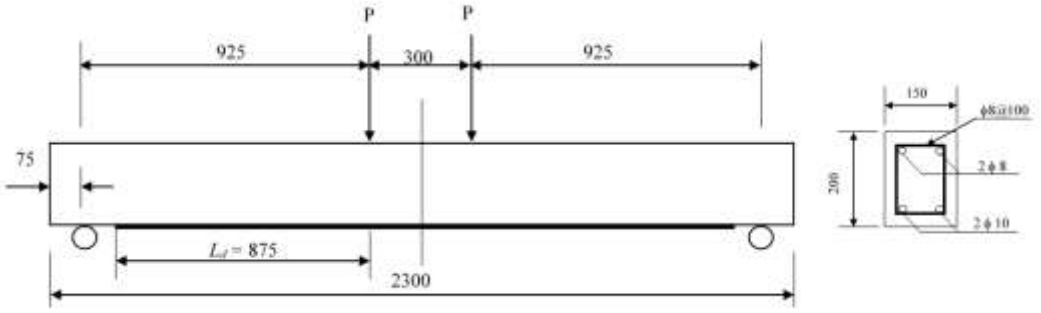

Figure 4-1 Dimension of FRP-strengthened RC beams

Table 4-1 Information of FRP-strengthened RC beams for accelerated laboratory tests

Serial number		Specimen type	Specimen size	FRP type	Adhesive type	Exposure duration	Quantity
L-GS	L-GS-0m	RC beam	150×200×2300	**G**FRP sheet	Sika330	0 month	1
	L-GS-6m					8 months	1
	L-GS-12m					12 months	1
	L-GS-18m					18 months	1
	L-GS-24m					24 months	1
L-CS	L-CS-0m	RC beam	150×200×2300	**C**FRP sheet	SW-3C	0 month	1
	L-CS-6m					8 months	1

	L-CS-12m					12 months	1
	L-CS-18m					18 months	1
	L-CS-24m					24 months	1
L-CP1	L-CP1-0m	RC beam	150×200×2300	**C**FRP plate	Sika30	0 month	1
	L-CP1-6m					8 months	1
	L-CP1-12m					12 months	1
	L-CP1-18m					18 months	1
	L-CP1-24m					24 months	1
L-CP2	L-CP2-0m	RC beam	150×200×2300	**C**FRP plate	Araldite106	0 month	1
	L-CP2-6m					8 months	1
	L-CP2-12m					12 months	1
	L-CP2-18m					18 months	1
	L-CP2-24m					24 months	1

Table 4-2 Information of FRP-strengthened RC beams for field exposure tests

Serial number		Specimen type	Specimen size	FRP type	Adhesive type	Exposure duration	Quantity
F-GS	F-GS-18m	RC beam	150×200×2300	GFRP sheet	Sika330	18 months	1
	F-GS-36m					36 months	1
	F-GS-60m					60 months	1
	F-GS-96m					96 months	1
	F-GS-144m					144 months	1
F-CS	F-CS-18m	RC beam	150×200×2300	CFRP sheet	SW-3C	18 months	1
	F-CS-36m					36 months	1
	F-CS-60m					60 months	1
	F-CS-96m					96 months	1
	F-CS-144m					144 months	1
F-CP1	F-CP1-18m	RC beam	150×200×2300	CFRP plate	Sika30	18 months	1
	F-CP1-36m					36 months	1
	F-CP1-60m					60 months	1
	F-CP1-96m					96 months	1
	F-CP1-144m					144 months	1
F-CP2	F-CP2-18m	RC beam	150×200×2300	CFRP plate	Araldite106	18 months	1
	F-CP2-36m					36 months	1
	F-CP2-60m					60 months	1
	F-CP2-96m					96 months	1
	F-CP2-144m					144 months	1

4.2.2 Specimen preparations

The steel reinforcement cages were carefully fabricated to ensure the internal steel reinforcements are accurately positioned. Two strain gauges were set on the tensile bars at mid-span of the beam (Figure 4-2 (a)). Another pair of strain gauges were applied at 100 mm from the mid-span in case the former ones are damaged. The gauges were protected with

two layers of water-resistant adhesives. On one end of the steel cage, lead wire was planted for the purpose of corrosion monitoring (Figure 4-2 (b)). The beams were cast using the same batch of concrete which was well mixed and vibrated. The beams were all carefully cured indoors for more than 28 days.

Figure 4-2 Measurement of tensile steel reinforcement (a) strain gauges; (b) lead wires for corrosion monitoring

After more than 28 days' curing of RC beam, FRP reinforcement was applied (Figure 4-3). The application of FRP sheets/plates followed the introduction in Chapter 3. It should be noted that there are much more technical difficulties to produce a high-quality FRP-concrete bond on RC beams than on concrete prisms because of the much larger bond area. It is not only required to apply the FRP sheets plainly and uniformly, but also made sure that the epoxy was free of air bubbles while mixed despite the very large quantity.

Figure 4-3 Bottom view of FRP-strengthened RC beams

4.2.3 Test procedures and instrumentations

The specimens were loaded by a hydraulic loading system (Figure 4-5). A steel beam was installed on the mid-top of the beam to distribute the load to two load points with a span of

300 mm (Figure 4-1). Ahead of loading, the beams and the loading frame were carefully aligned. The increment of load was set as 1 kN per step before concrete cracked. After the first crack was discovered, the load was set as 2-4 kN per step, according to the predicted ultimate load of each beam. After tensile bars yielded, the increment of mid-span displacement was set as 2 mm per minute and 1 mm for each step.

At each load step, the load forces, displacements and strains in the beam were monitored (Figure 4-4). Two load cells were installed at loading points. Two LVDTs were installed on the top of supports, and another two were set at mid-span on both sides of the beam due to limited space (Figure 4-6). The location of the reference plates is 75 mm downwards from the top surface of the beams so that the reference plates would not be interfered by cracks. Twenty-one 5 mm strain gauges at spacing of 100 mm were installed on the FRP laminate along the longitudinal orientation; one 100 mm strain gauge was installed on the top of compressive zone at the mid-span of the beam. In addition, two 100 mm strain gauges were attached on one side of the beam at vertical spacing of 50 mm from the top surface to monitor crack propagations.

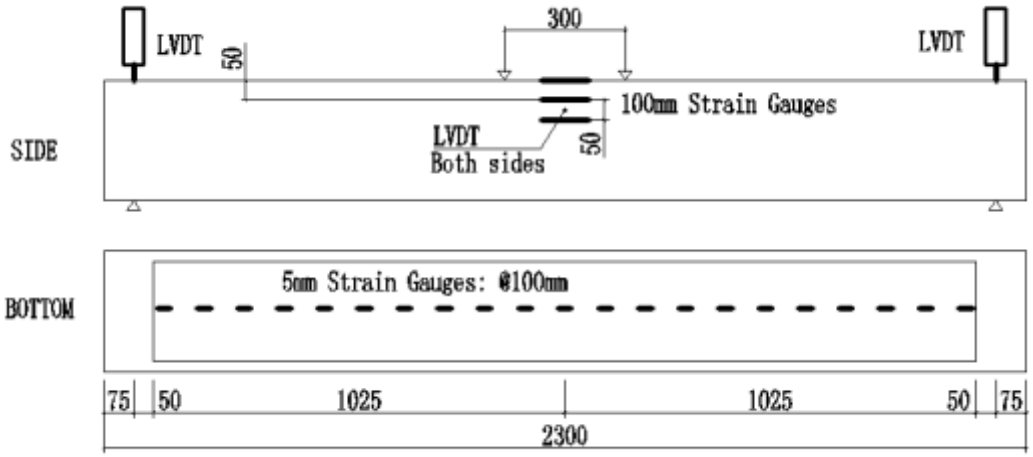

Figure 4-4 Layout of strain gauges and LVDTs

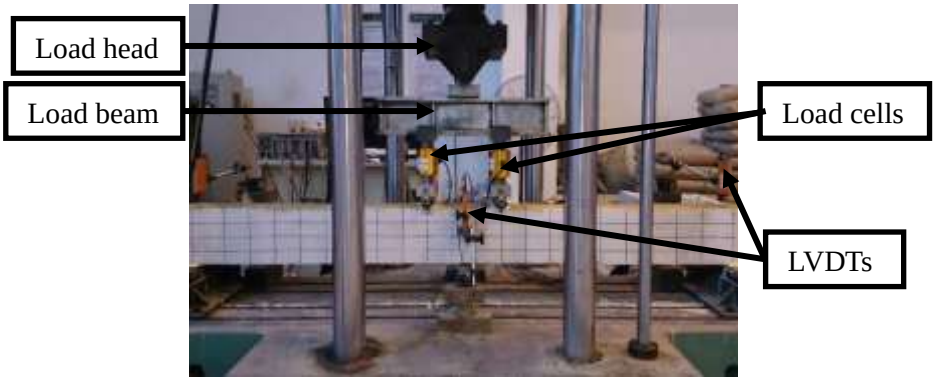

Figure 4-5 Loading set-up of beams

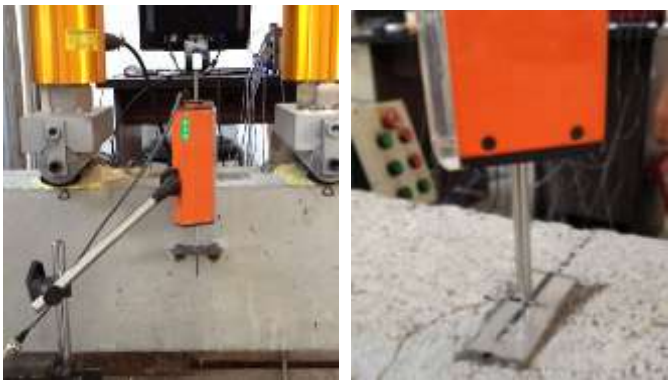

Figure 4-6 Locations of LVDTs at mid-span and two supports

4.2.4 Test results and observations

Considering the very long period of the experiment and the limited time for the master study, only 0-month and 8-month accelerated laboratory tests were completed. This section reports the test results of these beams. For simplicity, all the specimens mentioned in the following sections of this chapter refer to accelerated laboratory tests.

The ultimate loads of beams are listed in Table 4-3. The ultimate loads of non-exposed beam CP1-0m, CP2-0m, CS-0m and GS-0m were 77.65kN, 75.07kN, 56.36kN and 46.53kN respectively. The load capacity showed a good positive correlation with the FRP stiffness. Different scales of degradation in load capacities of beams were observed in exposed beams. After 8-month exposure, the ultimate load of CP1-8m, CP2-8m, CS-8m and GS-8m decreased by 2.6%, 10.8%, 1.4% and 7.9%, respectively. The load-deflection curves of all

beams are presented in Figure 4-7. Three stages can be observed clearly in all curves: (a) the beams behaved linearly before concrete cracking. In non-exposed beams, the stiffness was found very close although they were strengthened in beams with different FRP composites. (b) Obvious variations in stiffness of beams appear after concrete cracked. The stiffness of beams corresponded to the stiffness of FRP reinforcement ($E_{cp}t_{cp}>E_{cs}t_{cs}>E_{gs}t_{gs}$). (c) In the third stage when the tensile bars yielded, the stiffness of beams further decreased towards a brittle failure. After 8-month exposure, the CP beams suffered decrease in stiffness and ultimate load, while the CS and GS beams behaved in a stiffer response but also a slight lower load capacity. The mechanisms of the changes will be discussed in detail in Section 4.3.2.6

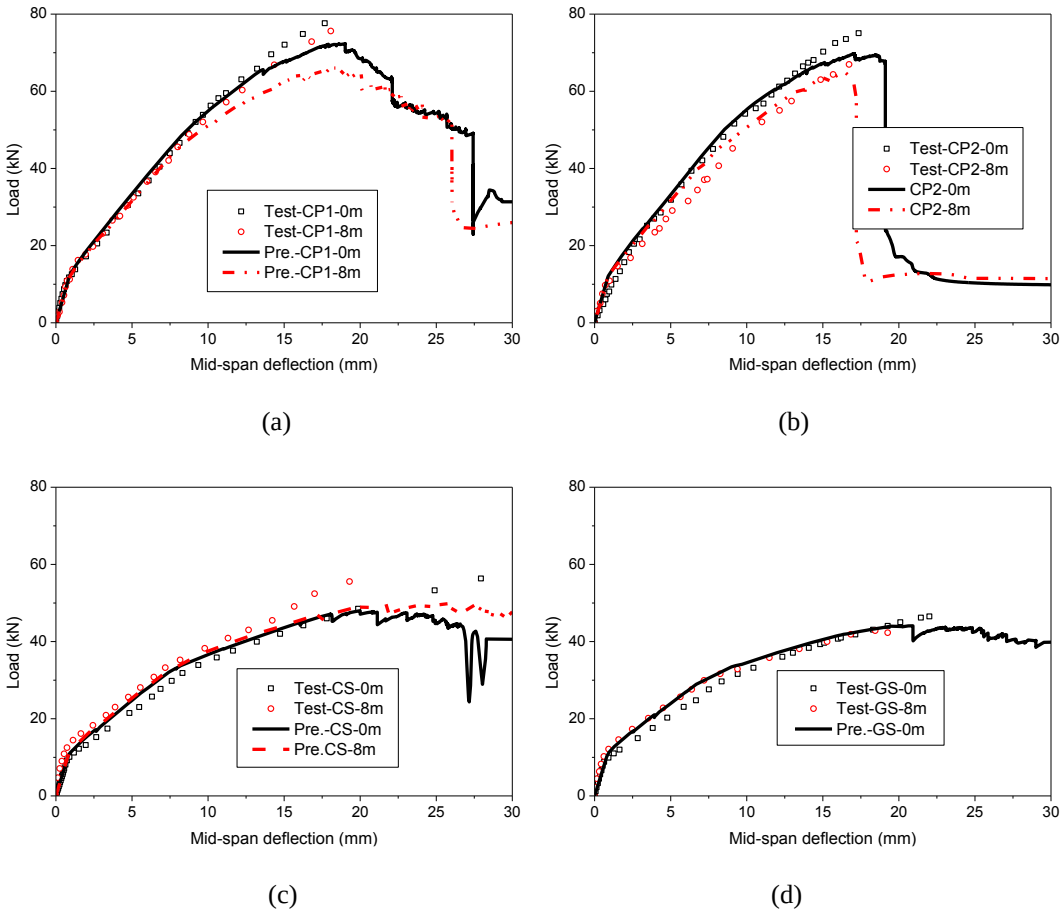

Figure 4-7 Test and predicted load vs. mid-span deflection curves (a) CP1 (b) CP2 (c) CS (d) GS

Table 4-3 Predicted vs. test results of FRP-strengthened RC beams

Specimen	Results	Maximum FRP strain at peak load ε_p	$\varepsilon_{p.pre.}/\varepsilon_{f.test}$	Concrete compressive strain at peak load ε_c	$\varepsilon_{c.pre}/\varepsilon_{c.test}$	Maximum load P_u (kN)	$P_{u.pre.}/P_{u.test}$
CP1-0m	Test	6077	\	-2644	\	77.65	\
	Ana.1	6200	1.02	-2100	0.79	72.22	0.93
	Ana.2	5890	0.97	-2668	1.01	72.32	0.93
CP1-8m	Test	5972	\	-2102	\	75.61	\
	Ana.1	6400	1.07	-2100	1	74.12	0.98
	Ana.2	5310	0.88	-2077	0.99	66.31	0.88
CP2-0m	Test	5394	\	-2658	\	75.07	\
	Ana.1	6200	1.15	-2100	0.79	79.00	1.05
	Ana.2	5360	0.99	-2444	0.92	69.75	0.93
CP2-8m	Test	4964	\	-2178	\	66.95	\
	Ana.1	6400	1.29	-2100	0.96	74.12	1.11
	Ana.2	4990	1.01	-2368	1.09	64.96	0.97
CS-0m	Test	12020	\	-3165	\	56.36	\
	Ana.1	10000	0.83	-2400	0.76	56.35	1.00
	Ana.2	7040	0.58	-2375	0.75	47.99	0.85
CS-8m	Test	10415	\	-2296	\	55.56	\
	Ana.1	10300	0.99	-2400	1.05	58.90	1.06
	Ana.2	8290	0.80	-2193	0.96	50.70	0.91
GS-0m	Test	9421	\	-2920	\	46.53	\
	Ana.1	9900	1.05	-2400	0.82	57.88	1.24
	Ana.2	8700	0.92	-2744	0.94	44.09	0.9478
GS-8m	Test	8354	\	-2302	\	42.84	\
	Ana.1	10200	1.22	-2400	1.04	59.23	1.38
	Ana.2	\	\	\	\	\	\

Note: The calculated FRP debonding strain is 1.3 times of the value determined according to Lu et al. (2007).

All beams failed by IC induced debonding regardless the FRP systems and exposure history (Figure 4-8 to Figure 4-11). The crack patterns of the debonding side of the beams are illustrated in Figure 4-17 in the appendix. Crack propagations and failure in beams are similar: the presence of the first crack was at 8 kN to 12 kN. As the load increased, more cracks were developed in the constant moment zone and distributed uniformly. It was followed by the presence of more cracks in the bending-shear area of beams at spacing of stirrups. The height of cracks propagated fast until the load reached 50% of the maximum load. After yielding of tensile bars, substantial secondary cracks were observed between the

existed cracks. At the meantime, the width of cracks in the constant zone increased rapidly, while the height of the cracks increased very slowly. The crack peak reached 50 mm from the top surface at the final stage of loading. The dominating cracks, at which the FRP sheets/plates debonding initiated, were observed in the constant moment zone or under the loading point. The FRP laminate debonded with a thin concrete layer, which was approximately 3mm-5mm in thickness. In particular, a part of concrete cover was split off between the dominating crack and one adjacent crack in CS and CP1. It also should be noted that although the GFRP sheets fractured in bonded joint tests, the GFRP strengthened RC beams stilled failed by FRP debonding. The most possible reason of the difference is that the GFRP sheets used in beams were thicker than that used in the bonded joints, which was more resistant to corrosion by exposure.

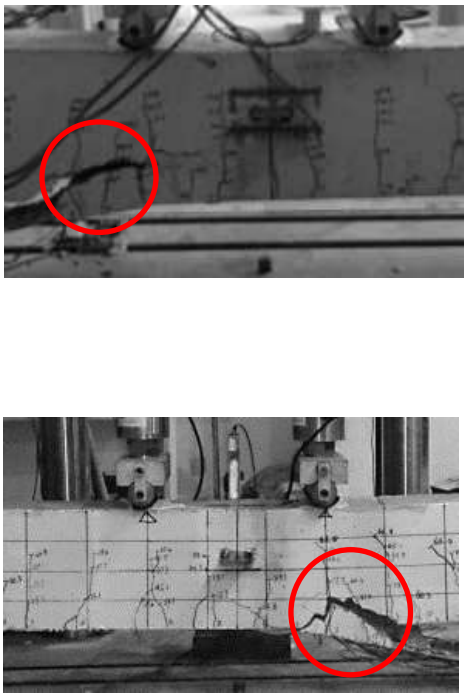

Figure 4-8 Failure of beams CP1-0m (left) and CP1-8m (right)

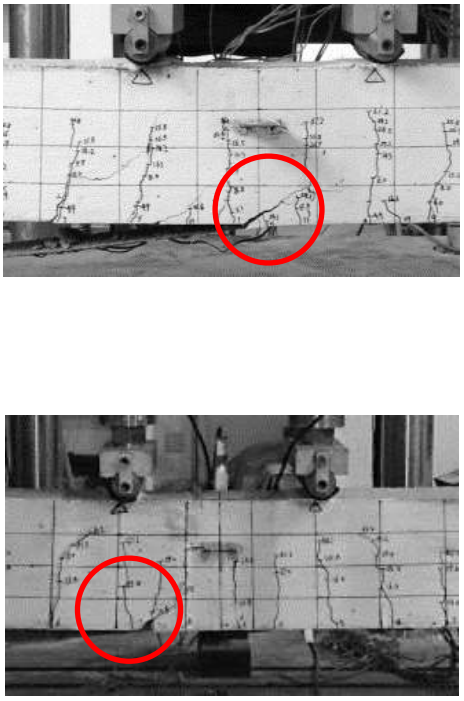

Figure 4-9 Failure of beams CP2-0m (left) and CP2-8m (right)

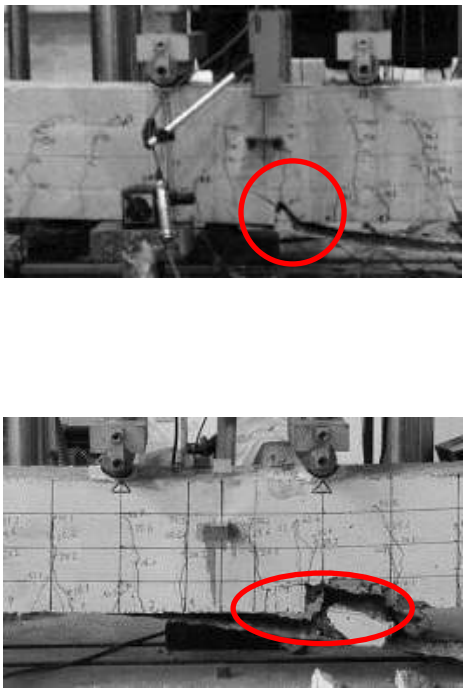

Figure 4-10 Failure of beams CS-0m (left) and CS-8m (right)

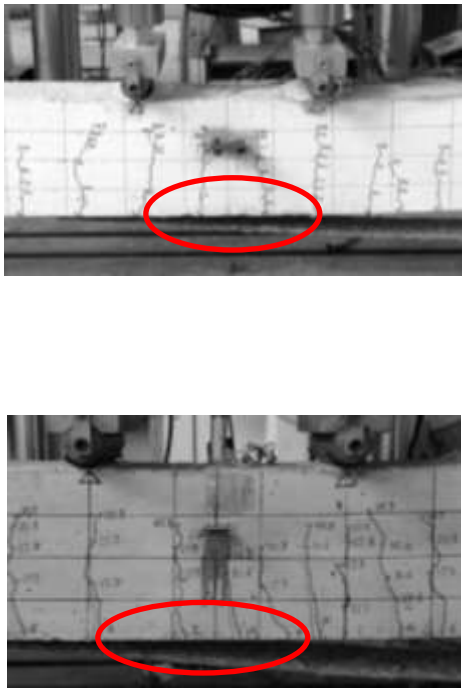

Figure 4-11 Failure of beams GS-0m (left) and GS-8m (right)

4.3 ANALYTICAL OBSERVATIONS

In this section, analytical studies were conducted for the tested FRP-strengthened RC beams. The debonding strain of FRP was first studied using Lu et al. (2007)'s model. Finite Element (FE) simulations were then conducted to explore the global performance of beams.

4.3.1 Prediction of FRP debonding strain in FRP flexural strengthened RC beams

An analytical study was conducted to predict the FRP debonding strain. The FRP debonding strain is deduced following Lu's model (2007):

$$\varepsilon_f^{IC} = \mathrm{C} \times 0.114(4.41-\alpha)\ \ \tau_{\max} / \sqrt{E_f t_f} \qquad \text{(eq. 4-1)}$$

in which

C= modified factor, use C=1.3 due to the conservative prediction of the original model.

$$\alpha = 3.41 L_{ee} / L_d \quad \text{(eq. 4-2)}$$

$$L_{ee} = 0.228\sqrt{E_f t_f} \quad \text{(eq. 4-3)}$$

$$\tau_{\max} = 1.5\beta_w f_t = 1.5 f_t \sqrt{\frac{2.25 - b_f / b_c}{1.25 + b_f / b_c}} \quad \text{(eq. 4-4)}$$

where L_d = distance from the loaded section to the end of the FRP plate (Figure 4-1). The predicted values of FRP debonding strain are listed in Table 4-3. Good agreement is met between predicted and test results. Due to the short-term nature of the model, the debonding strains could not reflect the weathering effect of the wet-dry cycles.

The plane-section assumption was adopted to calculate the ultimate load in beams. For a given section, the force equilibrium can be represented as the addition of the force in concrete, steel reinforcement and FRP laminates:

$$\sum F = F_c + F_{s1} + F_{s2} + F_{frp} = 0 \quad \text{(eq. 4-5)}$$

in which

$$F_c = k_1 f_{cu} b_c \quad \text{(eq. 4-6)}$$

$$F_{s1} = A_{s1} f_{s1} \quad \text{(eq. 4-7)}$$

$$F_{s2} = A_{s2} f_{s2} \quad \text{(eq. 4-8)}$$

$$F_{frp} = t_{frp} b_{frp} f_{frp} \quad \text{(eq. 4-9)}$$

where

$$k_1 = \begin{cases} 0.67\left(\frac{\varepsilon_{cf}}{\varepsilon_{co}} - \frac{\varepsilon_{cf}^{\ 2}}{3\varepsilon_{co}^{\ 2}}\right), \varepsilon_{cf} < \varepsilon_{co} \\ 0.67\left(1 - \frac{\varepsilon_{co}}{3\varepsilon_{cf}}\right), \varepsilon_{cf} > \varepsilon_{co} \end{cases} \quad \text{(eq. 4-10)}$$

$$\begin{cases} \varepsilon_{co} = \sqrt{f_{cu}} / 4100 \\ \varepsilon_{cr} = 0.0035 \end{cases} \quad \text{(eq. 4-11)}$$

$$\sigma_{si} = \begin{cases} \varepsilon_{si} E_{si}, \varepsilon_{si} < \varepsilon_y \\ f_y, \varepsilon_{si} \geq \varepsilon_y \end{cases} \quad \text{(eq. 4-12)}$$

$$\sigma_{frp} = \varepsilon_{ic,frp} E_{frp} \quad \text{(eq. 4-13)}$$

$$\varepsilon_{cf} = \frac{\varepsilon_{frp} x}{\left(x - d_{frp}\right)} \quad \text{(eq. 4-14)}$$

$$\varepsilon_{si} = \frac{\varepsilon_{frp}\left(x - d_{s1}\right)}{\left(x - d_{frp}\right)} \quad \text{(eq. 4-15)}$$

in which d_{s1}, d_{s2}, d_{frp} represent the height from the top of the compression zone to the center of the tensile bars, compressive bars and FRP laminates, respectively. The height of compressive zone, x can be deduced from eq. 4-5 by an iteration process. A MATLAB program was compiled to conduct the calculation. Once the x is known, the strains in concrete and steel reinforcement can then be deduced by eq. 4-14 and eq. 4-15. The ultimate moment, M_u, can then be calculated by eq.4-16:

$$M_u = k_1 f_{cu} b_c x\left(\frac{h}{2} - k_2 x\right) + \sigma_{s1} A_{s1}\left(\frac{h}{2} - d_{s1}\right) + \sigma_{s2} A_{s2}\left(\frac{h}{2} - d_{s2}\right) + \sigma_{frp} A_{frp}\left(\frac{h}{2} - d_{frp}\right)$$

(eq. 4-16)

And the ultimate load can be obtained by eq.4-17:

$$F_u = 2M_u / \left(L_d + 50\right) \quad \text{(eq. 4-17)}$$

in which L_d is the length from mid-span of the beam to the FRP plate end and (L_d + 50) = length of the beam span. The calculated ultimate loads, strains in concrete and FRP at peak load were listed in Table 3-3. Relatively good agreement was achieved although the effect of

wet-dry cycles was not considered.

4.3.2 Finite element analysis

In the simulation of FRP-strengthened RC beams, the accurate simulation of concrete is the most complex part. Generally, two common approaches are used in FE analysis for the modeling of concrete cracking: (a) the discrete crack approach and (b) the smeared-crack approach. The discrete-crack model simulates a crack as a geometrical identity. However, discontinuities arise from these modeled cracks. Another problem is that the cracks modeled in discrete-crack approach are commonly located along element boundaries which introduce mesh bias (ACI 1997). Several automatic remeshing algorithms were developed for the purpose of solving this problem (e.g., Yang el al. 2003), but it is still a challenge to overcome the computational difficulties caused by remeshing (De Borst et al. 2004). Some studies on FRP-strengthened RC beams were based on the discrete-crack approach, such as Yang et al (2003); Niu and Wu (2005); Pham et al. (2006) and Camata et al. (2007).

In the smeared-crack approach, the cracked concrete is assumed as a continuum, and the deterioration process of cracked concrete is presented by a constitutive relationship. Therefore, there is no need to consider the issues of mesh bias and topology changes in discrete-crack. However, the smeared-crack approach also has its drawbacks. The main problem is the strain localization phenomenon (Chen et al. 2011), which can induce the mesh-nonobjective effect for the models. Among several attempts of solving this problem, crack band model (Bazant and Planas 1998) is one of the most successful solutions. The crack band model relates the size of elements to the constitutive law of concrete, thus the fracture energy becomes independent to the element size. Several models for debonding failure in FRP-strengthened RC members were developed using this approach [Wond and Vecchio (2003); Teng et al. (2004); Lu et al. (2007); Pham and Al-Mahaidi (2005); Coronado and Lopez (2006) Neale et al. (2006); Baky et al. (2007); Kotynia et al. (2008) Nour et al. (2007) and Chen et al. (2010 & 2011)].

4.3.2.1 General

In order to obtain a better understanding of the behavior of FRP flexural strengthened RC beams subjected to wet-dry cycles, Finite Element (FE) simulations were conducted. The method by Chen et al. (2011) was followed in this study. In this model, the behaviors of all components in the beams were represented, including the concrete, steel bars, FRP and the interfaces between them. Only half of the beam was modeled considering its symmetry. The support was modeled with plane stress elements using steel materials, and the mid-bottom of the support was fixed in both *x* and *y* directions. The load was applied onto a steel plate first then spread to the concrete, in order to overcome the stress centralization on the load point in concrete. The boundary on the symmetry axis was defined with symmetric boundary condition.

4.3.2.2 Modeling of Concrete

The concrete is modeled using 2-dimension plane stress elements CPS4 in ABAQUS (2004). The concrete was meshed into very fine elements for purpose of accuracy and good representation of cracks in the form of logarithmic strains in elements. The size of the concrete element was 12.5mm×10mm. The concrete material was defined using the concrete damaged plasticity (CDP) model. The CDP model adopts concepts of scalar damaged elasticity in combination with isotropic tensile and compressive plasticity to represent the inelastic behavior of concrete.

The uniaxial compression and tension behavior of concrete need to be defined in the CDP model. The equation for concrete under uniaxial compression is represented as (Saenz 1964) [Figure 4-12 (a)]:

$$\sigma = \frac{\alpha\varepsilon}{1+[(\alpha\varepsilon_p/\sigma_p)-2](\varepsilon/\varepsilon_p)+(\varepsilon/\varepsilon_p)^2} \qquad \text{(eq. 4-18)}$$

in which

σ and ε =compressive stress and compressive strain, respectively;

α =experimentally determined coefficient representing the initial modulus, which is set to equal to the elastic modulus of concrete E_c. E_c was obtained by using ACI (2008) equation: $E_c = 4730\sqrt{f_c}$, in which f_c is the concrete compressive strength f_c from standard concrete cylinder tests.

σ_p and ε_p were set to f_c and 0.0002 respectively following Chen et al. (2011)

In CDP model, the uniaxial compression stress-strain response is defined linear until the initial yield is reached, which was set as 1/3 of the ultimate stress (Chen et al. 2011). In the plastic regime the response is typically characterized by stress hardening followed by strain softening beyond the ultimate stress.

For concrete under uniaxial tension, the tension-softening curve proposed by Hordijk's (1991) was adopted (Figure 4-12 (b)) which can be represented by the following equations:

$$\frac{\sigma_t}{f_t} = [1 + (c_1 \frac{w_t}{w_{cr}})^3] e^{(-c_2 \frac{w_t}{w_{cr}})} - \frac{w_t}{w_{cr}}\left(1 + c^3\right) e^{-c_2} \quad \text{(eq. 4-19)}$$

$$w_{cr} = 5.14 \frac{G_F}{f_t} \quad \text{(eq. 4-20)}$$

where

w_t =crack opening displacement;

w_{cr} =crack opening displacement when the stress or fracture energy in concrete is fully released;

f_t is the concrete uniaxial tensile strength, which can be obtained by eq. 4-21 (CEB-FIP, 1993):

$$f_t = 1.4\left(\frac{f_c - 8}{10}\right)^{(2/3)} \quad \text{(eq. 4-21)}$$

G_F =fracture energy required to create a stress-free crack over a unit area, which can be

estimated by the following equation (CEB-FIP, 1993):

$$G_F = \left(0.0469 d_a^2 - 0.5 d_a + 26\right)\left(\frac{f_c}{10}\right)^{0.7} \quad \text{(eq. 4-22)}$$

where $d_a = 10mm$ is the maximum aggregate size; and $c_1 = 3.0$ and $c_2 = 6.93$, which were determined from tensile tests of concrete (Chen et al. 2011).

Under uniaxial tension the stress-strain response follows a linear elastic relationship until the value of the tensile strength is reached. Beyond the tensile strength, a nonlinear descending curve was adopted to represent the formation of micro-cracks by lose of stress capacity along with growing local strain.

In the CDP model, the uniaxial tension and compression behavior are user-defined in the form of strain-stress data array obtained by eq. 4-18 and eq. 4-19. The evolution of the yield surface is controlled by two hardening variables, namely compressive equivalent plastic strain $\overline{\varepsilon}_c^{pl}$, and tensile equivalent plastic strain $\overline{\varepsilon}_t^{pl}$, which can be simply represented by the following equations:

$$\begin{aligned} \sigma_t &= \sigma_t\left(\overline{\varepsilon}_t^{pl}\right) \\ \sigma_c &= \sigma_c\left(\overline{\varepsilon}_c^{pl}\right) \end{aligned} \quad \text{(eq. 4-23)}$$

When the concrete is unloaded from any point on the strain softening branch of the stress-strain curves, the unloading response, i.e. the elastic stiffness of concrete is likely to degrade. The degradation of the elastic stiffness is characterized by two damage variables, d_t and d_c, which can be valued from zero to one, representing the change of materials from undamaged state to total loss in strength. For simplicity without losing much accuracy, compression damage in concrete was ignored herein since the loading is monotonic. Definition of damage evolution in tension followed the recommendation of Yu (2006) [Figure 4-12 (c)]:

$$d = 1 - \frac{\sigma_c}{f_t} \qquad \text{(eq. 4-24)}$$

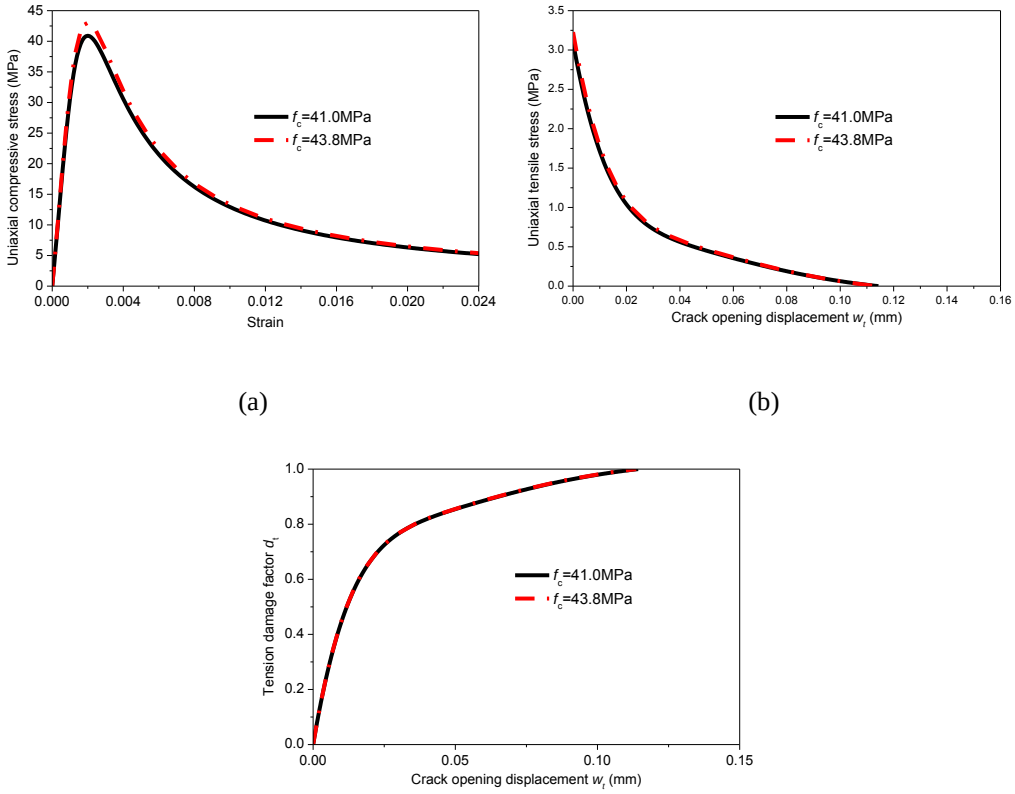

(a) (b)

(c)

Figure 4-12 Descriptions of concrete constitutive models: (a) uniaxial compression; (b) uniaxial tension; (c) tension damage factor d_t

4.3.2.3 Modeling of steel and FRP reinforcements

In this study, both the steel and the FRP reinforcements were modeled with one-dimensional truss elements in ABAQUS. The steel reinforcement was assumed to be elastic-perfectly plastic, while the FRP reinforcement was assumed to be linear elastic-brittle. The length of truss elements was the same with the length of concrete elements (12.5 mm) so that the element nodes on the interfaces were aligned, which improved convergence of the simulation.

4.3.2.4 Modeling of interfaces

SPRING2 elements were used to simulate bond behavior of the interfaces between concrete and steel reinforcement. The spring2 elements can couple a force with a relative displacement acting in one fixed directions between two points. In each couple of adjacent nodes of concrete and steel reinforcement, a pair of spring2 elements was set to define the load-slip behavior in transverse and normal directions respectively. The nonlinear constitutive bond-slip model in CEP-FIP (1993) was used as the spring constitutive model in transverse direction as recommended by Chen et al. 2011. The force-slip relationship in a spring is an element-size based constitutive model since the interfacial load is applied on discrete interfacial nodes instead of the element surfaces. Meanwhile, an elastic spring with relatively large stiffness is defined in the normal direction (Huang 2009). In addition, the stirrups were set embedded into the concrete element, which had few influences on test results, but improved the convergence of the simulation.

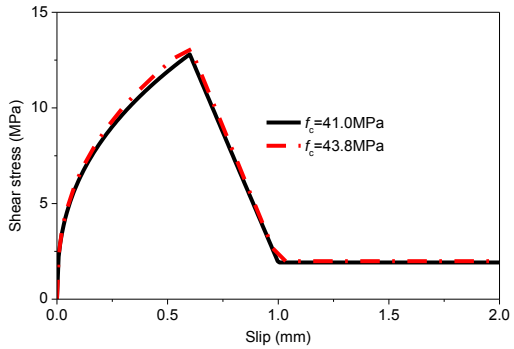

Figure 4-13 Bond stress-slip model for steel-to-concrete interface

The concrete-to-FRP interface was modeled with cohesive elements which are particularly designed for modeling bonded interfaces in ABAQUS. In a two dimensional rectangular cohesive element, four nodes and two directions (normal and transverse) were defined (Figure 4-14). The surface 1-2 and 3-4 were embedded with FRP and concrete element surfaces respectively so that the adjacent FRP and concrete elements are connected. Since the adhesive layer is very thin, modeling the interface with real continuum seems very difficult. In such a case, the traction-separation type cohesive elements were adopted. Instead of modeling the macroscopic material properties, the traction-separation cohesive

element resorts to a fracture mechanics based approach, which can simulate all stages of interfaces, i.e. the initial loading, the initiation of damage and the propagation of damage leading to eventual failure. In this present study, the displacement-stress mode of traction-separation cohesive element is used. The traction and separation (i.e. relative displacement in transverse and normal direction) between two surfaces 1-2 and 3-4 were coupled with stress based on the predefined constitutive laws which were converted from the proposed bond-slip models in Section 3.4.2.3. The following variables were defined: (a) initial stiffness in normal and transverse direction; (b) maximum shear strain that damage initiates; and (c) damage variables versus traction after initiation of damage. The damage variable is used to describe the degradation in the stiffness of cohesive elements, which can vary from 0 to 1, meaning from no loss to eventual loss in stiffness. Due to the nature of debonding mechanics which is mainly concerned with transverse shearing, the damage in normal direction was ignored, and the normal stiffness was defined 100 times of the initial transverse stiffness (Huang, 2009). By such a definition, the cohesive had a nonlinear stress-slip behavior only in shear direction. The stress-displacement behavior was firstly linear until the maximum shear strain criterion was reached. After the initiation of damage, the damage factor increased as a function of traction, which defined a nonlinearly ascending stress-slip curve before the maximum stress was reached and a descending curve beyond the maximum stress. Considering the interfacial contact area in beams was different from the bonded joints in Chapter 3, the width factor (Chen and Teng, 2001) was adopted to calculate the width of the section of cohesive elements:

$$b_{co} = b_{p2} \times \frac{\beta_{w2}}{\beta_{w1}} = 100 \times \frac{\sqrt{\left(2 - b_{p2}/b_{c2}\right)/\left(1 + b_{p2}/b_{c2}\right)}}{\sqrt{\left(2 - b_{p1}/b_{c1}\right)/\left(1 + b_{p1}/b_{c1}\right)}} = 100 \times \frac{0.8944}{1.118} = 80mm$$

(eq. 4-25)

in which b_{co} =width of cohesive element; b_{p1}, b_{p2} =width of FRP sheet/plate in bonded joints and beams, respectively; b_{c1} , b_{c2} =width of concrete prism of bond joints and beams,

respectively; β_{w1}, β_{w2} =width factor of FRP-to-concrete interface of bonded joint and FRP strengthened RC beams, respectively.

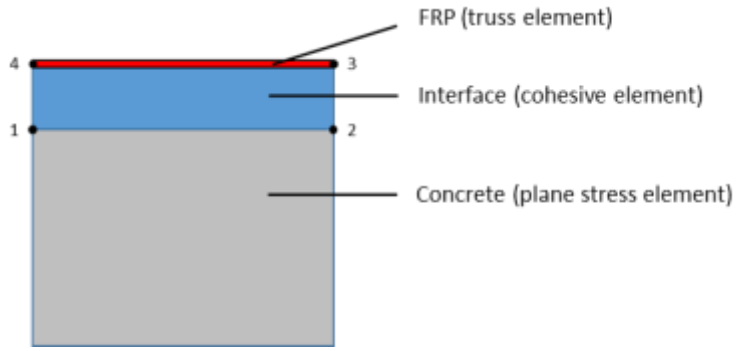

Figure 4-14 Modeling of FRP-to-concrete interface

4.3.2.5 Convergence issues

The beam was simulated using ABAQUS Standard which was an implicit calculation process. Due to the complexity of the model and severe nonlinearity in constitutive models, the convergence issue was a critical problem. Efforts were taken to overcome this difficulty: (a) The determination of the element size of concrete was very important. A fine mesh could produce a precise crack distribution. Chen et al. (2011) reported that if the element size is smaller than 20mm, the numerical results changed very slightly. However, if the element size is too small, there might be convergence issues caused by severe singularity of stiffness matrix after cracking (Lu et al. 2004). As a result, 12.5mm×10mm was used as the size of concrete elements and other elements used matching sizes. (b) An automatic stabilization scheme built in ABAQUS was adopted in static calculation. In this scheme, viscous forces induced by artificial damping were added into the global equilibrium equation so that severe local energy releases can be stabilized. Unfortunately, the value of damping factors varied largely from case to case and was heavily based on experience. Many trials were made to find a suitable value. It was found that using a relatively small damping factor (2E-10) was a

reasonable solution. A smaller damping factor than 2E-10 could cause severe convergence problem; on the contrary, if a larger damping factor was used, the ratio of the energy dissipated by viscous damping to the total strain energy will increased largely, which could affect the accuracy negatively. A visible error using a large damping factor was that the concrete crack was smeared in a very large area, which indicated the energy dissipated to the ambient elements very efficiently. As a result, the strain distribution on the FRP laminate was very smooth, was not consistent with the actual situation. (c) The initial, maximum and minimum increment value in calculation steps, and maximum step numbers as well as cutback times of incrementations were adjusted properly without losing accuracy.

4.3.2.6 Results and discussions

The predicted ultimate loads of beams from FE simulations are listed in Table 4-3. The load-mid-span deflection curves are illustrated in Figure 4-7. (a) Similar to the test results of CP1 and CP2, slight decrease in stiffness and load capacity was found in predicted curves, which was mainly contributed by the decrease in stiffness of the FRP-to-concrete interface. On the other hand, larger fracture energy of the FRP-to-concrete interface improved the ductility of beams, which could be concluded by comparing the deflection of CP1-0m and CP1-8m at peak load. (b) As observed in tests, CS-8m had larger stiffness than CS-0m. however, the difference between predicted CS-0m and CS-8m load-displacement responses varied very slightly although the trend was captured by considering the increase of concrete strength, changes in FRP stiffness and variations in FRP-to-concrete interfacial behavior which were all obtained by previous tests and analysis. Some other factors are proposed to affect the beam's stiffness. The most possible one is the slight corrosion of the steel reinforcement. As reported by Li et al. (2012), if there was no corrosion crack yet in concrete, the bond-slip behavior could be restrained and larger bond strength was observed between concrete and corroded steel reinforcement. Other scholars also reported similar phenomenon for relatively low corrosion levels (e.g. Abdullah et al. 1996, Stanish 1999). As described in Chapter 2, the steel bars were probably slightly corroded after exposure, which was not severe enough to

induce corrosion cracks. As a result, the stiffened concrete-to-steel interface increased the stiffness of the beam. (c) Due to lack of bond-slip model of FRP-to-concrete interface for GS-8m, the load-displacement curve was not simulated. However, by comparing the tested results of GS-0m and GS-8m, it can be inferred that the GFRP-to-concrete might obtained a stiffer bond-slip curve but a lower fracture energy after exposure, which is similar to CS as they were all produced by wet-layup method and had similar matrix structures.

The logarithmic strains (LE) of concrete elements which can indicate the crack behavior are illustrated in Figure 4-18 in the appendix. The cracks distributed similarly with the tested beams.

Predicted strain distributions in FRP at peak load are compared with test results in Figure 4-15. The strains in the constant moment zone increased very fast as the load increases. The maximum strains in FRP sheet/plate were generally located in the constant moment zone, near the toe of the critical cracks. The strain generally descended along the longitudinal axis of the beam. The strains at the free end remained very small even at the final stage of loading. The fluctuations in strain distributions indicated the existence of cracks. If there is a crack in concrete, a peak strain in FRP would appear under the crack. The strains in debonding area of FRP laminate were relatively high and constant which was especially obvious in CP2-0m. The distributions of FRP-to-concrete interfacial stress are illustrated in Figure 4-16. Correspondingly, it can be seen that there were fluctuations of stress under every crack. The stress peak was very low in some areas (except the plate end), which indicated the interface was totally damaged and the FRP laminate was debonded.

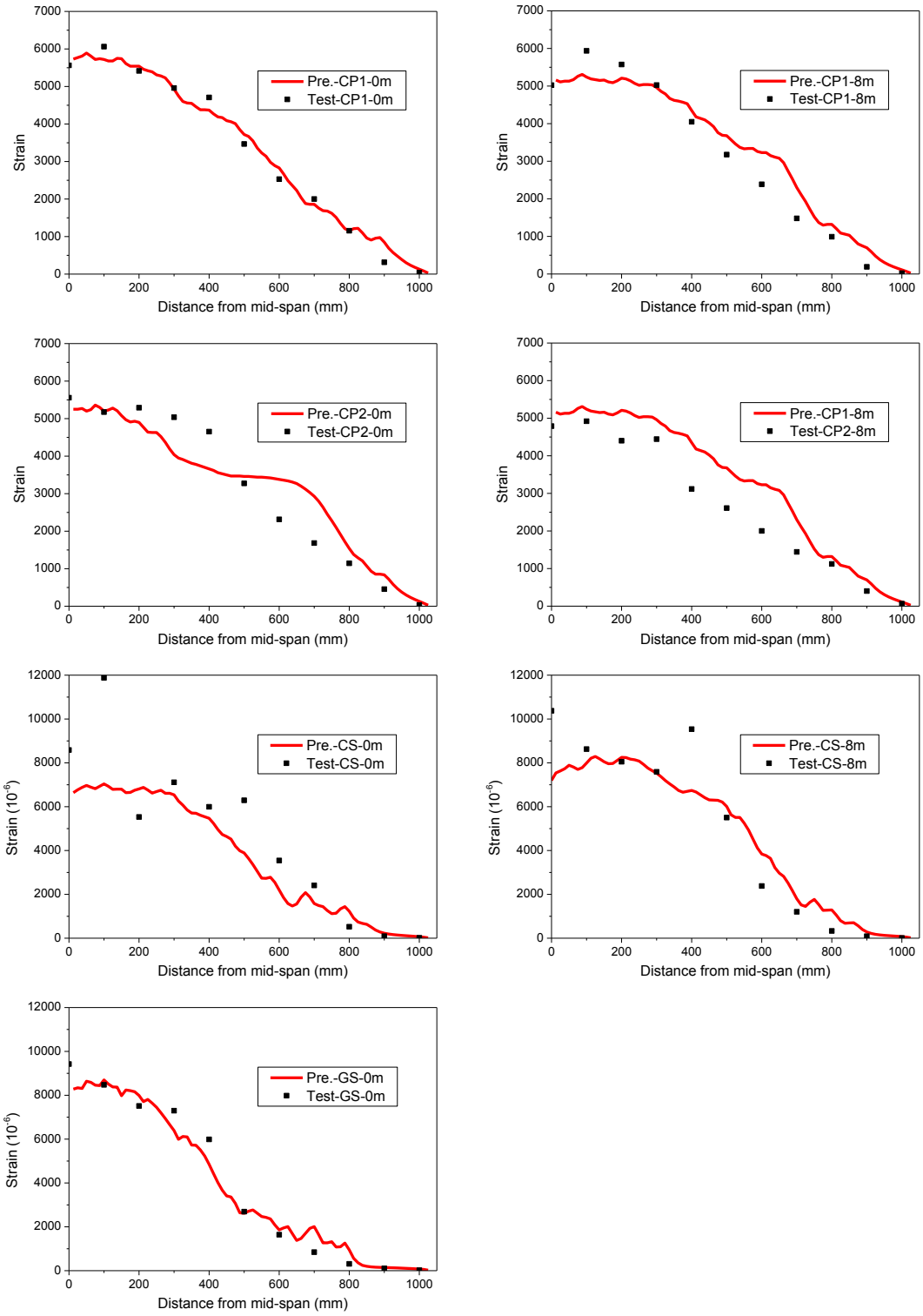

Figure 4-15 Predicted strain distribution in FRP at peak load

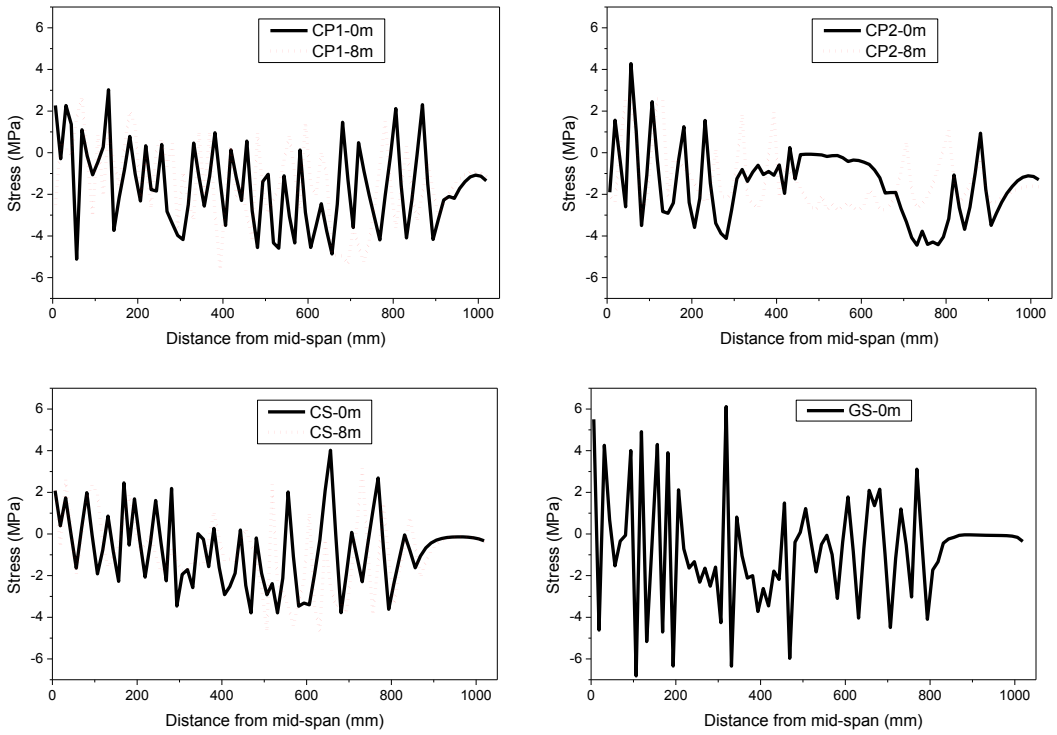

Figure 4-16 Interfacial shear stress of FRP-to-concrete interface

4.4 CONCLUSIONS

This chapter presents an experimental and analytical study on the durability performance of FRP-strengthened RC beams subjected to 8-month wet-dry cycles. The following findings were obtained:

(a) The ultimate loads were 77.65kN, 75.07kN, 56.36kN and 46.53kN for CP1-0m, CP2-0m, CS-0m and GS-0m, respectively. The load capacity showed a positive correlation with the FRP stiffness. CP1 and CP2 with the highest FRP strengthening ratio responded in higher stiffness and larger load capacity, while CS and GS specimens which were strengthened with smaller ratio had lower load capacity but better ductility.

(b) Degradation in load capacities was observed of beams under wet-dry cycles. After 8-months exposure, the ultimate load of beams decreased by 2.6%, 10.8%, 1.4% and 7.9%

for CP1-8m, CP2-8m, CS-8m, GS-8m, respectively. The stiffness of beams slightly decreased in CP1-8m and CP2-8m but increased in CS-8m and GS-8m, which was supposed to be contributed by a combination of many effects, such as aging of concrete, variations in FRP stiffness and FRP-to-concrete interfacial behavior, and possibly corrosion in steel bars.

(c) FE simulations were conducted in present study. The proposed model properly simulated all the components of FRP strengthened RC beams. The simulated results interpreted the mechanism of IC debonding. The models also provided good predictions for the exposure effects of wet-dry cycles by properly considering variations of material and interfacial properties of all components of the beams.

4.5 APPDENDIX

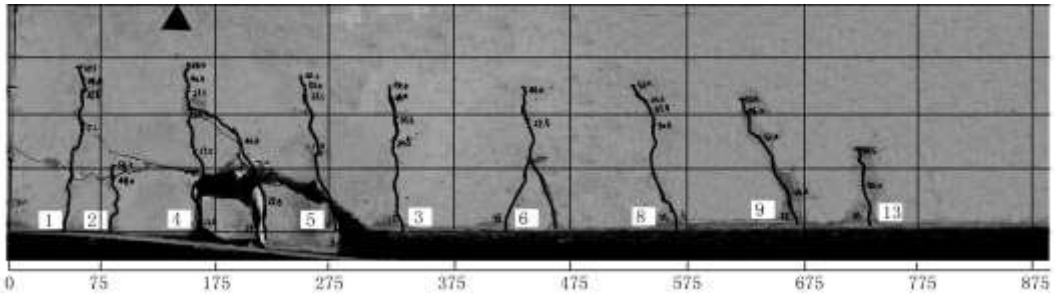

(a)

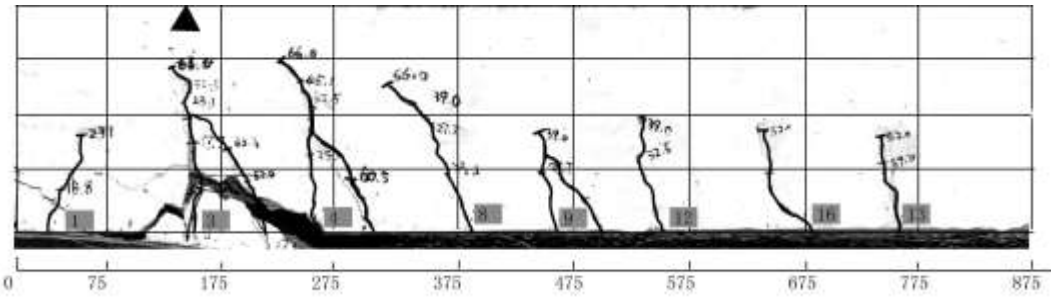

(b)

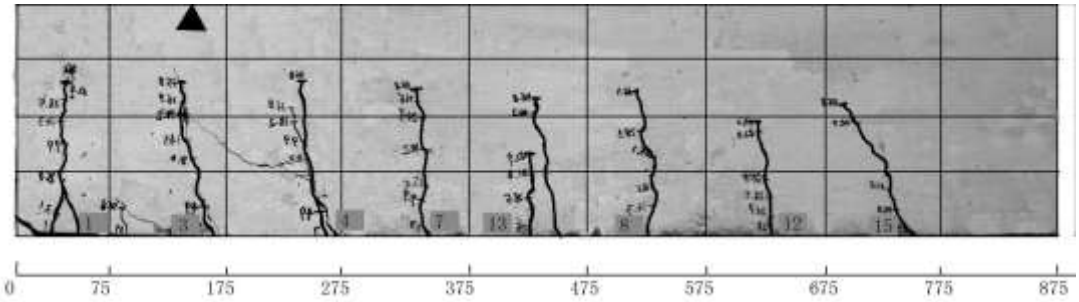
0
75
175
275
375
475
575
675
775
875

(c)

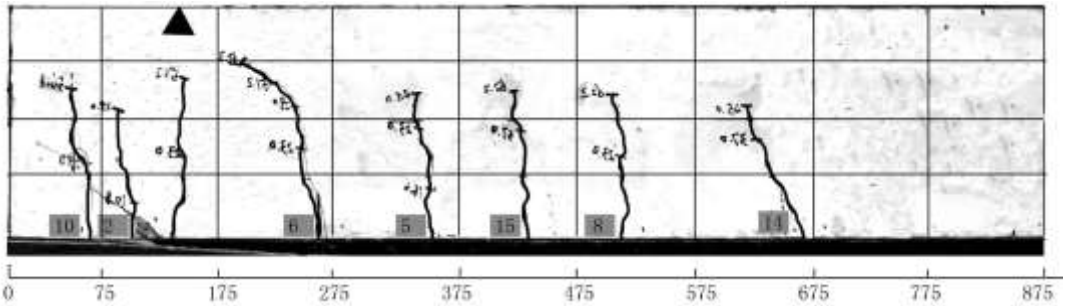
0
75
175
275
375
475
575
675
775
875

(d)

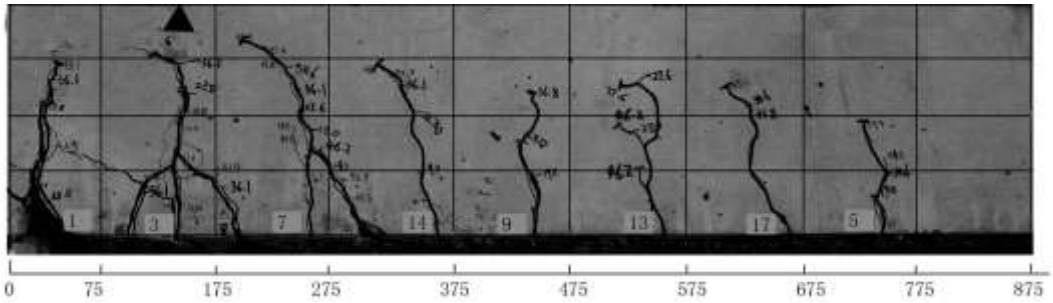
0
75
175
275
375
475
575
675
775
875

(e)

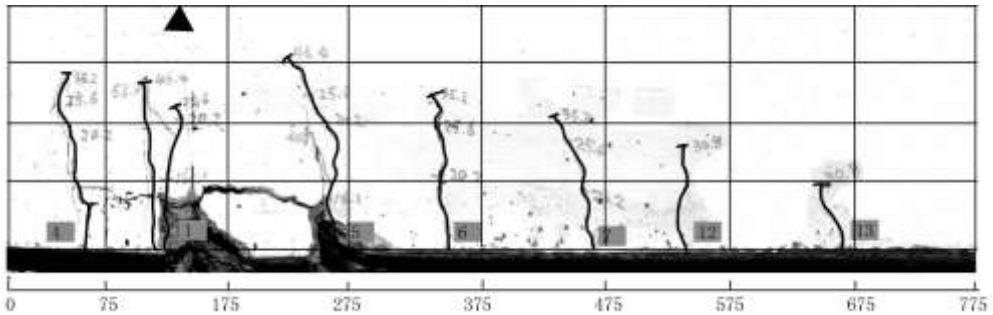
0
75
175
275
375
475
575
675
775

(f)

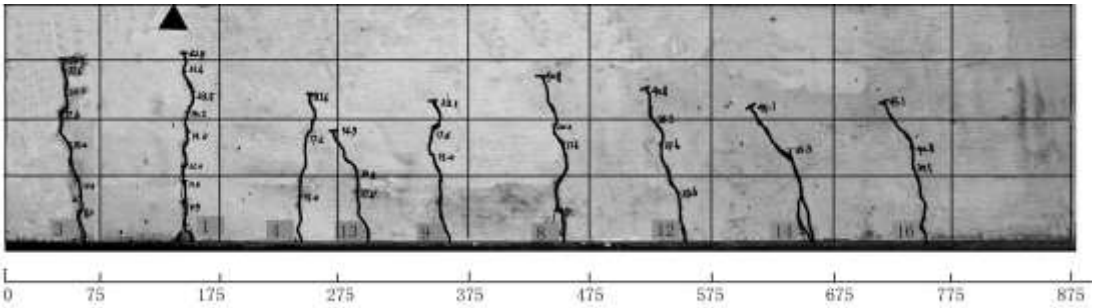

(g)

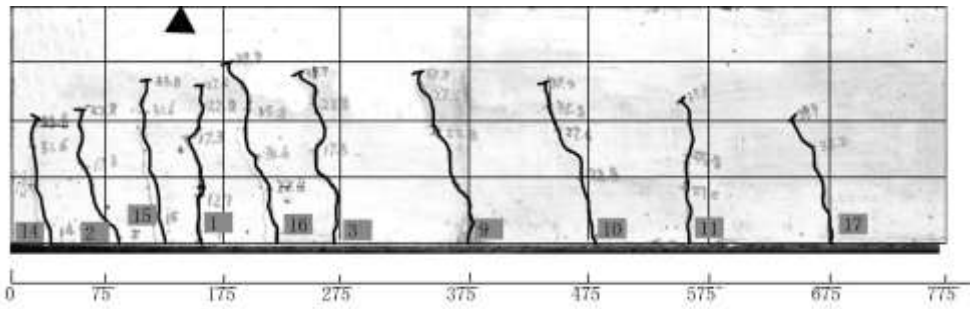

(h)

Figure 4-17 Crack pattern of beams (a) CP1-0m (b) CP1-8m (c) CP2-0m (d) CP2-8m (e) CS-0m (f) CS-8m (g) GS-0m and (h)GS-8m

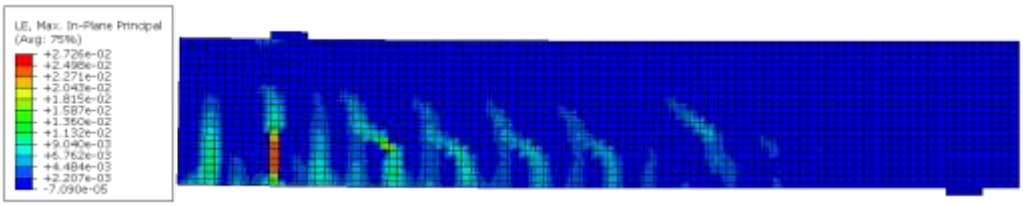

(a)

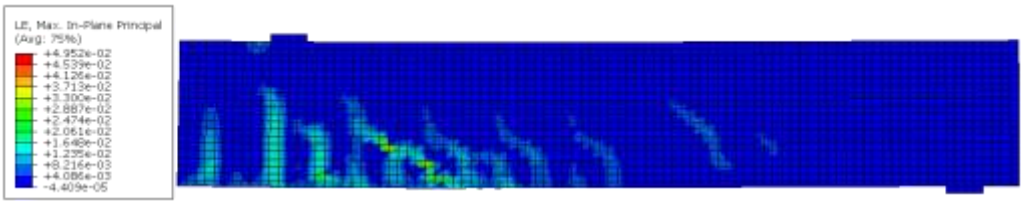

(b)

Figure 4-18 Simulated crack patterns of CP1-0m at (a) steel yielding (b) peak load

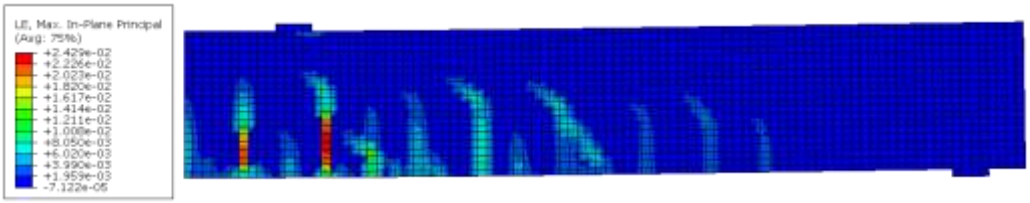

(a)

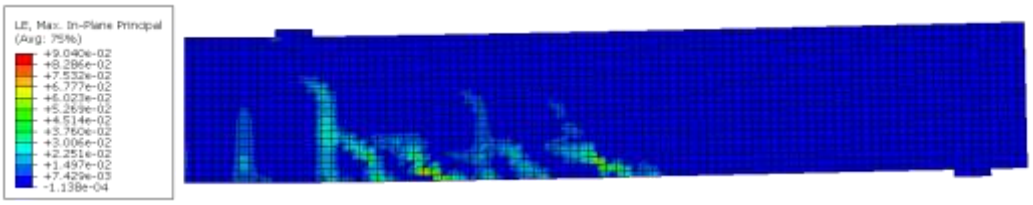

(b)

Figure 4-19 Simulated crack patterns of CP1-8m at (a) steel yielding (b) peak load

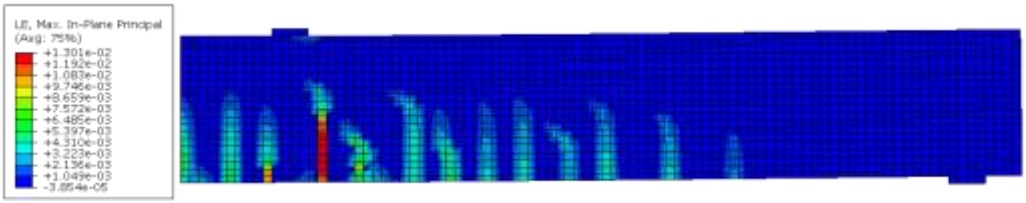

(a)

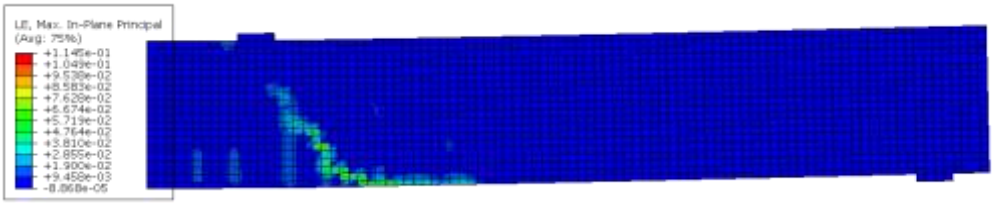

(b)

Figure 4-20 Simulated crack patterns of CP2-0m at (a) steel yielding (b) peak load

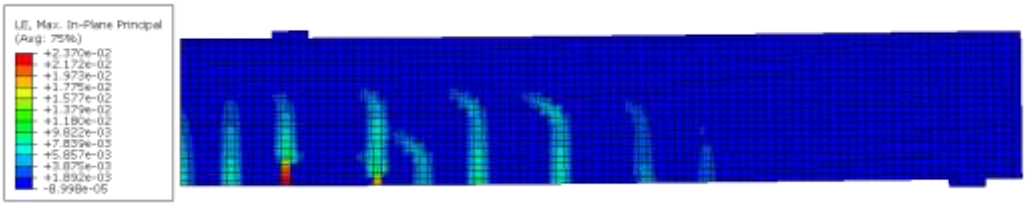

(a)

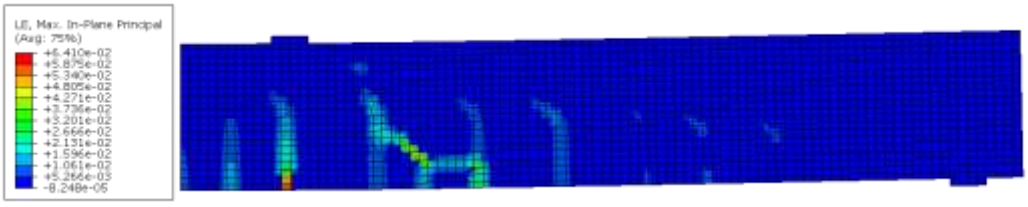

(b)

Figure 4-21 Simulated crack patterns of CP2-8m at (a) steel yielding (b) peak load

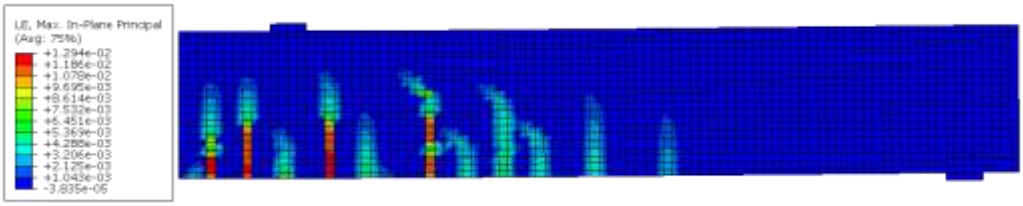

(a)

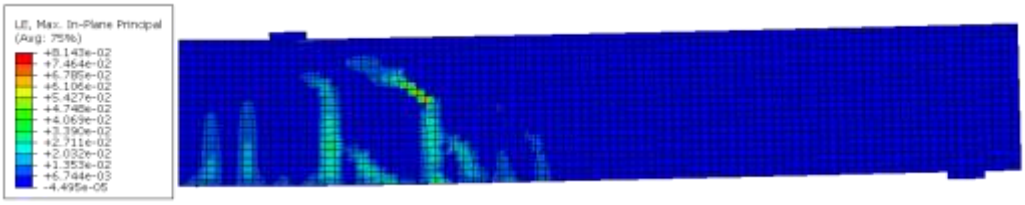

(b)

Figure 4-22 Simulated crack patterns of CS-0m at (a) steel yielding (b) peak load

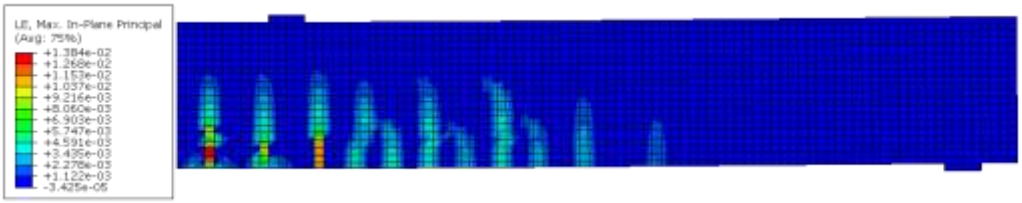

(a)

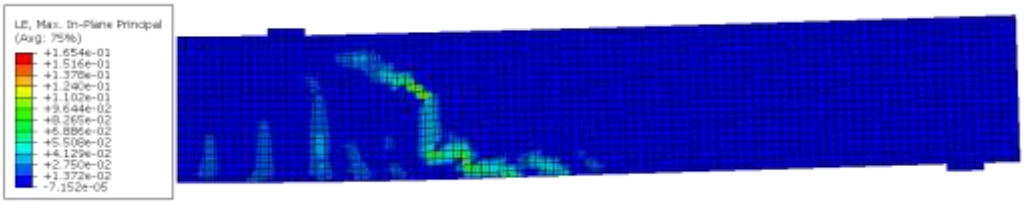

(b)

Figure 4-23 Simulated crack patterns of CS-8m at (a) steel yielding (b) peak load

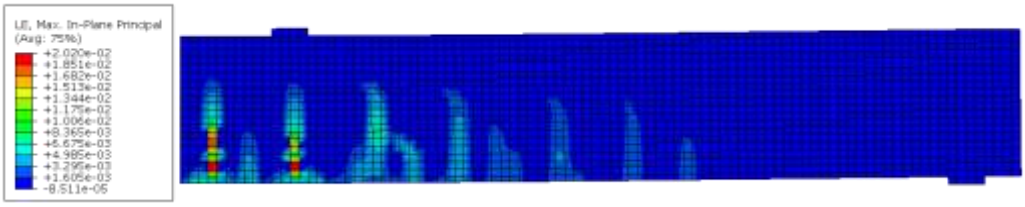

(a)

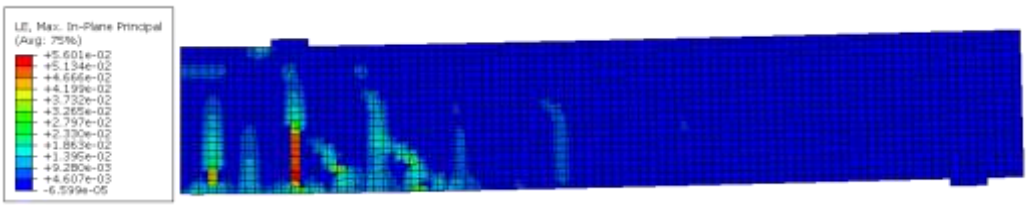

(b)

Figure 4-24 Simulated crack patterns of CS-8m at (a) steel yielding (b) peak load

CHAPTER 5

LONG-TERM BEHAVIOR OF FRP-STRENGTHENED RC BEAMS SUBJECTED TO SUSTAINED LOAD

5.1 INTRODUCTION

The FRP-strengthened structures are subjected to service load throughout their service life. When a FRP-strengthened RC beam is subjected to service load, sustained stress arises inside all the components of the beam, particularly if the FRP strengthening system is pre-stressed or applied to carry additional load. Time-dependent deflections and post cracks are supposed to occur in RC beams subjected to load, which are the dominating serviceability criteria for a flexural RC member. The long-term deflection is mainly contributed by creep and shrinkage of concrete. Moreover, it has been reported by many researchers that creep in the FRP reinforcement could contribute a noticeable proportion of deflection in FRP-strengthened RC beams. The FRP reinforcement is effective in reducing the instantaneous deflection of the beam by increasing stiffness of the beam. Although the creep in FRP composites is very small, which can be neglected within the service life of structures (Ascione et al. 2012); however, the creep in adhesive layer could be significant under service load within a very short period (Choi *et al.* 2007). In the present chapter, the time-dependent behavior of the FRP-to-concrete interface is analyzed first, and then the time-dependent behavior of FRP-strengthened RC beams under sustained load are evaluated through both experimental and analytical study. The ultimate load capacity of FRP-strengthened RC beams is also evaluated after sustained loading tests.

5.2 EXPERIMENT I: SUSTAINED LOAD TESTS

5.2.1 Experiment outline

In the present study, four RC beams in total were tested (Table 5-1). Two sustained load levels, 15.1 kN and 25.2 kN, were evaluated. Under the load levels the concrete cracked but the steel reinforcement did not yield. Two types of FRP systems, CFRP sheet and CFRP plate were used. The dimensions of beams, FRP strengthening schemes are identical with those used in the beams for exposure tests in Section 4.2.1.

Table 5-1 Information of FRP-strengthened RC beams under sustained load

Serial number		Load P	P/P_{max}	Exposure condition	FRP type	FRP stiffness $E_p t_p$ (kN/mm)
SL-1	CS1	15 kN	30%	Indoor (Temperature = 15~30 ℃; Humidity = 50%~95%)	CFRP Sheet	81.5
	CP1		23%		CFRP Plate	198
SL-2	CS2	25 kN	51%		CFRP Sheet	81.5
	CP2		39%		CFRP Plate	198

5.2.2 Test procedures and instrumentations

The set-up is illustrated in Figure 5-1. The beams were placed bottom-to-bottom in pairs, and there were one CS (upper) and one CP (lower) in each pair. The load was applied with a pre-stressed frame at the mid-span of the beams. The frame consisted of two steel rods and two steel beams. The frame was fastened with screw nuts at both ends of steel rods. When the frame was loaded, an oil jack was installed on top of the frame (Figure 5-2).

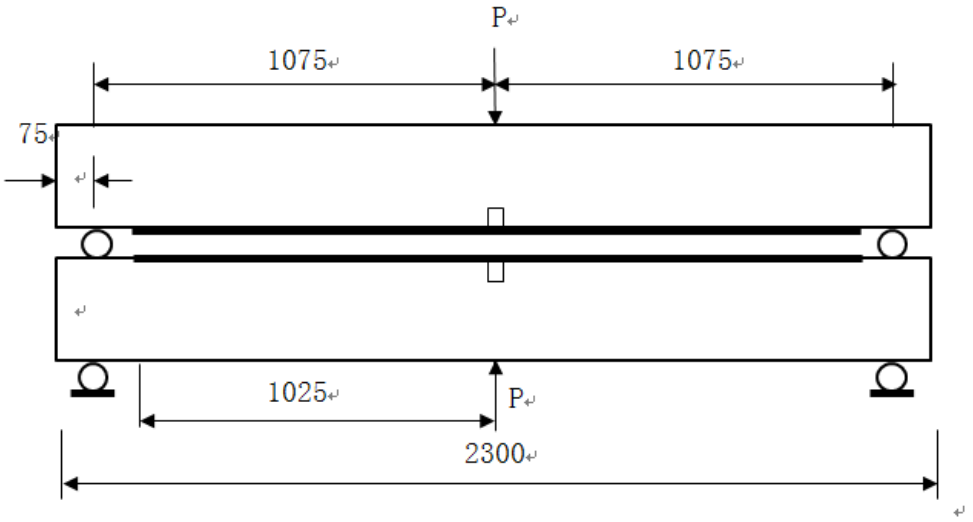

Figure 5-1 Schematic of the test set-up for sustained loading tests

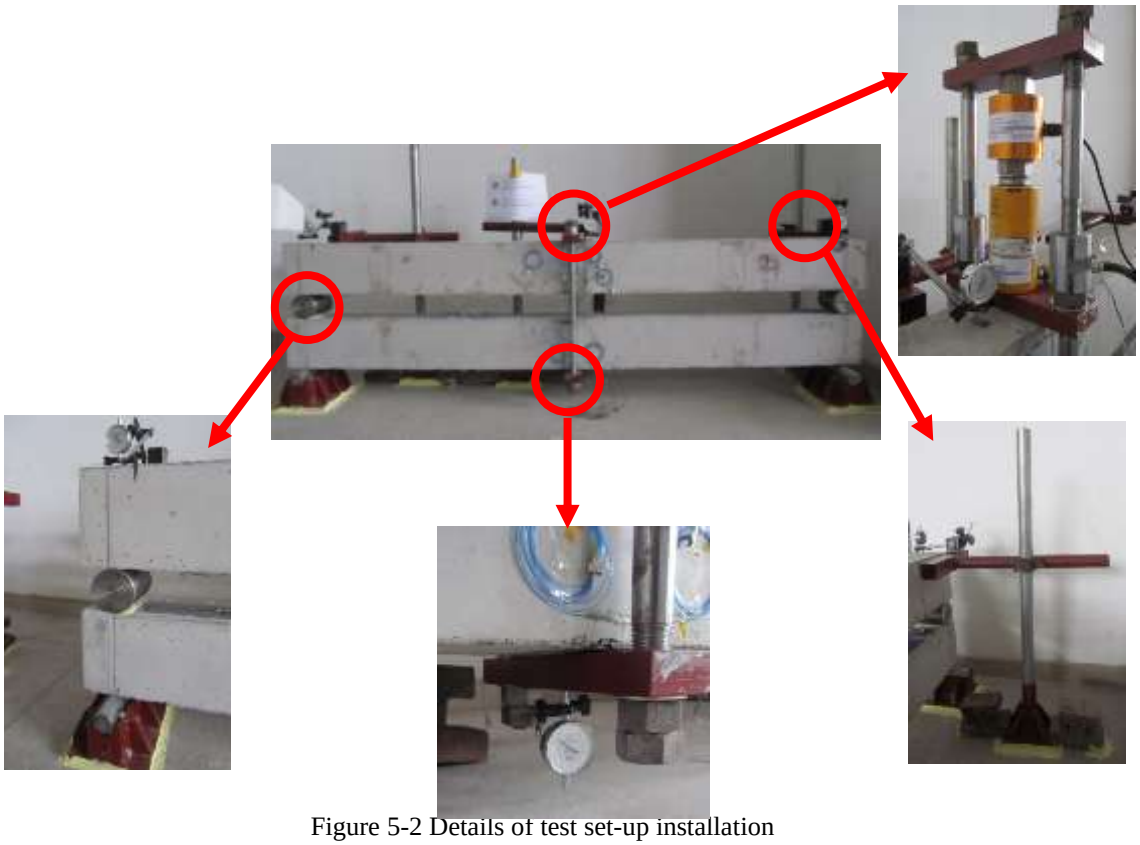

Figure 5-2 Details of test set-up installation

The instruments used in this present test are shown in Figure 5-3. The load was monitored with a load cell. Mechanical dial gauges were installed at the top of the beams and supports. Fiber Bragg Grating (FBG) fiber optic sensors (FOS) were applied to measure strains in FRP and concrete because of their stability and convenience for long-term use. Unlike strain

gauges, status of FBG sensors could be read in absolute values so that it was possible to track data time by time. FBG sensors were attached on the FRP laminate at spacing of 100 mm. An FBG sensor was attached on each side of the beam, 25mm downward from the top surface of the compressive zone. FBG sensors were also applied on the pre-stressed steel rods so as to monitor the load level. Sensors were read by an optical sensing interrogator. Each sensor has an inherent wavelength; when the fiber was tensioned, the sensor's inherent wavelength would change accordingly. The relationship between the increment of wavelength and strain can be represented as (Zhu, 2009):

$$\frac{\Delta L_n}{L_n} = \psi_\varepsilon \Delta\varepsilon + \psi_T \Delta T \qquad \text{(eq. 5-1)}$$

in which

L_n =reference wave length of *n*th gating under a reference temperature;

ΔL_n =difference in wave length between present reading and reference value;

ΔT = difference in temperature between present and reference time;

$\Delta\varepsilon$ =difference in strain; and

$$\psi_\varepsilon = 0.783$$
$$\psi_T = 6.78E-6 \qquad \text{(eq. 5-2)}$$

Therefore, by testing the difference in wave length of sensors with temperature compensation, the strains in the test point can be obtained accordingly.

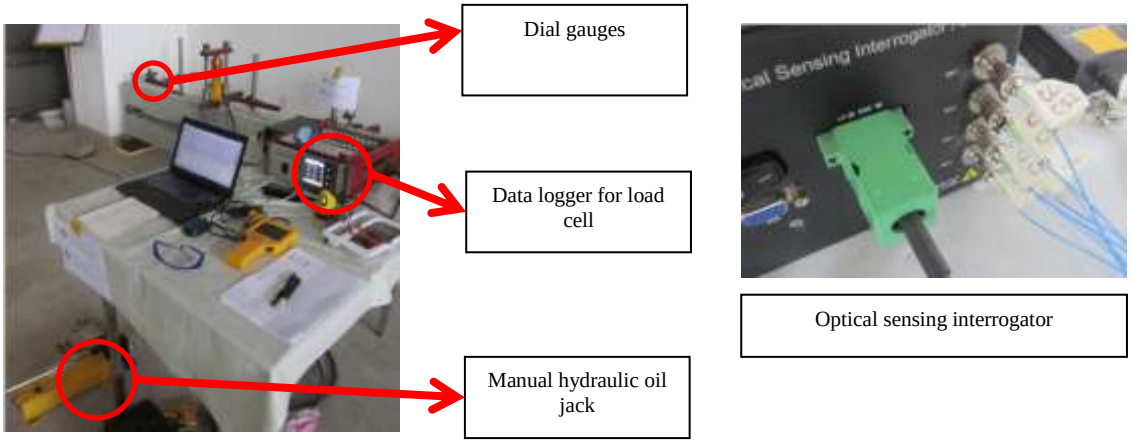

Figure 5-3 Details of test instrumentation

The application procedures of FBG sensors are as follows: (a) the sensor was tensioned at the initiation. The FBG sensor only works in tension within the range of 0-7 nm in the wavelength according to the manufacture. In present tests, 3nm offset was set for compression test point; while for tensile test point, 0.5 nm offset was set to provide as long work range as possible; (b) after being tensioned to required state, the fibers were fixed with quick-drying adhesive onto the test points; (c) once the fibers were fixed, the fibers were coated with epoxy coating adhesive, which could protect the fiber sensor against damage and corrosion and force the sensor deforming simultaneously with the tested surface.

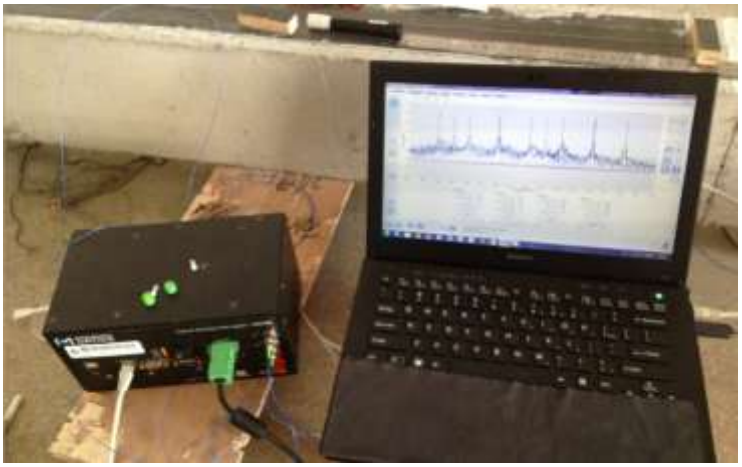

(a)

(b)

(c)

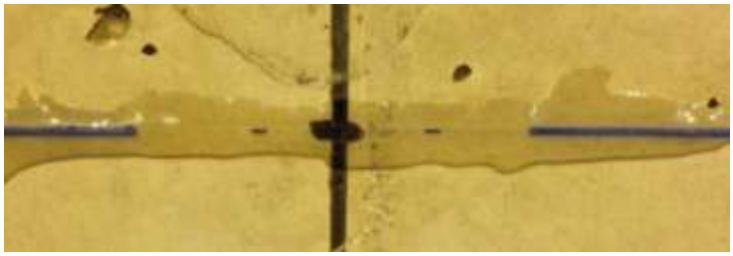

(d)

Figure 5-4 Preparation of FOS: (a) pre-tensioning; (b) fixing; (c) surface coating; (d) completion

Loading procedures are shown in Figure 5-5. The beams were firstly loaded to required load levels (i.e. 15 kN or 25 kN) using the oil jack, and the strains in steel rods, ε_1 and ε_2 were recorded as references. The beam was then loaded 5% higher than the required load; afterwards, the frame was fastened with screw nuts. This process was to offset the stress loss in rods when the oil jack was released. After the release of the oil jack, the strains in rods, ε'_1 and ε'_2, were checked and compared with reference strains. It was required that the difference was within 5% between the sum of strains $(\varepsilon'_1+\varepsilon'_2)$ and reference strain $(\varepsilon_1+\varepsilon_2)$. If the requirement was not met, the load procedure was repeated. As the beam deflected, the stress in rods decreased gradually. The strains in the steel rods were checked from time to time to make sure the load was always above 85% of the required load level; once the threshold was reached, the loading procedure was conducted to regain the load to the required level. It has been found that at the initiation of the test, the load dropped quickly and reloading is relatively frequent. As time went on, the frequency of reloading reduced gradually. The time spacing between two reloading processes were 2 day at the initiation and 20 days after 9 months, respectively.

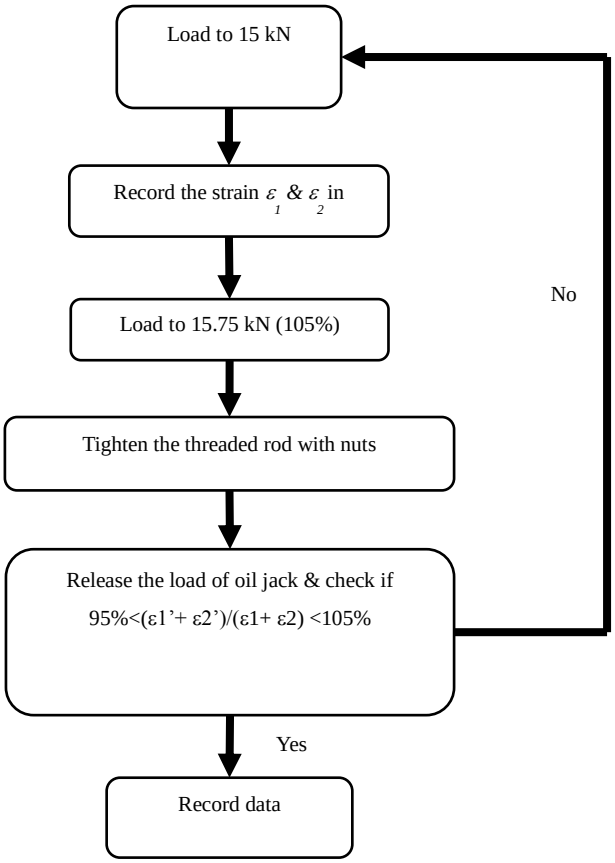

Figure 5-5 Procedures for implemeting the sustained load

5.2.3 Test observations

Test and normalized total deflections in beams are shown in Figure 5-6 and Figure 5-7, respectively. After initial loading, the instantaneous deflections in CS1, CP1, CS2 and CP2 were 2.96mm, 2.65mm, 6.18mm and 4.46mm, respectively. It can be seen from the curves that the deflection increased very quickly at the beginning of loading; with the development of time, the increase of deflections decelerated. After the beams were loaded for 150 days, deflections in beams became relatively stable. The time dependent deflections after 299 days

in CS1, CP1, CS2 and CP2 were 7.50mm, 6.88mm, 9.28mm and 7.66mm, which were 2.53, 2.60, 1.50 and 1.72 times the initial deflections, respectively. It can be seen that: (a) the higher the load level, the larger instantaneous and time-dependent deflections; however, higher load led to a smaller ratio of time-dependent to instantaneous deflections. This is mainly due to the increase in instantaneous deflection was larger than the increase in time-dependent deflection with the increase of load. Similar phenomena were also observed by other studies (e.g., Tan et al. 2006). (b) Under the same load level, higher FRP stiffness led to lower instantaneous and time-dependent deflections. Moreover, with the increase of load, the contribution of FRP in reducing the time-dependent deflections became more significant. After 9 months, the time-dependent deflections of CP1 and CP2 were 8.3% and 17.5% less than CS1 and CS2, respectively. Lastly, the larger the FRP stiffness, the larger the ratio of the time-dependent to instantaneous deflection. This phenomenon became less significant with the increase of load level.

Table 5-2 Deflection of FRP strengthened RC beams

Beam	Instantaneous deflection (mm)	Time-dependent deflection (mm)	Total deflection (mm)	Time-dependent/ instantaneous deflection
CS1	2.96	7.50	10.46	2.53
CS2	2.65	6.88	9.53	2.60
CP1	6.18	9.28	15.46	1.50
CP2	4.46	7.66	12.12	1.72

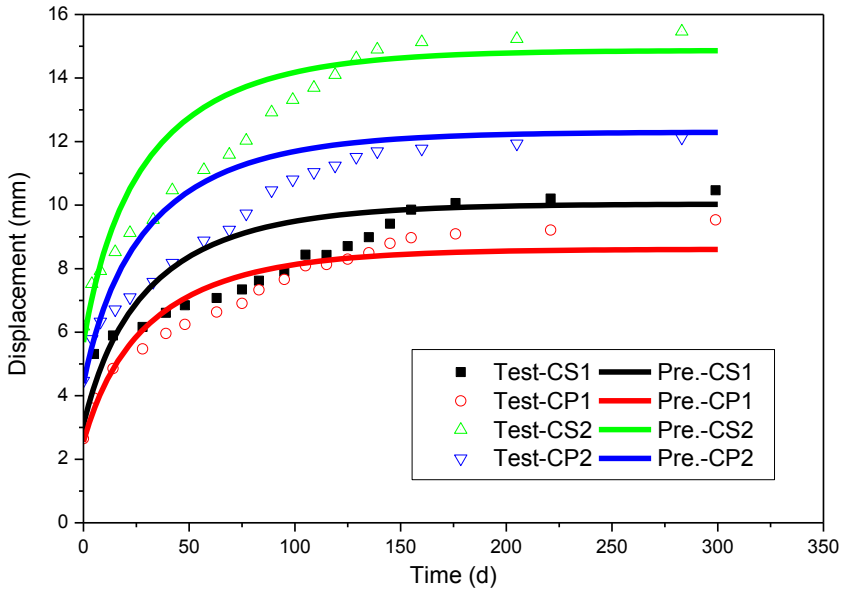

Figure 5-6 Test and predicted time-dependent mid-span deflection

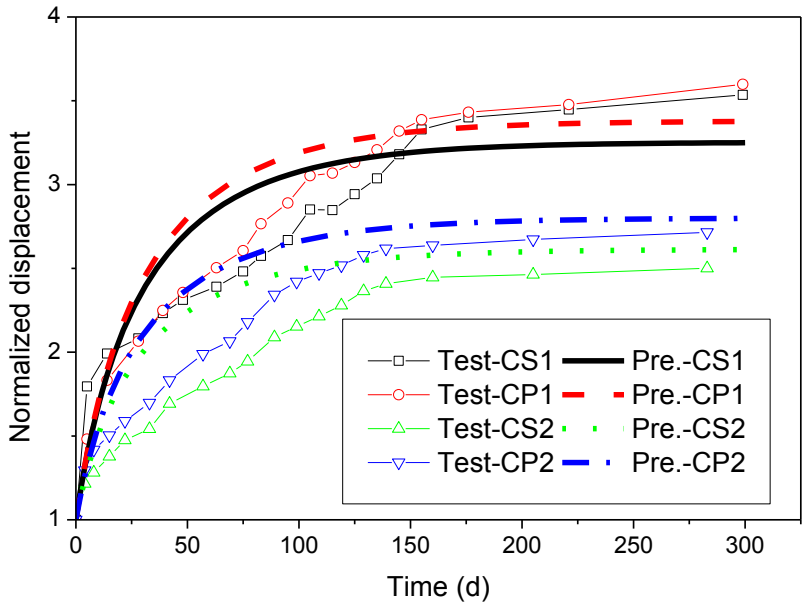

Figure 5-7 Normalized time-dependent mid-span deflection

Strain evolutions in concrete and FRP laminates over time are illustrated in Figure 5-8 and Figure 5-9, respectively. It can be seen that strains in concrete and FRP laminates increased fast in the early stage and became stable at the end. By the end of sustained load test, the concrete compression strain increased by 309%, 279%, 250% and 200% and the maximum strain in FRP increased by 242%, 272%, 238% and 175% in CS1, CP1, CS2 and CP2, respectively.

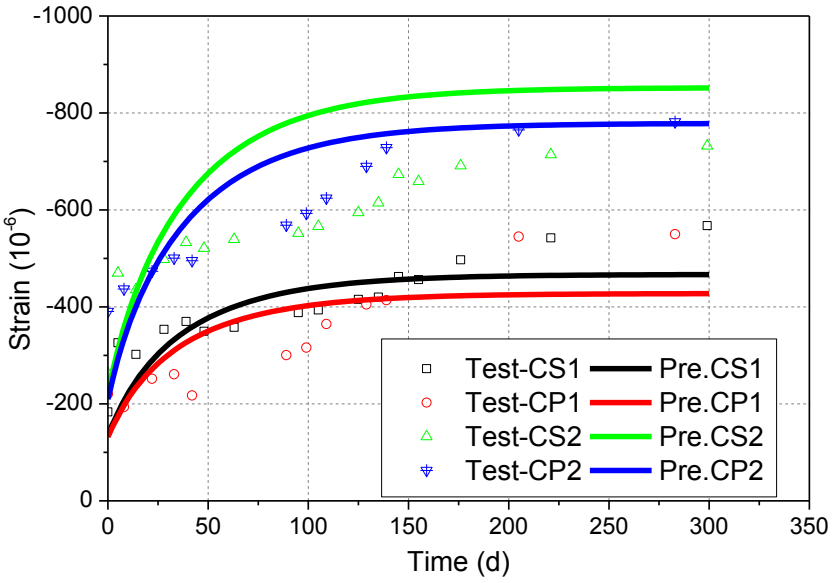

Figure 5-8 Evolutions of compressive strains in concrete at the mid-span of different beams under sustained load

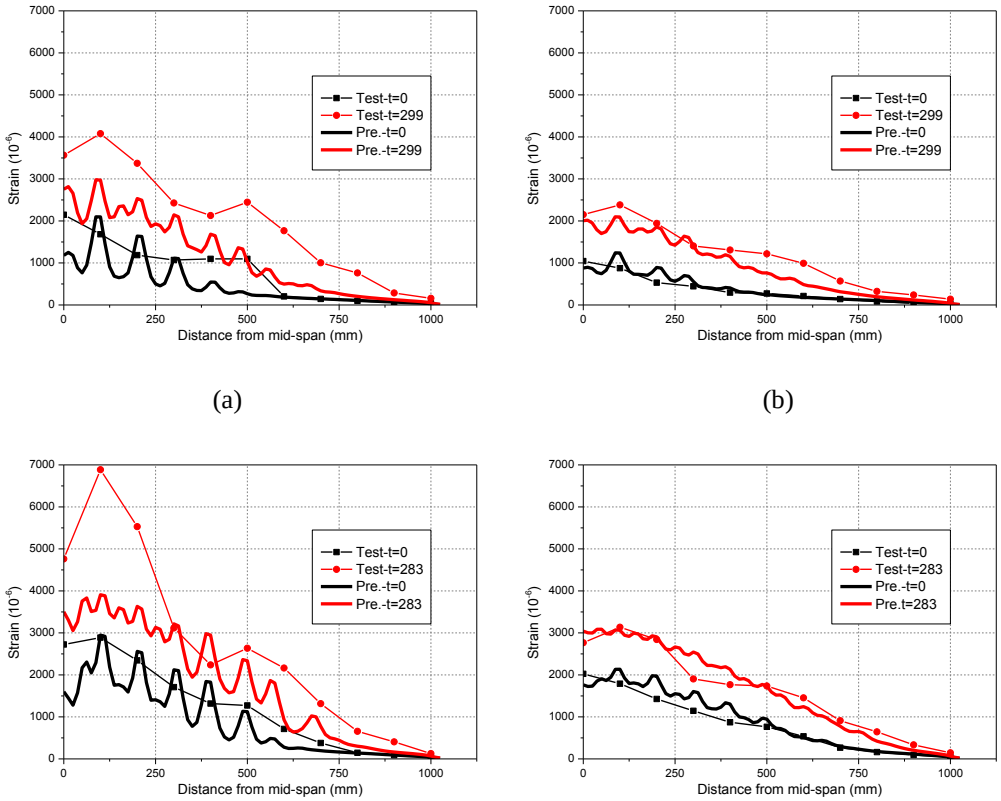

Figure 5-9 Time-dependent strain evolutions in FRP sheets/plates in different beams under sustained load (a)CS-15kN (b) CP-15kN (c) CS-25kN (d) CP-25kN

5.3 FINITE ELEMENT SIMULATIONS ON SUSTIANED LOAD TESTS

5.3.1 Modeling of FRP-strengthened RC beams

FE simulations were conducted for predicting the behavior of FRP-strengthened RC beams subjected to sustained load. The FE simulations were on the basis of the models used in Chapter 4; however, additional modifications were made in order to achieve the simulation of time-dependent behaviors of beams (Table 5-3).

Table 5-3 Details of FE models for FRP-strengthened RC beams under sustained load

Material	Element	Material Property
Concrete	2-D plane stress element	Damaged plasticity + nonlinear creep behavior
Steel	Truss	Elasto-plastic
Concrete-steel interface	Spring element	Nonlinear bond-slip model
FRP composites	2-D truss element	Elasto-brittle
FRP-to-concrete interface	Traction-separation cohesive element	Elastic + nonlinear creep

5.3.1.1 Outline

The dimensions of beams were identical with the modeled beams in Chapter 4. Half span of the beam was modeled by taking advantage of symmetry. The support was modeled with plane-stress elements and steel materials, and the mid-bottom of the support was fixed in 1 and 2 directions. The load point was covered by a steel plate to overcome the stress centralization. The boundary at the mid-span was defined with symmetric constraint condition.

5.3.1.2 Modeling of creep behavior in FRP-to-concrete interfaces

The creep in FRP-to-concrete interface was firstly modeled so that it can be implemented in the simulation of beams. Due to lack of experimental explorations, the tests by Choi et al. (2007) were used. In this test, the FRP bonded concrete joints were loaded by a sustained load, forcing the interface to shear slip over time. An FE model was built to simulate this process (Figure 5-10). In the FE model, the dimensions of the beam model followed the tested beams. The concrete joint was modeled with the 2-D plane-stress model. The concrete material was modeled using the concrete damage plasticity model. The FRP reinforcement was modeled with 2-D truss elements with elasto-brittle material property. The creep in FRP composites and concrete tension was neglected because they were very limited (Choi et al. 2007; Ascione et al. 2012). The interface was modeled using traction-separation cohesive elements. The bond stress-slip behavior was defined linearly considering the relatively low stress state in the creep test. The interfacial creep coefficient was presented by the following

equation (Choi et al. 2007):

$$\phi(t,t_0) = \phi_u(t_0)\left[1-\exp\left(-t/\tau^*\right)\right] \quad \text{(eq. 5-3)}$$

where

$\phi(t,t_0)$ = creep coefficient

$\phi_u(t_0)$ =ultimate creep coefficient at infinite time

τ^* =retardation time denoting the time when 63% of the creep has occurred.

$\phi_u(t_0)$ and τ^* are constant parameters which can be obtained from tests. According to Choi et al. (2007)'s experimental exploration, $\phi_u(t_0)=1.17$ and $\tau^*=43.3$ was used for the FRP-to-concrete interface bonded with epoxy adhesives. By knowing creep coefficient, the time-dependent effective shear modulus of the interface could be deduced with the following equation:

$$\overline{E} = \frac{\sigma}{\varepsilon} = \frac{\sigma}{\varepsilon_{cr}+\varepsilon_e} = \frac{E}{1+\phi} = \frac{E}{1+\phi_u(t_0)\left[1-\exp\left(-t/\tau^*\right)\right]} \quad \text{(eq. 5-4)}$$

in which

$\overline{E}$ =effective shear modulus of the interface;

ε_{cr} =creep strain in the interface; and

ε_e =elastic strain in the interface.

The time-dependent effective interfacial shear modulus was realized by using an ABAQUS subroutine: the User Defined Field (USDFLD). ABAQUS subroutines are composed in FORTRAN, which is saved as .for files and can be called by ABAQUS during calculation processes. Users can define the value of a field as a function of specified variables through the USDFLD. Herein the USDFLD was used to define the shear modulus as a function of step time. At the beginning of every time increment, ABAQUS updated the interfacial shear modulus corresponding to the step time as defined in USDFLD and then calculated the new equilibrium equation. The predicted slip-time curve is illustrated in Figure 5-11, which

matches well with the original test results. Figure 5-13 shows distributions of maximum principal stress in concrete before and after creep. The creep in the interface induced stress redistribution in concrete. In this case, a more significant stress concentration was found at the both ends of FRP laminate.

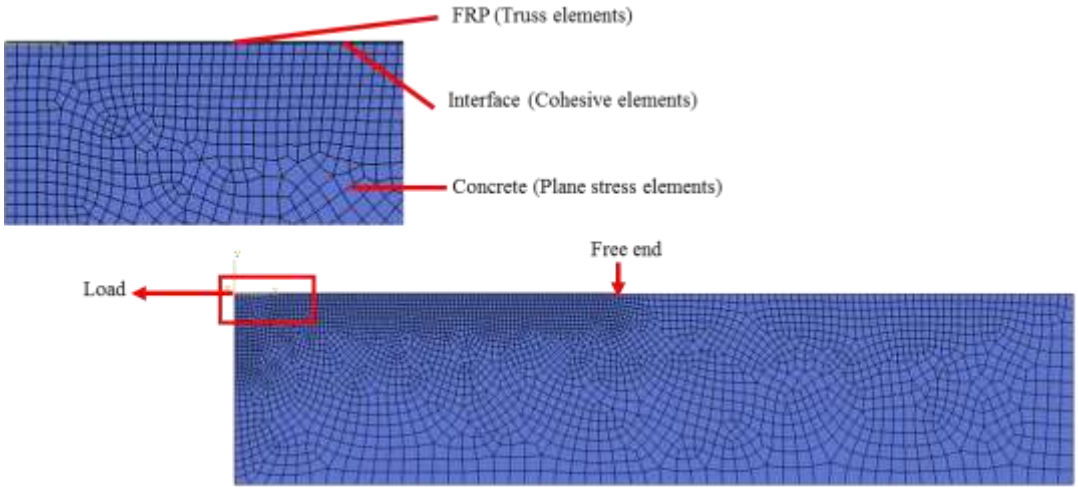

Figure 5-10 Schematic of creep test on FRP bonded concrete joints

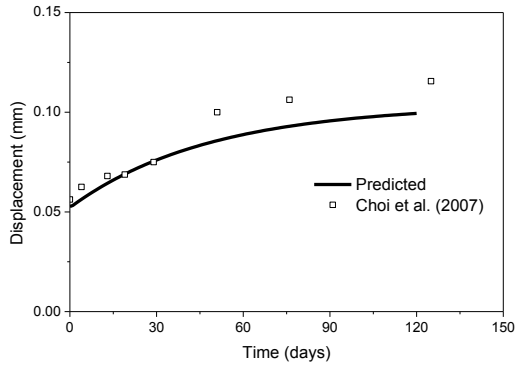

Figure 5-11 Predicted versus test slip-time curves

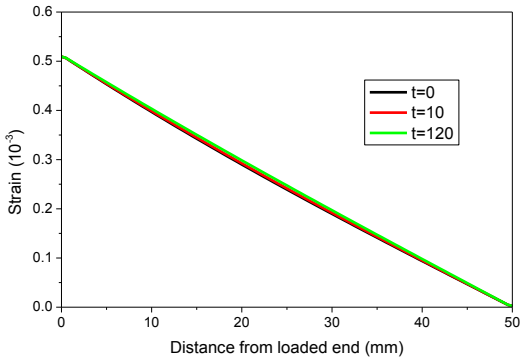

Figure 5-12 Predicted strain distributions in the FRP laminate

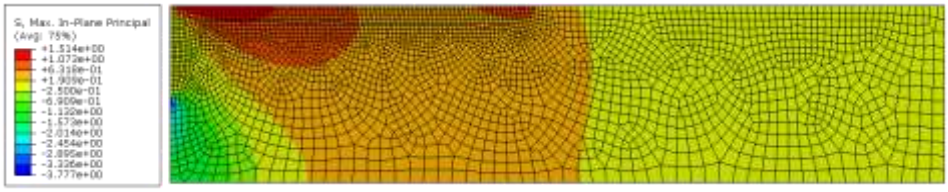

(a)

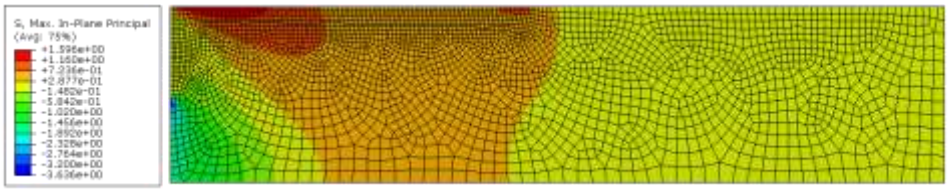

(b)

Figure 5-13 Predicted stress distribution in concrete (a) t = 0 day (b) t = 120 days

The linear-viscous FRP-to-concrete interface model was implemented to the beam models. The initial shear modulus was defined as the initial modulus of the bond-slip model proposed in Chapter 3 since the shear slip was very small (less than 0.05mm) based on analytical observations.

5.3.1.3 Modeling of creep behavior in concrete

The concrete creep law can be represented as (Choi et al. 2010):

$$\dot{\varepsilon}_{cr,i}(t) = \frac{1}{E_c \bar{\tau}} \phi_u \sigma_i \exp\left(-t/\bar{\tau}\right) \qquad \text{(eq. 5-5)}$$

where

$\dot{\varepsilon}_{cr,i}(t)$ =component creep strain rate at time t;

E_c =concrete Young's modulus;

$\bar{\tau}$ =retardation time, denoting the time when 63% of the creep has occurred, which can be obtained from tests;

ϕ_u =creep coefficient, which can be obtained from tests;

σ_i =stress component applied at time t

Following Choi et al. (2010), each component of creep strain rate was assumed to develop

only from the corresponding stress component. The tension creep component was set to zero since it's very limited. Assuming that the strain rate is constant in each increment, the incremental creep strain can then be obtained by multiplying the strain rate with the length of time increment. At the beginning of each increment, the creep strain increment was calculated for each integration point. The total strain of an integration point was obtained by summing the incremental creep strain and initial strain. New equilibrium could then be obtained with the updated strain state.

The modeling of creep in concrete was realized by using the subroutine USDFLD and UXPAN. The function of USDFLD was used to retrieve the stress components and step time as state-dependent variables. The creep strain increment was then calculated by eq.5-5 in UXPAN and output as expansion strains in ABAQUS.

5.3.1.4 Definition of calculating procedures

Two steps were defined. Step 1 was defined to apply initial loading, in which an instantaneous deflection occurred but the creep was restrained; step 2 was used to simulate time-dependent behavior. In this step, the load remained constant and the step time was set equal to real time. Creep in concrete and FRP-to-concrete interface was activated. The time increment of step 2 was set as small as 24 hours for satisfactory accuracy based on trial calculations.

5.3.2 Results and discussions

To evaluate the creep in concrete, proper determination of the variables in the creep model of concrete are necessary. In Choi et al. (2010)'s study, $\bar{\tau} = 365$ and $\phi_u = 2.65$ were recommended based on a reference RC beams creep test for 2500 days. Unfortunately, due to lack of reference tests in present study, it is difficult to determine the value of these two variables directly from tests. It has been found by Choi et al. (2010) that the variables varied

largely according to many factors such as the age and components of the concrete, temperature and humidity. Therefore, it is not reasonable to use the variables directly obtained from other tests. Under these circumstances, a series of trial calculations were conducted to find the most suitable values based on the least square method. As a result, when $\bar{\tau} = 49$ and $\phi_u = 9.4$, the simulations can give closest predictions for the test results. The simulated mid-span deflection-time curves are illustrated in Figure 5-6, which could give good predictions for the test results. The predicted strain evolutions in concrete and FRP are also shown in Figure 5-8 and Figure 5-9, respectively. A relatively good agreement was achieved. The stress distributions in beam CP1 are illustrated in Figure 5-14, which indicate the stress redistribution in beams during loading history.

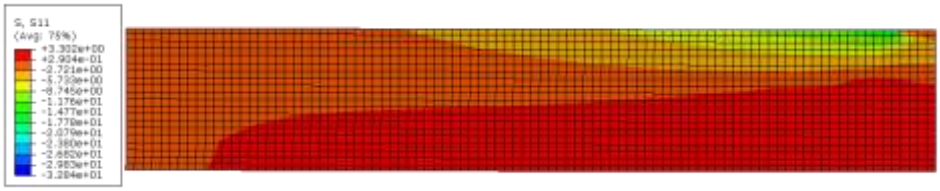

(a)

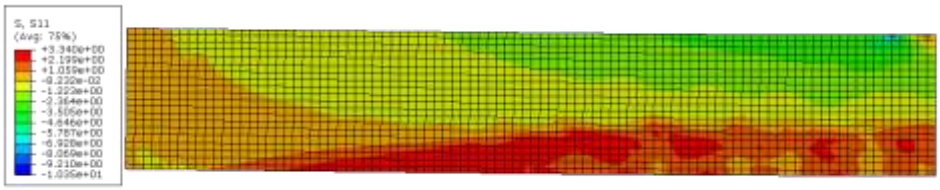

(b)

Figure 5-14 Stress distribution in concrete of beam CP2 (a) t=0 (b) t=300

The contribution of FRP reinforcement was explored using a parametric study. Taking CS1 as example, the long-term performance under the following three cases were evaluated: (a) CS1; (b) CS1 without adhesive creep and (c) RC beam without FRP reinforcement. The predicted displacement-time curves are shown in Figure 5-15. The following can be observed: (1) The initial deflection of (a) and (b) were the same and 48% smaller than (c); (2) the ratios of time dependent deflection to instantaneous deflection in (a) (b) and (c) were 3.62, 3.47 and 3.39, respectively. The ratio of long-term to instantaneous deflection in FRP strengthened RC beams was larger than those of the beam without FRP reinforcement; at the

meantime, the ratio is larger if adhesive creep is considered.

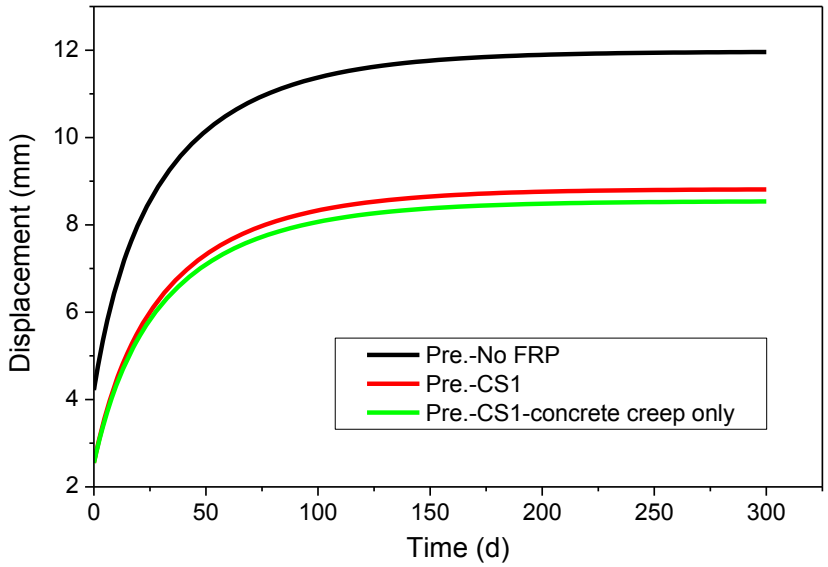

Figure 5-15 Predicted displacement-time responses

5.4 EXPERIMENT II: DESTRUCTIVE BENDING TEST

After being loaded for about 300 days, the beams were loaded to damage using four-point-bending tests to check their ultimate load capacities. The load scheme was identical to the bending tests in Chapter 4. Figure 5-16 illustrates the load-displacement curves of these four beams. It can be seen that (a) the initial stiffness of beams decreased largely since they had been loaded to crack in previous sustained load tests. The curves remained almost linear until the tensile steel reinforcements yielded; (b) the curves of SL-1 and SL-2 beams with the same type of FRP reinforcement were identical, indicating that the different load levels had little different influences on the load-deflection responses of beams; (c) After being loaded for 9 months, severe deformation occurred in beams and was not fully recovered although the sustained load was released. This caused the reduction in ductility of beams, especially in CS1 and CS2; (d) however, the ultimate load capacities were not largely affected.

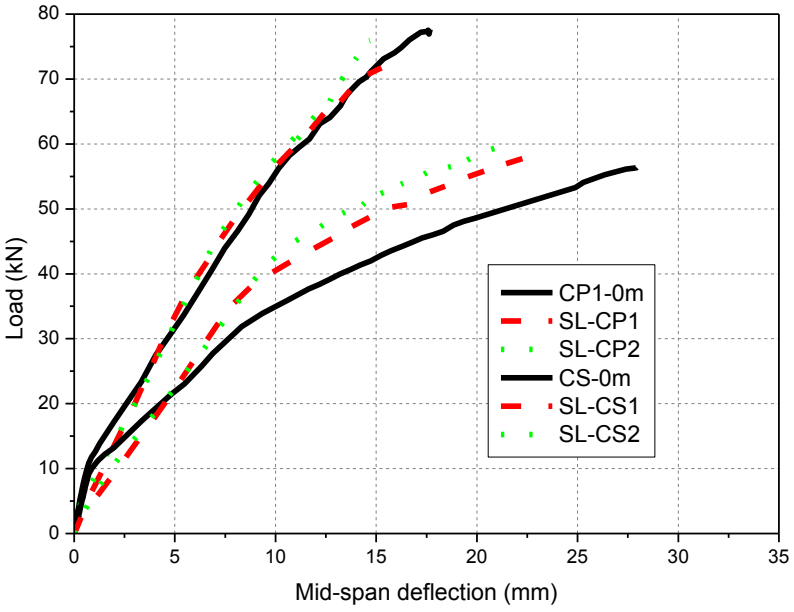

Figure 5-16 Load vs mid-span deflection curves of different beams tested at the end of sustained loading process

5.5 CONCLUSIONS

This chapter introduced explorations on the influences of sustained load on the long-term performances of FRP-strengthened RC beams. CFRP sheet and CFRP plate-strengthened RC beams were subjected to 9-month sustained loading with two service load levels: 15kN and 25kN. The beam deflected as a function of the load level and time. The long-term deflections were 201%~246% of their instantaneous deflections. FE simulations were used to study the process. According to the test and analytical observations, the following findings were obtained: (a) A higher FRP strengthening ratio can reduce the absolute value of instantaneous deflection and long-term deflection; however, the long-term deflections occupied a larger proportion of total deflection in this case. (b) No significant change in the load capacity of strengthened beams was observed on the after being loaded for 9 months regardless of the sustained load levels. (c) Both the stiffness and the ductility of strengthened beams reduced after the sustained loading.

CHAPTER 6

CONCLUSIONS AND RECOMMENDATIONS

In the present study, the long-term performance of FRP-to-concrete interfaces and FRP-strengthened RC beams subjected to accelerated wet-dry cycles, which simulate sub-tropical environments, was investigated. The thesis consists of four parts of work: (1) The degradation of material components in the FRP-strengthened RC structures subjected to 8-month wet-dry cycles was evaluated; (2) The long-term performance of FRP-to-concrete interface subjected to 8-month exposure was examined using single-lap shear tests, and exposure-based interfacial bond-slip models were established accordingly. Degradations were observed in FRP-to-concrete interfaces after 8-month exposure, and the degradations were well interpreted by the proposed models; (3) The durability of FRP-strengthened RC beams was assessed under 8-month exposure in dry-wet cycles. FE analysis was conducted to simulate their performances with due consideration of the degradation of materials and FRP-to-concrete interfaces and good predictions were achieved. (4) The long-term performance of CFRP sheet and CFRP plate-strengthened RC beams under sustained load were tested. Four beams were loaded under two service load levels for 9 months. FE simulations were conducted to simulate the time-dependent behavior in beams, which were in good agreement with the test results. Load capacity of beams was also tested at the end of sustained load tests.

6.1 DEGRADATION IN MATERIALS SUBJECTED TO WET-DRY CYCLES

After 8-month exposure, the compressive strength of concrete, tensile strengths of CFRP sheets and CFRP plates obtained 6.9%, 6.0% and 12.3% increase, while the Young's modulus remained the same. On the contrary, the ultimate tensile strength of the GFRP sheets (GS) decreased by 48.9%, which was a severe degradation. At the same time, the resins 3C, Sika330, Sika30 and Araldite106 obtained 37.9%, 40.8%, 52.4% increase in tensile strength and no change in their stiffness, while the Araldite106 underwent 15.0% decrease in the tensile strength but a 48.9% increase in its stiffness.

6.2 DEGRADATION IN FRP-TO-CONCRETE INTERFACES SUBJECTED TO WET-DRY CYCLES

Both experimental and analytical studies were conducted on the exposure-dependent behavior of FRP-to-concrete interfaces. The FRP bonded concrete joints were exposed in wet-dry cycles for 8 months, in which four different combinations of FRP and epoxy adhesives were used. Single-lap shear tests were used to evaluate the bond performance after exposure. The following conclusions are made based on the above work:

(a) Arch-shape strain distributions emerged in the FRP laminates during exposure, and the residual strains were not likely to fully recover even the bonded joints were fully dried and placed back to the original indoor environment.

(b) The exposure in wet-dry cycles induced changes of the failure mode of joints. Most of the specimens (CP1-8m, CP2-0m, CS, GS-0m) failed in concrete; however, two of CP1-0m failed in the adhesive layer; CP2-8m failed in the adhesive-epoxy interface combined with FRP delamination; and GS-8m failed by FRP sheet fracture. Changes in the failure mode indicate that the exposure has brought out different effects on the interfaces or the FRP composites. The 8-month exposure improved the cohesion

between the primer and resins in CP1 but weakened the cohesion between the FRP plate and adhesive in CP2 and the strength of GFRP sheets.

(c) Variations in bond strengths were also observed: 13.7% and 2.8% increase in CP1 and CP2 while 3.2% and 16.4% decrease in CS and GS, respectively. The ultimate bond strength of GS series decreased largely due to rupture of GFRP sheets.

(d) Predicted bond stress-slip models were proposed. The parameters were regressed from tests. Bond degradation was well interpreted by variations in parameters B and G_f. Good agreement was found between predicted and test results.

(e) It is proved that a soft adhesive layer could improve the bond performance. In present study, CP1 with a softer adhesive layer achieved higher bond strength than CP2 using the same FRP plate but a stiffer adhesive layer.

6.3 BEHAVIOR OF FRP-STRENGTHENED RC BEAMS SUBJECTED TO WET-DRY CYCLES

In the present study, the durability performances of FRP-strengthened RC beams under wet-dry cycles were evaluated by both experimental and analytical study and the following findings were obtained:

(a) The ultimate loads were 77.65kN, 75.07kN, 56.36kN and 46.53kN for CP1-0m, CP2-0m, CS-0m and GS-0m, respectively. The load capacity showed a positive correlation with the FRP stiffness. CP1 and CP2 with the highest FRP strengthening ratio responded in higher stiffness and larger load capacity, while CS and GS specimens which were strengthened with smaller ratio had lower load capacity but better ductility.

(b) Degradation in load capacities was observed of beams under wet-dry cycles. After 8-months exposure, the ultimate load of beams decreased by 2.6%, 10.8%, 1.4% and 7.9% for CP1-8m, CP2-8m, CS-8m, GS-8m, respectively. The stiffness of beams slightly decreased in CP1-8m and CP2-8m but increased in CS-8m and GS-8m, which was supposed to be contributed by a combination of many effects, such as aging of concrete, variations in FRP stiffness and FRP-to-concrete interfacial behavior, and possibly corrosion in steel bars.

(c) FE simulations were conducted in present study. The proposed model properly simulated all the components of FRP strengthened RC beams. The simulated results interpreted the mechanism of IC debonding. The models also provided good predictions for the exposure effects of wet-dry cycles by properly considering variations of material and interfacial properties of all components of the beams.

6.4 BEHAVIOR OF FRP-STRENGTHENED RC BEAMS SUBJECTED TO SUSTAINED LOAD

CFRP sheet and CFRP plate-strengthened RC beams were subjected to 9-month sustained loading in two service load levels: 15kN and 25kN. The beam deflected as a function of the load level and time. The time-dependent deflections were 1.73~2.60 times the instantaneous deflections, which varied according to sustained load level and FRP stiffness. FE simulations were used to study the process. According to the test and analytical observations, the following findings were obtained: (a) the higher the load level, the larger instantaneous and time-dependent deflections; however, higher load led to a smaller ratio of time-dependent to instantaneous deflections. (b) under the same load level, larger FRP stiffness led to lower instantaneous and time-dependent deflections. Moreover, with the increase of load, the

contribution of FRP in reducing the time-dependent deflections became more significant. Lastly, the larger the FRP stiffness, the larger the ratio of the time-dependent to instantaneous deflection. This phenomenon became less significant with the increase of load level. (c) no significant change in load capacity of the strengthened beams was observed after they were loaded for 9 months regardless of the sustained load levels. (d) both the initial stiffness and the ductility of beams reduced in all beams subjected to sustained load.

6.5 RECOMMENDATIONS FOR FUTURE WORK

The completed work in this present study is a part of a long-term project named "durability of bond between FRP and concrete exposed to a humid subtropical environment". The project is aiming at (a) obtaining a good understanding of long-term bond behavior of the FRP-to-concrete interface; (b) evaluating the global performance of FRP-strengthened structures using degraded FRP reinforcement; (c) establishing a relationship between accelerated tests and field exposure tests; and (d) establishing a reliable predictive method to measure long-term performance of bond. Due to limitation of time of the master study, only 8-months accelerated laboratory tests were completed. 4 more durations of accelerated laboratory tests and five durations of field tests were designed and prepared by the author.

6.5.1 Accelerated laboratory tests and field exposure tests

In present study, 120 FRP bonded-joints, 48 FRP-strengthened RC beams and materials coupons were prepared for both accelerated laboratory tests (5 durations) and field exposure tests (5 durations) (Figure 6-1). Detailed information of specimens are listed in Table 2-1, Table 2-2, Table 2-6, Table 2-7, Table 3-1, Table 3-2, Table 4-1 and Table 4-2, respectively. Figure 6-1 shows the specimens prepared for field exposure tests.

Figure 6-1 Specimens for future field exposure tests

6.5.2 On-going experiment on combined effects of moisture and sustained load

This test was designed to evaluate the combined effects of moisture and sustained load. For ease of comparison, the set-up of the test was the same with the sustained load test in Chapter 5; additionally, a coating sponge was settled between the two beams covering the FRP bonded area of RC beams. The sponge was soaked with pure water so as to provide a moisture submerging environment for the FRP-to-concrete interface. The beams were subjected to 15 kN and 25kN sustained load respectively. Mid-span deflections and strains in concrete and FRP were monitored by mechanical dial gauges and FOS, respectively.

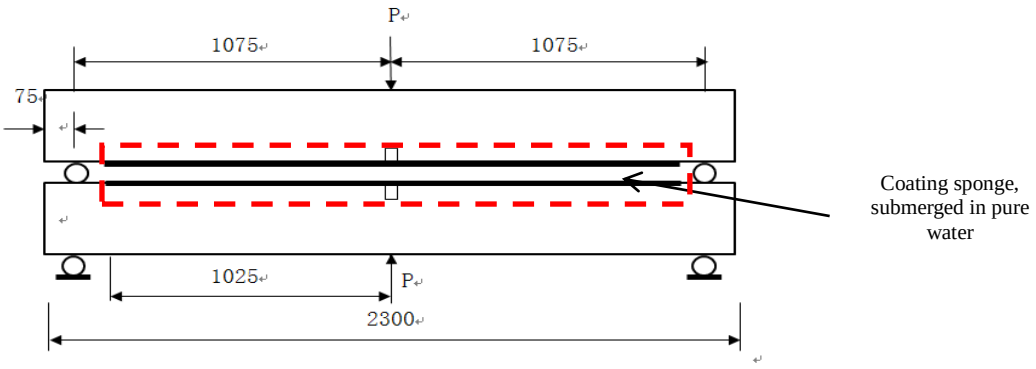

Figure 6-2 Specimens for future sustained load tests

Figure 6-3 Test set-up of sustained loading test

REFERENCES

Abdullah A., A., Ahmad S., AI-G., Abdur, R.A. and Rasheeduzzafart. (1996) "Effect of reinforcement corrosion on bond strength." *Construction and Building Materials,* **10**(2): 123-129.

Ahmed, E. and Sobuz, H.R. (2011). "Experimental study on long-term behaviour of CFRP strengthened RC beams under sustained load." *Structural Engineering and Mechanics,* **40**(1): 105-120.

Al Chami, G., Thériault, M. and Neale, K.W. (2007). "Creep behaviour of CFRP-strengthened reinforced concrete beams." *Construction and Building Materials,* **23**(4): 1640-1652.

Ali, O., Bigaud, D. and Ferrier, E. (2012). "Comparative durability analysis of CFRP-strengthened RC highway bridges." *Construction and Building Materials,* **30**: 629-642.

Almusallam, T.H. (2006). "Load-deflection behavior of RC beams strengthened with GFRP sheets subjected to different environmental conditions." *Cement & Concrete Composites,* **28**(10): 879-889.

Attard, M.M. and Kim, M. (2010). "Lateral buckling of beams with shear deformations - A hyperelastic formulation." *International Journal of Solids and Structures,* **47**(20): 2825-2840.

Au, C. and Buyukozturk, O. (2006). "Peel and shear fracture characterization of debonding in FRP plated concrete affected by moisture." *Journal of Composites for Construction,* **10**(1): 35-47.

Bank, L., Gentry, T. and Barkatt, A. (1995). "Accelerated test methods to determine the long-term behavior of FRP composite structures - environmental-effects." *Journal of Reinforced Plastics and Composites,* **14**(6): 559-587.

Bažant, Z., Wu, P., Wu, S. and Wu, T. (1974). "Rate- type creep law of aging concrete based on Maxwell chain." *Matériaux et Construction,* **7**(1): 45-60.

Benyoucef, S., Tounsi, A., Adda bedia, E.A. and Meftah, S.A. (2007). "Creep and shrinkage effect on adhesive stresses in RC beams strengthened with composite laminates." *Composites Science and Technology,* **67**(6): 933-942.

Cao, S., Wu, Z. and Wang. X. (2009). "Tensile properties of CFRP and hybrid FRP composites at elevated temperatures." *Journal of Composite Materials*, **43**(4): 315-330.

CEB-FIP. (1993). CEB-FIP Model Code 90, Thomas Telford, London.

Ceroni, F., Cosenza, E., Gaetano, M. and Pecce, M. (2006). "Durability issues of FRP rebars in reinforced concrete members". *Cement and Concrete Composites*, 28(10): 857–68.

Chajes, M.J., Thomson, T.A. and Farschman, C. A. (1995). "Durability of concrete beams externally reinforced with composite fabrics." *Construction and Building Materials,* **9**(3): 141-148.

Chen, G.M., Teng, J.G., Chen, J.F. and Rosenboom, O.A. (2008). "Finite element model for intermediate crack debonding in RC beams strengthened with externally bonded FRP reinforcement." *Proceedings of the 4th International Conference on FRP Composites in Civil Engineering (CICE2008)*, CD-ROM, Paper No: 8C3, Zurich, Switzerland, July 22-24.

Chen, G.M., Teng, J.G. and Chen, J.F. (2011). "Finite-element modeling of intermediate crack debonding in FRP-plated RC beams." *Journal of Composites for Construction,* **15**(3): 339-353.

Chen, J.F. and Teng, J.G. (2001). "Anchorage strength models for FRP and steel plates bonded to concrete." *Journal of Structural Engineering-ASCE*, **127**(7): 784-791.

Choi, K., Meshgin, P. and Taha, M.M.R. (2007). "Shear creep of epoxy at the concrete-FRP interfaces." *Composites Part B-Engineering*, **38**(5-6): 772-780.

Choi, K., Taha, M.M.R., Masia, M.J., Shrive, P.L. and Shrive, N.G., (2010). "Numerical Investigation of Creep Effects on FRP-Strengthened RC Beams." *Journal of Composites for Construction,* **14**(6): 812-822.

Dai, J., Ueda, T. and Sato, Y. (2005). "Development of the nonlinear bond stress-slip model of fiber reinforced plastics sheet-concrete interfaces with a simple method." *Journal of Composites for Construction*, **9**(1): 52-62.

DAI, J.G., Ueda, T. and Sato, Y. (2006). "Unified analytical approaches for determining shear bond characteristics of FRP-concrete interfaces through pullout tests." *Journal of Advanced Concrete Technology,* **4**(1): 133-145.

Dai, J.G., Kato, E., Iwanami, M. and Yokota, H. (2008). "Durability of carbon strand sheet to concrete bond interface under moisture condition", *Proceedings of the 4th International Conference on FRP Composites in Civil Engineering (CICE 2008)*, CD-ROM, Paper No: 3D3, Zurich, Switzerland, July 22-24.

Dai, J.G., Yokota, H., Iwanami, M. and Kato, E. (2010). "Experimental Investigation of the Influence of Moisture on the Bond Behavior of FRP to Concrete Interfaces." *Journal of Composites for Construction;* ASCE, **14**(6): 834-844.

Davalos, J.F., Kodkani, S.S. and Ray, I. (2006). "Fracture mechanics method for mode-interface evaluation of FRP bonded to concrete substrates." *Journal of Materials in Civil Engineering*, **18**(5): 732-742.

El-Dieb, A., Aldajah, S., Biddah, S. and Hammami, A. (2012) "Long-Term Performance of RC Members Externally Strengthened by FRP Exposed to Different Environments." *Arabian Journal for Science and Engineering*, **37**(2): 325-339.

Frigione, M., Aiello, M.A. and Naddeo, C. (2006). "Water effects on the bond strength of concrete/concrete adhesive joints." *Construction and Building Materials,* **20**(10): 957-970.

Grace, N. and Singh, S. (2005). "Durability evaluation of carbon fiber-reinforced polymer strengthened concrete beams: Experimental study and design." *ACI Structural Journal,* **102**(1): 40-53.

Hamed, E. and Bradford, M.A. (2010). "Creep in concrete beams strengthened with composite materials." *European Journal of Mechanics A-Solids*, **29**(6): 951-965.

Hamed, E. and Bradford, M.A. (2012) "Flexural time-dependent cracking and post- cracking behaviour of FRP strengthened concrete beams." *International Journal of Solids and Structures*, **49**(13): 1595-1607.

Hackman, I. and Hollaway L.C. (2006). "Epoxy-layered silicate nanocomposites in civil engineering." *Composites Part A*, 37(8):1161–70.

Haque, A., Shamsuzzoha, M., Hussain, F. and Dean, D. (2003). "S2-Glass/epoxy polymer nanocomposites: manufacturing, structures, thermal and mechanical properties." *Journal of Composite Materials*, 37(20):1821–37.

Hollaway, L.C. (2010). "A review of the present and future utilisation of FRP composites in the civil infrastructure with reference to their important in-service properties." *Construction and Building Materials*, 24(12): 2419-2445.

Hollaway, L.C. and Head, P.R. (2011). "Advanced polymer composites and polymers in the civil infrastructure." Amsterdam ; New York : Elsevier Science.

Hordijk, D. A. (1991). "Local approach to fatigue of concrete." Ph.D. thesis, Delft University of Technology.

Huang, N. (2009). "Finite element analysis of locally corroded reinforced concrete beams for FRP strengthening" MSc dissertation, the Hong Kong Polytechnic University.

Jones, R.L., Chandler, H.D. (1985). "Strength loss in E-glass fibres after exposure to organics acids." *Journal of Material Science*, 20:3325–3328.

Karbhari, V., Chin, J., Hunston, D., Benmokrane, B., Juska, T., Morgan, R., Lesko, J., Sorathia, U. and Reynaud, D. (2003). "Durability gap analysis for fiber-reinforced polymer composites in civil infrastructure." *Journal of Composites for Construction*, **7**(3): 238-247.

Karbhari, V., Engineer, M. and Eckel, D. (1997). "On the durability of composite rehabilitation schemes for concrete: Use of a peel test." *Journal of Materials Science*, **32**(1): 147-156.

Karbhari, V. and Zhao, L. (1997). "Issues related to composite plating and environmental exposure effects on composite-concrete interface in external strengthening." *Composite Structures*, **40**(3-4): 293-304.

Katsuki, F. (1997). "Evaluation of alkaline resistance of fibre reinforcement for concrete." Thesis submitted to the University of Tokyo for PhD Degree. [in Japanese].

Li, F.M., Yuan, Y.S. (2012). "Experimental study on behavior of long-term bond-creep between corroded steel strands and concrete." *Industrial Construction*, 42(2):

Liu, W., Hoa, S., Pugh, H. (2005). "Epoxy–clay nanocomposites: dispersion, morphology

and performance." *Composites Science and Technology*, **65**: 307–16.

Lu, X.Z. (2004). "Studies on FRP-concrete interface." PhD dissertation, Tsing Hua University, Beijing, China.

Lu, X.Z., Teng, J.G., Ye, L.P. and Jiang, J.J., (2005). "Bond–slip models for FRP sheets/plates bonded to concrete." *Engineering Structures,* **27**(6): 920-937.

Lu, X.Z., Teng, J.G., Ye, L.P. and Jiang, J.J. (2007). "Intermediate crack debonding in FRP-strengthened RC beams: FE analysis and strength model." *Journal of Composites for Construction,* **11**(2): 161-174.

Lyons, J., Laub, D., Giurgiutiu, V., Petrou, M. and Salem, H. (2002). "Effect of hygrothermal aging on the fracture of composite overlays on concrete." *Journal of Reinforced Plastics and Composites,* **21**(4): 293-309.

Matthews F.L., Rawlings, R.D. (1999). "Composite materials: engineering and science." Cambridge, England: Woodhead Publishing.

Mather, B. (2004). "Concrete durability." *Cement and Concrete Composites,* **26**(1): 3-4.

Mufti, A., Onofrei, M., Benmokrane, B., Banthia, N., Boulfiza, M., Newhook, J. et al. (2005). "Report on the studies of GFRP durability in concrete from field demonstration structures." In: Hamelin et al., editors. *Proceedings of the composites in construction– 3rd international conference*, Lyon, France, July 11–13; 2005.

Mukherjee, A. and Arwikar, S.J. (2007) "Performance of externally bonded GFRP sheets on concrete in tropical environments. Part I: Structural scale tests." *Composite Structures,* **81**(1): 21-32.

Mukhopadhyaya, P., Swamy, R.N. and Lynsdale, C.J. (1998) "Influence of aggressive exposure conditions on the behaviour of adhesive bonded concrete–GFRP joints." *Construction and Building Materials,* **12**(8): 427-446.

Nakaba, K., Kanakubo, T., Furuta, T. and Yoshizawa, H. (2001). "Bond behavior between fiber-reinforced polymer laminates and concrete." *ACI Structural Journal,* **98**(3): 359-367.

Ouyang, Z. (2007). "Durability of bond between FRP and concrete in moist environments experimental, numerical and analytical study." Ph.D. thesis, Marquette University.

Rabinovich, O., and Frostig, Y. (2000). "Closed-form high-order analysis of RC beams strengthened with FRP strips", *Journal of Composites for Construction*, 4(2): 65-74.

Saenz, L. P. (1964). "Discussion of 'Equation for the stress-strain curve of concrete' by P. Desayi and S. Krishan." *Journal of American Concrete Institution*, 61(9): 1229–1235.

Sen, R., Shahawy, M., Mullins, G. and Spain, J. (1999). "Durability of carbon fiber-reinforced polymer/epoxy/ concrete bond in marine environment." *ACI Structural Journal*, **96**(6): 906-914.

Shrestha, J., Ueda, T., Zhang, D., Kitami, A. and Komori, A. (2012) "Durability of the FRP-concrete bond under the influence of moisture." *Proceedings of the First International Conference on Performance-based and Life-cycle Structural Engineering (PLSE 2012)*, Hong Kong, China.

Silva, M.A.G. and Biscaia, H. (2008). "Degradation of bond between FRP and RC beams." *Composite Structures*, **85**(2): 164-174.

Soudki, K., El-Salakawy, E. and Craig, B. (2007). "Behavior of CFRP strengthened reinforced concrete beams in corrosive environment." *Journal of Composites for Construction; ASCE*, **11**(3): 291-298.

Stanish, K.D. (1999). "Corrosion effects on bond strength in reinforced Concrete." Master of Applied Science dissertation, University of Toronto, Canada.

Taha, M., Masia, M.J., Choi, K.K., Shrive, P.L. and Shrive, N.G. (2010) "Creep effects in plain and fiber- reinforced polymer-strengthened reinforced concrete beams." *ACI Structural Journal; ACI Structural Journal*, **107**(6): 627-635.

Tan, K.H. and Saha, M.K. (2006). "Long-term deflections of reinforced concrete beams externally bonded with FRP system." *Journal of Composites for Construction*, **10**(6): 474-482.

Tan, K.H. and Saha, M.K. (2008). "Cracking characteristics of RC beams strengthened with FRP system." *Journal of Composites for Construction*, **12**(5): 513-521.

Tan, K.H., Saha, M.K. and Liew, Y.S. (2009) "FRP-strengthened RC beams under sustained loads and weathering." *Cement and Concrete Composites*, **31**(5): 290-300.

Teng, J.G., Chen, J.F., Smith, S.T. and Lam, L. (2002). "FRP-strengthened RC structures."

John Wiley and Sons, Inc., UK.

Teng, J.G., Smith, S., Yao, J. and Chen, J.F. (2003). "Intermediate crack-induced debonding in RC beams and slabs." *Construction and Building Materials*, **17**(6-7): 447-462.

Teng, J.G. and Chen, J.F. (2009). "Mechanics of debonding in FRP-plated RC beams." *Proceedings of the Institution of Civil Engineers-Structures and Buildings*, **162**(5): 335-345.

Toutanji, H.A. and Gómez, W. (1997). "Durability characteristics of concrete beams externally bonded with FRP composite sheets." *Cement and Concrete Composites*, **19**(4): 351-358.

Tuakta, C. and Bueyuekoeztuerk, O. (2011). "Conceptual model for prediction of FRP-concrete bond strength under moisture cycles." *Journal of Composites for Construction*, **15**(5): 743-756.

Ueda, T. and Dai, J. (2005). "Interface bond between FRP sheets and concrete substrates: properties, numerical modeling and roles in member behaviour." *Progress in Structural Engineering and Materials*, **7**(1): 27-43.

Uomoto, T. and Nishimura, T. (1999). "Determination of Aramid, Glass and Carbon Fibres due to alkali, acid and water in different temperatures." In: *Proceedings 4th international symposium, FRPRCS-4, ACI SP-188, American Concrete Institute*, 515–22.

Uomoto, T. (2001). "Durability considerations for FRP reinforcements." In: Burgoyne CJ, editor. *Proceedings of 5th International Conference on fibre-reinforced plastics for reinforced concrete structures.* Cambridge, UK.

Wan, B., Petrou, M. and Harries, K. (2006). "The effect of the presence of water on the durability of bond between CFRP and concrete." *Journal of Reinforced Plastics and Composites*, **25**(8): 875-890.

Wu, Z.S., Iwashita, K., Yagashiro, S., Ishikawa, T. and Hamaguchi, Y. (2005). "Temperature effect on bonding and debonding behavior between FRP sheets and concrete." *Journal of the Society of Materials Science, Japan*, **54**(5): 474-480.

Yao, J., Teng, J.G. and Chen, J.F. (2005). "Experimental study on FRP-to-concrete bonded joints." *Composites Part B*, **36**(2): 99-113.

Yao, J. (2005). “Debonding failures in RC beams and slabs strengthened with FRP plates.” PhD dissertation, the Hong Kong Polytechnic University.

Zhu, H. (2009). “Fiber optic monitoring and performance evaluation of geotechnical structures.” PhD dissertation, the Hong Kong Polytechnic University.